Profile 1

● TEM
○ ERT
— SkyTEM

0   100   200 m

Level	0-16.5 m	16.5-36 m	36 – 42.2	42.2 – 71.1
Lithology (200m from 300 m mark)	Sand and clay	Till with thin coarse silt layer	Silt to thin clay	Coarse silts to sand
Level	0-5	5 – (30 to 40)	40 to bedrock at 75 to 80 m	At 45 m depth at central profile
Lithology (south)	sand	Till or clayey till and thin clay	Sand and gravel	Clay (1m thickness)

Grevie
2D INVERTED MODEL (mean residual 2.0%)

Distance[m]

sa,cl
till

Level[m]

15   18   22   26   32   38   46   56   68   83   100
Resistivity[ohm-m]

Profile 1, Grevie

UTM
387686   387748   387809   387872   387933   387995   388057   388118

T1   T2   T3   T4

DCI, SkyTEM

Using DCIP and TEM to investigate the geology of the Alnarp Valley in southwestern Scania, Sweden

Simon Gustafsson

Holger Larsson

Abstract

In southwestern Scania there is a paleovalley, the Alnarp Valley, which holds a confined aquifer called Alnarpsströmmen. Its geology consists mainly of sand and gravel and it is generally confined by one or more layers of clayey till above, and the limestone bedrock below. In collaboration with Region Skåne and SGU, this thesis aims to gather information about Alnarpsströmmen using two geophysical methods Direct-Currect and Induced Polarization (DCIP) and Transient Electromagnetic Method (TEM), both relying on measuring the ground's resistivity to electrical current and using those measurements together with information gathered from nearby boreholes to make geological interpretations. Before resistivity data could be interpreted, it had to go through inversion, where a mathematical model is generated that outputs data that are as similar as possible to the ones gathered in the field.

It was decided to focus mainly on the area around Grevietäkten, a groundwater supply area that today provides about a quarter of Malmö's drinking water. Some sites were chosen outside of this area to offer comparison. Sites were selected by examining data gathered via helicopter borne TEM measurements, or SkyTEM, as well as data gathered from boreholes, and they were selected to be interesting from a geological standpoint or to fill a gap in the datasets.

Fieldwork was carried out for three weeks. For two weeks starting on the 19th of April 2021 and concluding on the 30th of April 2021 DCIP measurements were conducted. Further fieldwork was delayed, and TEM fieldwork began on the 15th of November 2021 and concluded on the 19th. In total, 11 different profiles were investigated.

Inversion of DCIP data was done in the software Res2DINV, and TEM data was inverted in SPIA. Resistivity profiles including DCIP, TEM, and SkyTEM data, as well as nearby boreholes, were created by importing data into GeoScene3D. While interpreting, some general observations were made. The clayey till often appears as a low resistivity layer compared to the high resistivity layer that denotes the aquifer sediments. The bedrock is not reached via DCIP in most cases, but TEM and SkyTEM show that it generally has a very low resistivity and decreases with depth, indicating heavy fracturing and/or high ionic content. After interpretation, a table with the most commonly occurring materials and their resistivity values was created and is presented below.

Material, interpeted	Resistivity (Ohm·m)
Alnarp sediments	40-100
Clay	10-40
Gravel	300-400
Limestone	10-100
Sand	100
Till	30-80

Sammanfattning

I sydvästra Skåne finns en underjordisk dalgång, Alnarpsdalen, som rymmer en sluten akvifer vid namn Alnarpsströmmen. Den består huvudsakligen av sand och grus och är i allmänhet begränsad av ett eller flera lager av lerig morän ovanför och kalkstensberggrund nedanför. I samarbete med Region Skåne och SGU syftar detta examensarbete till att samla information om Alnarpsströmmen med hjälp av de geofysiska metoderna DCIP och TEM, som båda mäter markens resistivitet mot elektrisk ström, och använder dessa mätningar tillsammans med information från närliggande borrhål för att göra geologiska tolkningar. Innan resistivitetsdata kan tolkas måste den gå igenom inversion, där en matematisk modell genereras som matar ut data som är så lika de som samlats in i fält som möjligt.

Det beslutades att främst fokusera på området kring Grevietäkten, ett grundvattenförsörjningsområde som i dagsläget står för ungefär en fjärdedel av Malmös dricksvatten. Vissa platser valdes utanför detta område för att kunna göra jämförelser. Platser valdes ut genom att undersöka data som samlats in via helikopterburna TEM-mätningar, eller SkyTEM, samt från borrhål, och valdes ut för att vara intressanta ur någon geologisk synvinkel eller för att fylla en lucka i dataunderlaget.

Fältarbete utfördes under tre veckor, först med två veckor med start den 19 april 2021 och avslut den 30 april, då DCIP-mätningar utfördes. Ytterligare fältarbete försenades och TEM-fältarbetet började den 15 november 2021 och avslutades den 19:e. Totalt undersöktes 11 olika profiler.

Inversion av ERT-data gjordes i programvaran Res2DINV, och TEM-data inverterades i SPIA. Resistivitetsprofiler inklusive DCIP-, TEM- och SkyTEM-data, såväl som närliggande borrhål, skapades genom att importera data till GeoScene3D. Under tolkningen gjordes några allmänna observationer. Den leriga moränen uppträder ofta som ett lager med lägre resistivitet jämfört med det högre resistivitetslagret som betecknar akvifersediment. Berggrunden penetreras i de flesta fall inte via DCIP, men TEM och SkyTEM visar att den generellt har mycket låg resistivitet som minskar med djupet, vilket tyder på kraftig sprickbildning och/eller hög jonhalt. Efter tolkning skapades en tabell med Alnarpsdalens främst förekommande geologiska material och deras resistiviteter, som presenteras nedan.

Material, tolkade	Resistivitet (Ohm·m)
Alnarpssediment	40-100
Grus	300-400
Kalksten	10-100
Lera	10-40
Morän	30-80
Sand	100

Preamble

This thesis was written to conclude the authors studies at the Civil and Enviromental Engineering program, with a specialization in Water Resources Engineering at Lunds Tekniska Högskola. It corresponds to 30 credits and was initiated early in 2021. After some delays, the fieldwork was finished in November of the same year. It was then put on an extended hiatus but is now finally completed, more than two years later.

The thesis was initiated by a team of two authors, but after about one and a half years, one of the authors, Holger, had to stop working with it due to health reasons. The project was eventually concluded by me, Simon. However, Holger still did a very substantial amount of work and is therefore rightly recognized as an author. His contributions include much of the preparatory work for the fieldwork, such as finding suitable sites, as well as a larger part of the actual on-site fieldwork as I was ill for a week during this. Afterwards, he also did most of the data processing and created many of the images that go along with the profiles. As for me, I did most of the actual writing that ended up in the final report, although often continuing upon and refining work already done by Holger, as in the case of most interpretations. The geology and methodology sections are completely my own work, as well as the discussion. The rest of it, Holger had a hand in, in one way or another.

Table of Contents

1 Introduction

The Alnarp Valley (Figure 1) is located in southwestern Scania, Sweden. It stretches between the coastal line of the Baltic Sea (Ystad) to the Sound (Landskrona).

It is however part of a larger depression which continues underwater into the northern parts of the isle Zealand in Denmark. The Alnarp valley is completely filled with sediments, and thus not visible from the ground. Just above the bedrock lies a layer of sand, gravel and cobbles which houses two aquifers, the Alnarp stream (*Swedish: Alnarpsströmmen*) and the Skivarp stream (*Swedish: Skivarpsströmmen*). The groundwater flows in opposite directions from the depression's highest point, see Figure 1. Previous studies have referred to both aquifers as Alnarpsströmmen. Since its discovery, many cities and towns in the surrounding areas have relied on this aquifer to supply some or most of their water.
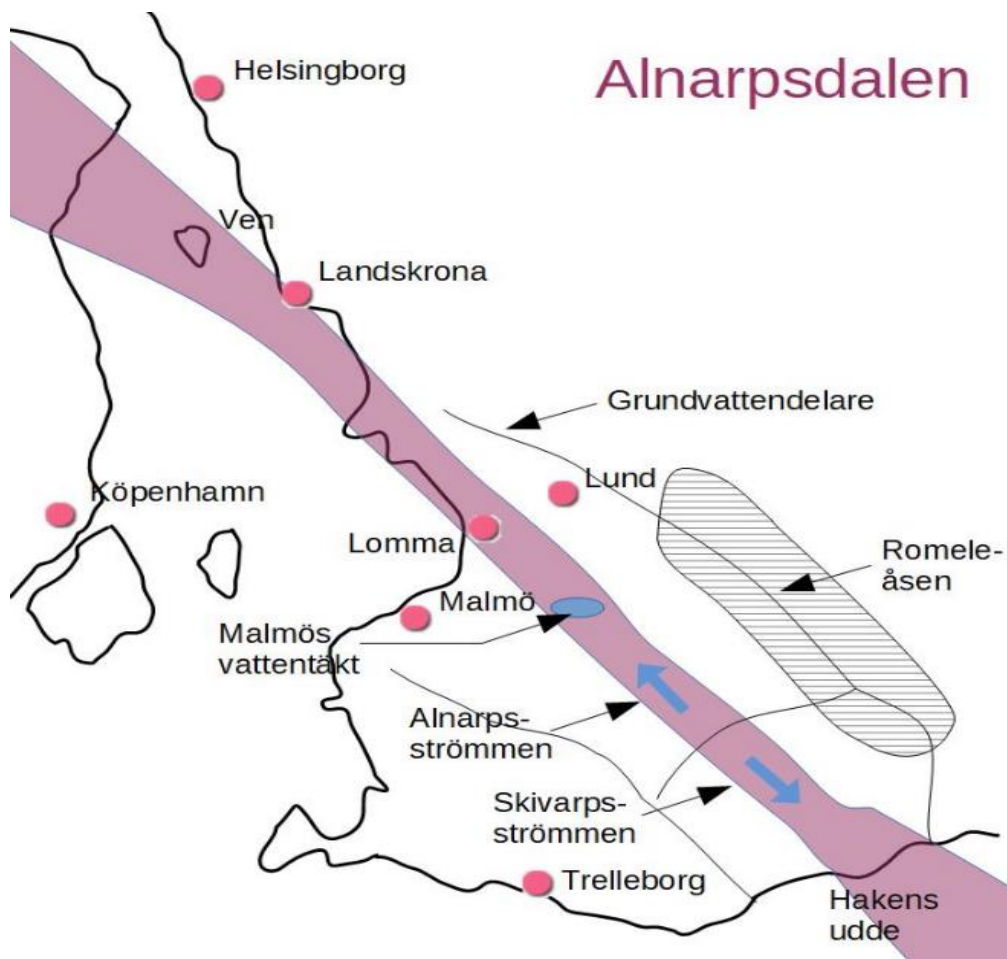

Figure 1. The Alnarp valley in its geographical context in southwestern Scania. Note: this figure is reused with permission from Leksunim (2018)

The oldest wells utilizing Alnarpsströmmen date back to before the 1850's, but it wasn't until the late 19th century that usage of the aquifer became more widespread. In the late 19th century, an investigation found that roughly 50 l/s was drained from the aquifer. The usage of the aquifer grew quickly, as many both private and public wells came into use. In the beginning of the 20th century, the city of Malmö started using water from the aquifer to meet its water demand. The water originated from the water supply area Grevietäkten, near the village of Staffanstorp. Here, as much as 400 l/s second was extracted from the aquifer until new surface water installations were constructed in the late 1940's. Many other towns in Scania, such as Lund, made their own installations, and in 1968 the sum total of groundwater extracted was roughly 500 l/s. Since then, this number has steadily decreased, and today the total sum is around 200l/s (Vattenbyggnadsbyrån, 1969; Malmö stad, 2021). Much of this water is still extracted at Grevietäkten, which also acts as a regional groundwater reserve (VA SYD, 2021).

This project is part of a Lund University collaboration between Sveriges Geologiska Undersökning (SGU) and region Skåne at the division of Engineering Geology, Lunds Tekniska Högskola (LTH). The aforementioned project aims to increase the knowledge of the groundwater reserves in Scania, with a focus on Alnarpsströmmen. This thesis will focus primarily on the geographical area around Grevietäkten. The main goal is to gather information about the geological conditions in this area. How the geology relates to hydrogeological conditions will be touched upon lightly, but otherwise left for another study. To investigate, the geophysical methods DCIP and TEM will be used. They will be explained in depth later, but they both rely on injecting the ground with electricity and measuring its resistivity response, which then can be used for interpretation.

The goals of the thesis are as follows:

1. Analyze existing background material, consisting of borehole logs, SkyTEM data, previous studies, and literature, to find sites that are interesting from a groundwater point of view, or where previous investigations are lacking. The study will be focused on the area around Grevietäkten, but some areas outside of this area will be studied to offer comparison.
2. Perform TEM and/or DCIP surveys in the selected areas.
3. Interpret the results of the geophysical surveys, using available borehole data as aid.
4. Characterize the materials that commonly appear in the studied areas in terms of resistivity.
5. Compare the results of TEM, DCIP, and SkyTEM in the studied areas.
6. Discuss the strengths and weaknesses of the applied methods.

2 Theoretical background

2.1 Geology

In southwestern Scania, much of the bedrock is sedimentary in nature, and was formed during the Paleozoic era. It consists mainly of reef limestone, shale, alum shale, sandstone, and conglomerate. In south-west Scania, where the Alnarp depression is situated, the dominating surface rock is Danian limestone belonging to the "Köpenhamnsledet" and it is occasionally covered by younger sedimentary rocks (Johansson, et al., 2006). The surface limestone contains cracks and fissures, due to unloading and loading during the ice ages (Landberg & Hartzén, 1987).

A tectonic zone, called the Tornquist zone, that runs through the Alnarp valley, is a crustal boundary between the Baltic shield to the north, and Avalonia, to the south (Liljegren & Björkman, 2004). It is not known how the Alnarp valley was created, but due to its location in the movement zone it can be speculated that tectonic movements in the Tornquist zone may have played a role in its development. Previous geologists however, attributed its formation to erosion by a preglacial river. In any case it is plausible that fluvial and glacial erosion has further increased the size of the depression (Ringberg, 1980).

The depression has a principal geometry measuring roughly 50km along its length, 5 to 10km across its width, with a depth varying between about 40m to 100m (Ringberg, 1987). The principal geology of the northwestern Alnarp valley, which this study focuses primarily on, is presented in Figure 2. It is filled with Quaternary deposits, often referred to as the Alnarp sediments, deposited directly on top of the underlying bedrock consisting of limestone. The bedrock is found to be quite eroded as a result of loading and unloading during Quarternary glaciations (Landberg & Hartzén, 1987).The grain size of these sediments varies with depth. Near the bedrock, sands and gravel can be found, and above that, making up the bulk of the sediment, fine sand, and silty fine sand (Ringberg, 1980). It is the coarser sediments and the fractured bedrock that are the most water-bearing and thus most interesting from a groundwater point of view, owing to their greater hydraulic conductivities (Barmen, 1992). Occasionally till deposits can be found between the Alnarp sediments and bedrock, possibly formed in the next-to-last glaciation (Miller, 1977). One or several layers of till/clay covers the sediments, with occasional layers of sediment interspliced (Ringberg, 1987). These tills are often divided into a very clay rich upper layer with a low content of gravel and larger grain sizes, while the lower layer consists mainly of coarse sediments. The upper clayey tills combined with the outright sorted clays acts as a mostly impermeable barrier for water, creating the confined aquifer. This is a simplified view, but it holds mostly true in the north-western parts of the depression, which is characterized by a thickness of the Alnarp sediments of approximately 40m, of which sediments coarser than silts make up to 25m. The stratigraphy of the southeastern part shows many more irregularities, where glacial forces have rearranged the sediment layers. This geographical area also features on average

much thicker Quaternary deposits, reaching depths of 180m in some parts (Gustafsson, 1978).
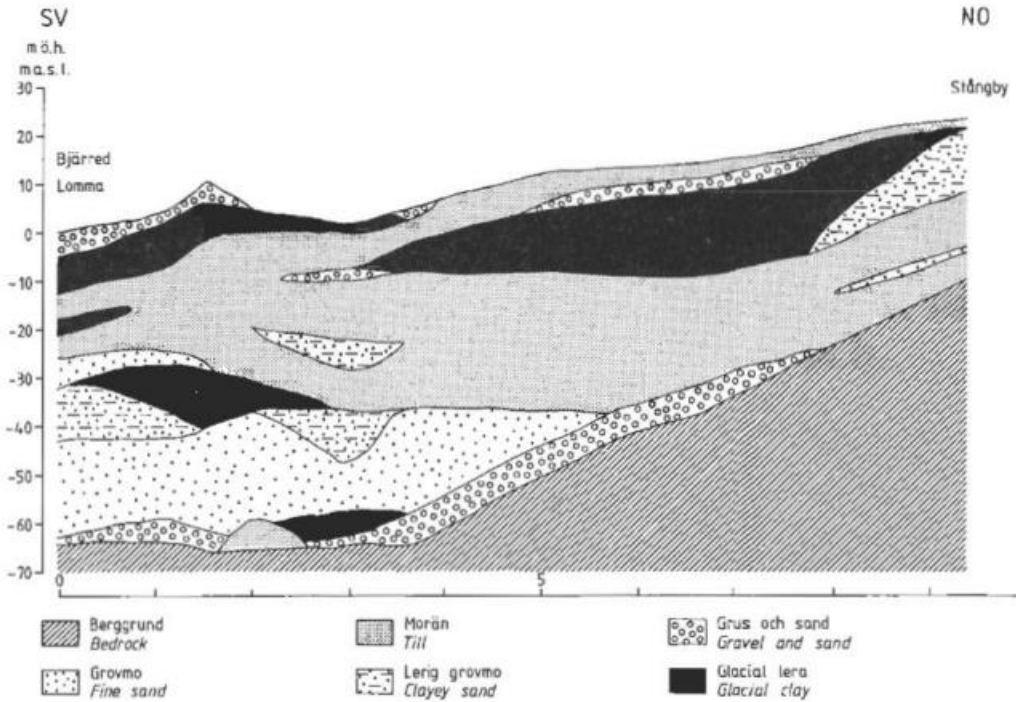
Figure 2. Principal geology of the northwestern parts of Alnaprsdalen. The cross-section is drawn between Bjärred and Stongby and is based on well drilling in the area. Note: this figure is reused with permission from Ringberg (1987) © SGU.

2.1.1 Hydrogeological conditions

The Alnarp sediments and the fractured bedrock can be considered the main part of the water-bearing materials in the paleovalley, however the pockets of sand and gravel found throughout the layers may contain enough water for local wells (Gustafsson, et al., 2005). Water flows predominantly in the northwestern direction as previously discussed. The clayey tills and fine-grained sediments create a mostly impermeable cover, which makes Alnarpsströmmen a confined aquifer. A confined aquifer is one that is situated between two layers of quasi-impermeable materials, in this case the bedrock and the clay rich materials above (ScienceDirect, 2023). Groundwater can still be found near the surface in a shallow and separate unconfined aquifer.

4

2.1.2 Recharge zones

As discussed, the geological layers that make up the aquifer are usually covered by layers of impermeable clay-rich materials, which does not allow for much recharge of precipitation. Along the Romele ridge (*Swedish: Romeleåsen*, Figure 1) however, the bedrock is only a few meters below the topographic surface. This coupled with its high elevation and the steep inclination of its sedimentary layers makes this an ideal recharge zone (Vattenbyggnadsbyrån, 1969). Another important recharge zone is an area around Svedala, referred to in literature as the hummocky till region due to its knolled surface, where sandy till dominates the topmost Quarternary deposits. In some cases, coarse-grained sediments reach the surface, connecting directly to the main aquifer body. Combined with the knolled surface, which reduces surface runoff, and the low hydraulic head in this area makes this another preferred recharge area (Ringberg, 1980). The two areas make up the main recharge zones for the aquifer, however other smaller recharge sources exist as well but will not be explained further (Barmen, 1992).

2.2 SkyTEM survey

During the years 2018-2020, the Geological Survey of Sweden (SGU) was tasked by the Swedish government to expand their knowledge of groundwater resources throughout Sweden. As a part of this assignment, a project was carried out in southwest Scania, which utilized the method helicopter carried transient electromagnetics, or SkyTEM, to find areas that are interesting from a groundwater perspective (Brolin, 2021). This technique is described in detail later on in the theis, but fundamentally SkyTEM uses electric and magnetic fields to obtain electrical resistivity profiles along the helicopters' flight path, which together with borehole observations gives an insight into the stratigraphy of an area. One drawback of the method is its sensitivity to electromagnetic fields generated by other sources such as powerlines. Such gaps exist in the resistivity profiles in many areas, where faulty data has been removed (Brolin, 2021). One way to combat this issue is by utilizing another geophysical method called DCIP to "fill in the gaps" caused by such disturbances.

2.3 Electrical currents in soil

Electrical currents in the ground can be conducted in three different ways. Electrolytic conduction is carried out by the movement of ions within the soil's pore water. This depends on factors such as ionic concentration, the type of ions present, and mobility. Electronic conduction is a flow of free electrons generally occurring in metals. Dielectric conduction occurs in materials that have very high resistivity. Here, an applied alternating current will cause electrons in the material to shift slightly compared to their nuclei.

In most circumstances, electrolytic conduction is the dominant form of conduction, except in subsurface materials containing large amounts of metallic minerals. Dielectric

conduction can generally be disregarded at the frequencies used in electrical resistivity methods (Reynolds, 2011).

As electrolytic conduction is dominant, the effective resistivity of a rock formation can be expressed as a function of porosity, saturation, and water resistivity. This is called Archie's Law, and is expressed as follows (Reynolds, 2011):

$$\rho = a\phi^{-m}s^{-n}\rho_w \text{ (Eq. 1)}$$

Where ρ and ρ_w are the effective rock resistivity and the resistivity of the porewater, ϕ is the porosity, s is the volume fraction of pores with water, a, m and n are constants where $0.5 \leq a \leq 2.5$, $1.3 \leq m \leq 2.5$, and $n \approx 2$ (Reynolds, 2011).

The water itself can vary greatly in resistivity. On one end of the spectrum, salty seawater can have resistivity as low as 0.05 Ohm·m; on the other end glacial meltwater can have resistivity as high as 1000 Ohm·m, owing to their vast difference in ionic content (Reynolds, 2011).

One material that is commonly found in the studied area deserves a bit of extra explanation, namely clay. When completely dry, it acts as an insulator just like other dry-nonmetallic soils. However, moisture affects its resistivity much more than other materials. Clay particles are so fine-grained that they are considered micro-crystals. During the formation of the clay via weathering, cations are adsorbed to the imperfections on the crystalline surface and remain there loosely attached. If the soil is moisturized, they can be exchanged with other ions and go into solution (McNeill, 1980). These ions contribute to electrical flow through the material as discussed above.

2.4 DCIP

2.4.1 Principle and History

Electrical resistivity tomography (ERT) measures resistivity through analyzing the ground's response to an electrical current. Every material has its own unique physical properties, including its ability to conduct electrical currents, and by measuring this property something can be said about the physical makeup of the subsurface. DCIP, direct current resistivity and induced polarization, is an extension of ERT, in that it measures resistivity, but also a property known as chargeability at the same time, using the same equipment.

The history of ERT goes back to the early 1900's, when direct current methods proved to be useful for sulphide mineral exploration. Equipment and interpretation methods were crude, limited by the technology available at the time. Something closer resembling the ERT of today first came to be in the 80's, when it was proved that some techniques used in medical electrical tomography could be applied to geology, although it would not be until the 90's that these systems were suitable for fieldwork (Daily, et al., 2005).

Today, ERT is a commonly used method for mapping geological variations including lithology, groundwater presence, salinity, and groundwater contamination (Olson Engineering, 2023). IP is often used in mineral exploration and hydrocarbon contamination detection (Slater & Lesmes, 2008).

2.4.2 DCIP

In the DCIP method, four electrodes are driven into the ground. Current passes between two of these electrodes, and the resulting voltage is measured between the remaining two. By doing this, the resistivity can be calculated. If the subsurface was completely homogenous, the measured resistivity would be the *true resistivity*. In a truly electrically homogenous cube, with the sides (L), a passing current (I) will suffer a potential drop (V) between the two sides, due to the resistance of the cube. This resistance (R) is proportional to (L), and inversely proportional to the cross-sectional area (A). This is depicted in Figure 3. Further, Ohm's Law states that the ratio of the potential drop to applied current (V/I) is also equal to resistance. These two expressions may be combined (Eq. 2) into a formula for resistivity (ρ) in a homogenous medium, having a resulting unit of Ohm·m.
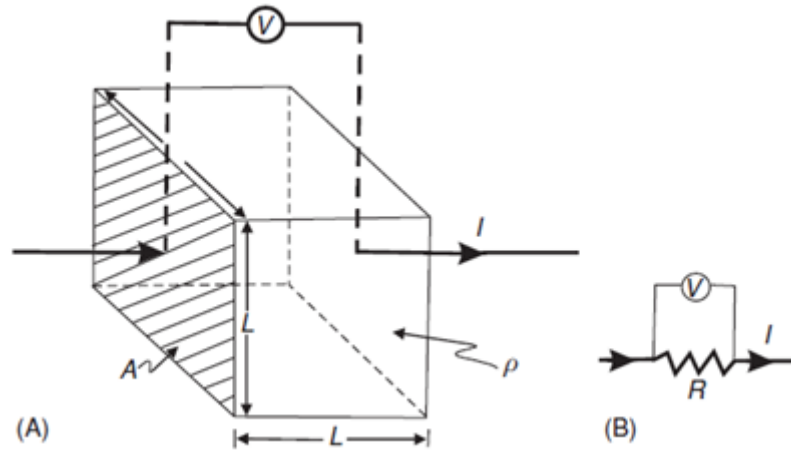
$$\rho = \frac{VA}{IL} \;\text{(Eq. 2)}$$

Figure 3. A current I is applied to a block with length L and resistance ρ (a), with a resulting potential drop V over the different sides, and the equivalent electrical circuit is shown in (b). Note: this figure is reused with permission from Reynolds (2011). © John Wiley & Sons Inc.

However, like in most natural materials, the ground is rarely homogenous. Instead, the measured values will be the mean value of all the present materials combined (Reynolds, 2011). This is referred to as the *apparent resistivity,* and is defined by the US Environmental Protection Agency as: "the resistivity of an electrically homogeneous and isotropic half-space that would yield the measured relationship between the applied current and the potential difference for a particular arrangement and spacing of electrodes" (U.S EPA, 2016). Mathematically (Eq. 3), this is a product of the resistance R, and a geometrical factor K.

$$\rho = R * K \text{ (Eq. 3)}$$

This geometrical factor is defined by Equation 4, where A, B are current electrodes, and M, N are potential (measuring) electrodes, as presented in Figure 4.

$$K = 2\pi \left(\frac{1}{AM} - \frac{1}{MB} - \frac{I}{AN} - \frac{I}{NB} \right)^{-1} \text{ (Eq. 4)}$$
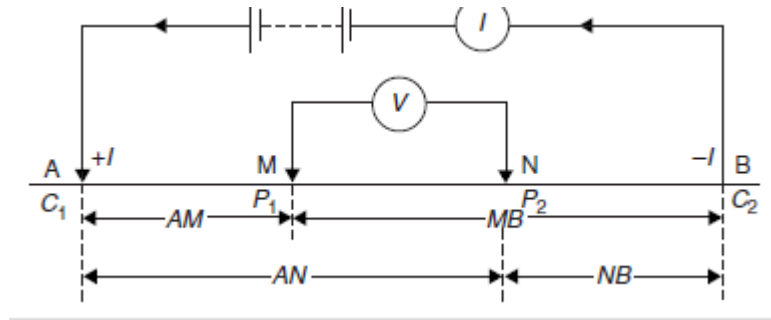
Figure 4. Two current electrodes (A, B) and two potential electrodes (M, N) in a generalized resistivity measurement schematic. Note: this figure is reused with permission from Reynolds (2011) © John Wiley & Sons Inc.

In Figure 4, the most basic electrode configuration where every electrode spacing is equal is shown, called the Wenner configuration. Apart from this one, there are hundreds of different recognized electrode arrays, most of which are rarely used. They each have their own advantages and disadvantages. Some may offer greater resolution, require more or less labor or available space, or are better at investigating horizontal or vertical structures (Reynolds, 2011). Another important aspect of electrode arrangement is depth of investigation, or the maximum depth which may be studied. As a rule of thumb, for a current-current electrode spacing of AB, the maximum depth of investigation is AB/5 (Greggio, et al., 2018). The true expression for depth of investigation is much more complex and is calculated using what's known as the Frechet derivative of the array (Loke, 2004).

A standard DCIP unit consists of a number of parts. The unit which controls outgoing current is called a transmitter. To generate current, these transmitters require an external battery. The receiver in turn handles incoming voltage measurements. Generally, these two components come integrated in a complete, single case solution, such as the Abem Terrameter LS2 (GuidelineGeo, 2023), presented in Figure 5 which is used in this study.

Figure 5. The Abem Terrameter Ls, featuring a built-in computer and graphical user interface. Here shown displaying a pseudosection. Note: This picture is reused with permission from: GuidelineGeo (2023) © Guideline Geo.

This central unit transmits current out to the electrodes via cables, which consists of a rubber casing surrounding several metal cores. Cables connect to electrodes via crocodile clips, connecting to exposed metal components along the cable, or take-outs. The distance between these components is called spacing. Cables intended for a certain type of central unit come with different spacings, but fixed amounts of metal components, creating cables of varying lengths. Cables are connected to each other using connectors. The electrodes themselves are simple metal stakes which may be pushed or hammered into the ground.

When performing a measurement, the instrument will vary which four electrodes are in use according to a predetermined schedule, depending on the array selected. For this survey, the multiple gradient method was selected, which is presented in Figure 6. This array is somewhat unique in that several potential readings are conducted in a single current injection.
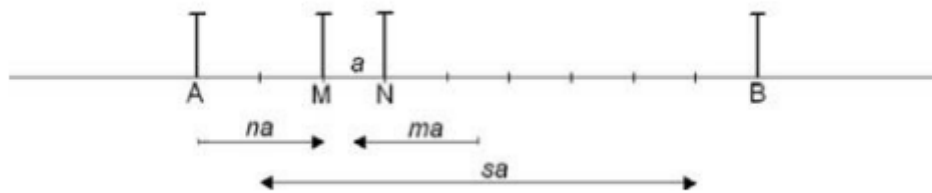

Figure 6. Sketch of multiple-gradient array electrode positions. Current electrodes AB with spacing (s+2)a and voltage electrodes with spacing a. Note: this figure reused with permission from Dahlin & Zhou (2006) © John Wiley & Sons Inc.

10

In Figure 6, s is the maximum number of potential readings for a current injection, a is the spacing in between potential electrodes, n is the relative spacing between the two potential electrodes, or the potential dipole, to the closest current electrode, whereas m is the position of the midpoint of the potential electrode dipole to the midpoint of the current electrode dipole. Measurements are done by varying both a and s, thus scanning across the whole length of the cable, creating a large number of measurement points at different depths (Dahlin & Zhou, 2006). Based on these points, the instrument creates a two-dimensional cross section image, or a pseudosection, a process which is illustrated in Figure 7. When creating the pseudosection, the instrument uses a method known as the pseudosection contouring method. Here, the vertical location of the plotting point is placed equidistant to the set of potential electrodes in use. The vertical distance is selected to be proportional to the electrode separation in some way. One common method of choosing this vertical distance is by placing the plotting point at the median depth of investigation, or pseudodepth, which depends on the electrode array in use. The result is a distorted, approximate view of the true resistivity distribution, and should therefore not be used for interpretation. What it is useful for is graphically displaying apparent resistivity values, and for finding noisy apparent resistivity measurements, which will often be very high or low compared to their surroundings (Loke, 2004). To get to the *actual* resistivity section which should be used in interpretation, this collected data needs to go through inverse modelling (Binley & Kemna, 2005).

One thing to note is that since there are fewer combinations of electrodes with large integers as a, and the depth of the point measured varies with *a*, more points are measured near the surface than deeper below, so the section will take on a vaguely truncated triangular shape.
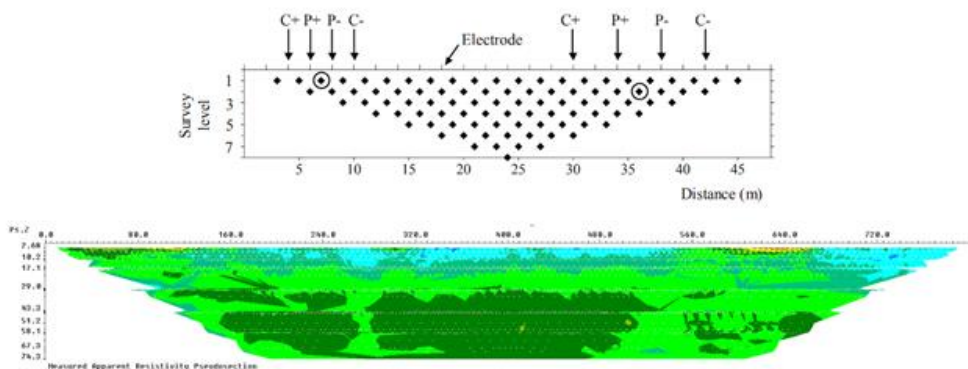

Figure 7. Current and potential electrodes at spacing a=1 and a=2 and their corresponding measurement points are shown in (a), and an example of a pseudosection is shown in (b). Note: figure (a) reused with permission from Binley & Kemna (2005) © John Wiley & Sons Inc., pseudosection (b) from own work.

Generally, during a measurement, four cables will be in use. Using the so-called roll-along method as presented in Figure 8, cross-sections longer than that of four cable lengths can be studied. In this method, after a sounding has been completed, the last cable is moved up to the front, and the instrument position is adjusted to once again be in the middle. The instrument position, or station, is then saved together with its corresponding sounding, and are then combined for modelling purposes. A sounding takes roughly fifteen minutes, in which time it may be possible to install a fifth cable ahead of time without connecting it to the others, so that when the sounding is finished only the instrument needs to be moved before another sounding can begin.
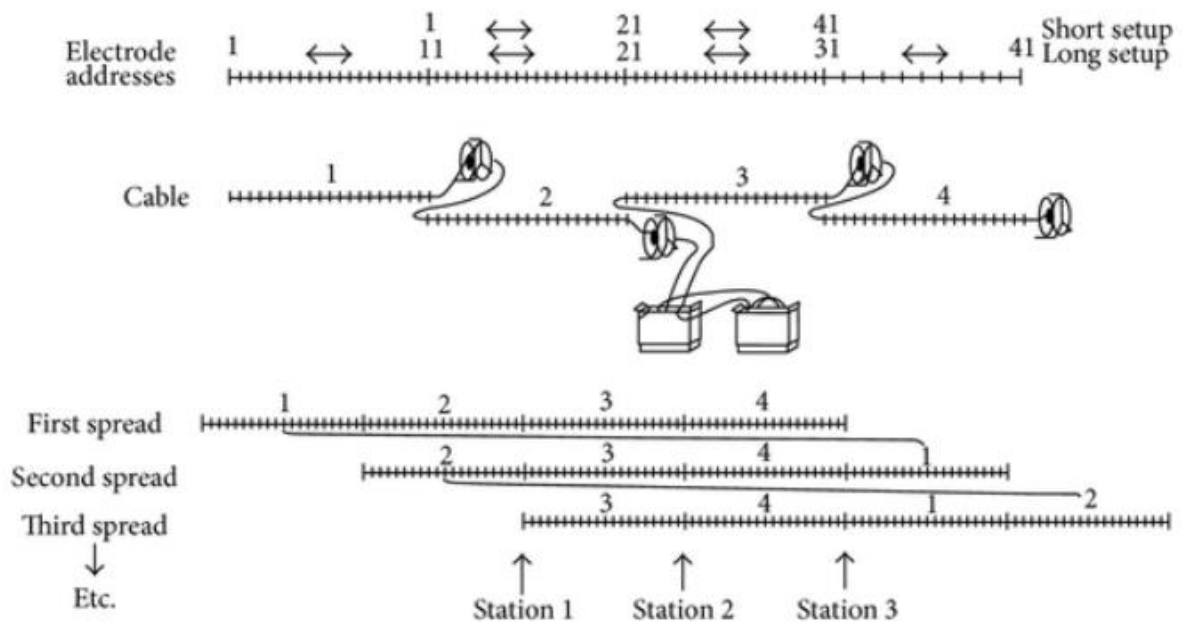

Figure 8. Presenting the roll along method. Note: this figure reused with permission from ABEM (2010) © GuidelineGeo.

2.4.3 The Induced Polarization effect

The other half of DCIP, induced polarization, is a phenomenon which creates a measurable additional voltage, called overvoltage, which decays to zero after current is turned off. While this phenomenon is not completely understood, the two main mechanisms are known to be grain polarization, also known as electrode polarization, and membrane polarization (Reynolds, 2011).

As previously mentioned, electric current in soil is usually conducted via ions. These ions travel through the various interconnected pores, fractures, and cracks in the subsurface. If such a channel is blocked by an electrically conducting grain, a charge will build up over the grain, owing to differently charged ions accumulating on opposite sides. When the applied voltage is removed, ions will diffuse and the potential difference over the grain dissipate, giving a measurable overvoltage used in chargeability calculations, a process which is illustrated in Figure 9 (Reynolds, 2011).
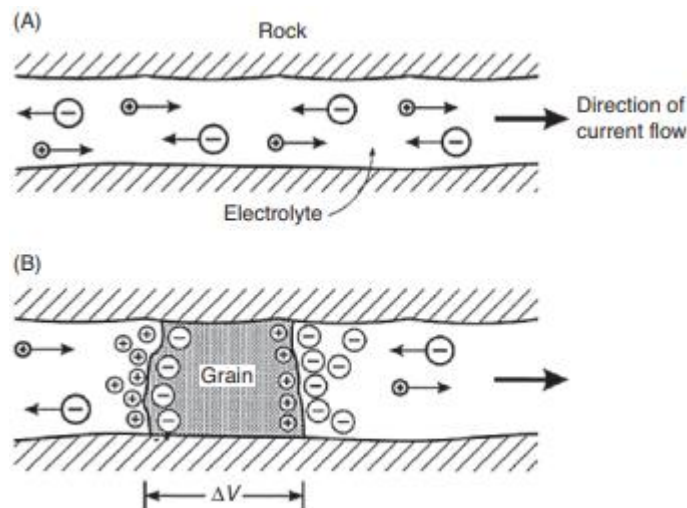
Figure 9. Uninterrupted ionic flow is shown in (a), and a situation where a grain is blocking ionic flow with a resulting potential difference is shown in (b) Note: this figure reused with permission from Reynolds (2011) © John Wiley & Sons Inc.

Membrane polarization has two causes. One is caused by constriction within a pore channel, and the other by clay being present in pore channels. For the first case, positive charges in the pore fluid attach to the negatively charged rock-pore fluid interface, whereas negatively charged ions bounce off. Should this effect be enough to clog up the channel, the flow of ions is blocked, and a charge builds up across the constriction, owing to the build-up of oppositely charged ions on both sides, as visualized in Figure 10 (a) (Reynolds, 2011) . When voltage is turned off this imbalance is normalized by diffusion. This diffusion causes the overvoltage to decay over time, giving rise to the measurable overvoltage decay, as seen in Figure 10 (a) (Reynolds, 2011).

Figure 10. The two different types of membrane polarization. Note: this figure reused with permission from Reynolds (2011). © John Wiley & Sons Inc.
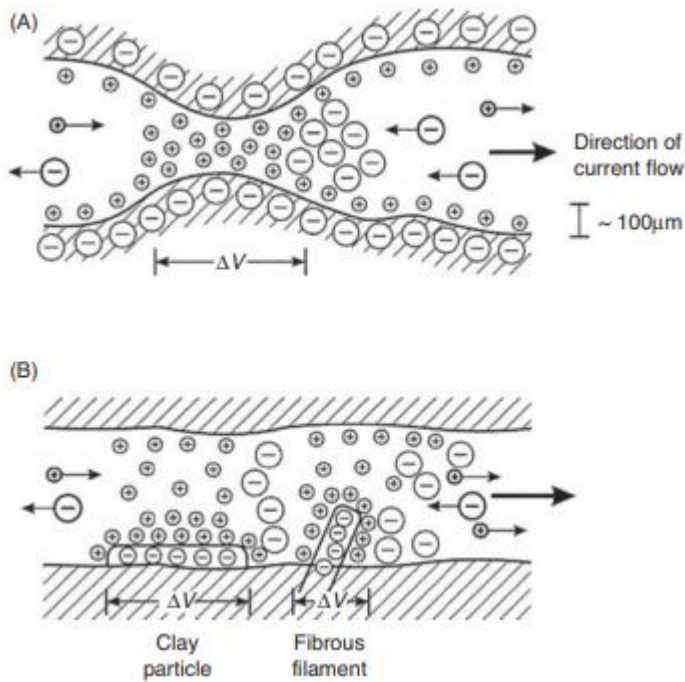
If clay particles, which usually have a net negative charge, are present in the flow network, they will attract positively charged ions in the water, creating a positively charged cloud. When a voltage is applied, the positively charged ions may move between these clouds, while the negatively charged ions are blocked, causing an imbalance in ionic concentration. As voltage stops, the situation returns to normal by diffusion, and an IP response can be measured, as visualized in Figure 10 (b) (Reynolds, 2011).

Induced polarization measurements can be done in time-domain and frequency-domain mode. In time-domain mode, a constant level of current is applied through on-off cycles. During the on-cycle, measured voltage increases to a constant level. This measured voltage (Vo) consists of two components, the voltage due to applied current (V), and the decaying overvoltage due to IP effects (Vp). The IP effect is usually quantified by the ratio Vp/Vo, or chargeability, generally expressed in the unit millivolts per volt, or alternatively in percent. It describes how well a material stores these charge differences. When current is switched off as the off cycle begins, the measured voltage immediately drops by V, as can be seen in Figure 11 (a) below that which remains is the overvoltage.

In Figure 11 (b), overvoltage is first measured at several equidistant points in time, and then integrated with respect to time to give the area beneath the overvoltage curve. (Reynolds, 2011).

When this overvoltage area is divided by the measured voltage, one receives the apparent chargeability, which is usually given in milliseconds. According to (Reynolds, 2011), *"the true chargeability is virtually impossible to measure in the field situation as each layer within the ground will have its own absolute value of chargeability and of true resistivity. What is measured is a complex function of all true resistivities and absolute chargeabilities for all the media being sampled within the range of the equipment"* Apparent chargeability can be a very useful measurement as for a certain charging time and a certain integration time, different soil types have different chargeability values (Reynolds, 2011).
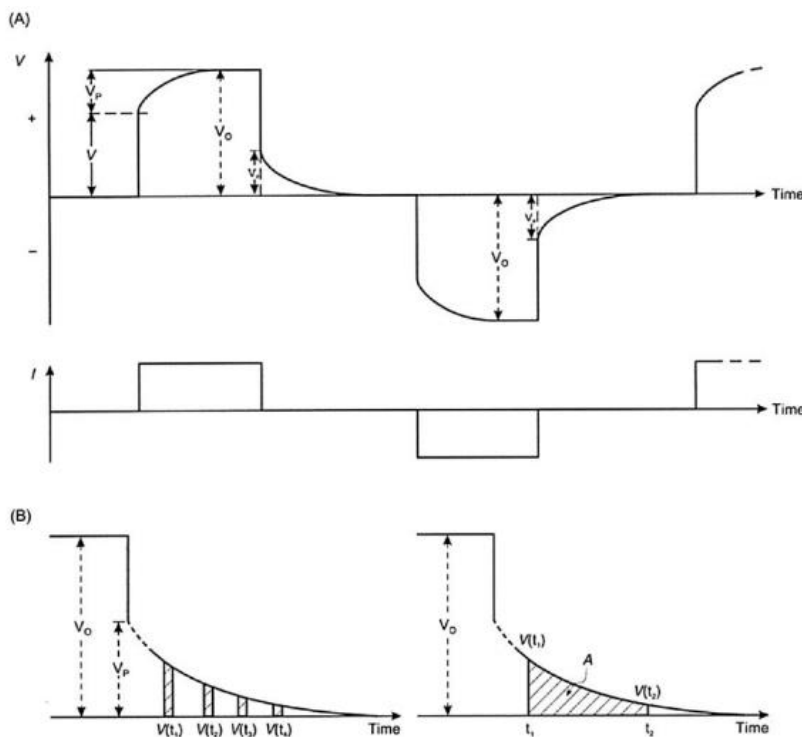
Figure 11. (a) a voltage with varying polarity V is applied. The resulting Vo and Vp are also shown. (b) Vp is measured at equally spaced points in time and integrated to form the area beneath the graph. Dividing this area with Vo produces the desired apparent chargeability. Note: this figure is modified and reused with permission from Reynolds (2011). © John Wiley & Sons Inc.

In Figure 11 above, a current with 50% operation time and 50% rest time is shown. In other words, the current is turned on only half of the time, which is the current standard for these types of measurements. Here, the overvoltage is measured during the rest time. However, a recent study by (Olsson, 2016) showed the viability of using a 100% operation type, and instead measuring overvoltage decay when polarity is reversed, with the obvious advantage of twice as quick measurements.

In frequency domain mode, the apparent resistivity is measured using alternating current at several different frequencies, usually in the range from 1 to 100Hz. The measured

resistivity will then be greater for the lower frequency. This is due to the fact that a higher charging time, i.e. lower frequency, will increase the overvoltage (Reynolds, 2011). Since this project uses time domain mode, this will not be expanded upon further.

2.4.4   Field problems

One of the greatest challenges when conducting DCIP surveys is achieving adequately low contact resistance in the electrodes. If contact resistance becomes too large, the applied current will decrease, and measurements will fail or be affected by low levels of signal to noise ratio. This is a common problem in areas where surface material contains media such as dry sand, boulders, gravel or where the topsoil is frozen (Reynolds, 2011). There are a few ways of remedying this. One approach is to apply a saline solution around the electrodes, thus increasing soil conductance. Another is to fill in holes with a clay slurry before inserting the electrode, which can be useful in coarse-grained surface material where little contact between the electrode and material can otherwise be achieved (Milsom & Eriksen, 2011). A third option is to use multiple electrodes in parallel, connected to the same take-out, acting as resistors in parallel and thus lowering the total resistance. These electrodes should be implanted at 90-degree angles to the profile to not affect the effective electrode separation (Reynolds, 2011). In some cases, it may be impossible to overcome this difficulty for one or more electrodes. Some instruments allow the user to exclude an electrode from the survey, but this should be done cautiously as the loss of a single electrode will result in a loss of many measurement points over the entire section when using the multiple gradient method (Reynolds, 2011).

Another challenge is keeping the survey line straight. If, for example, a cable is bent in such a way that one of the current electrodes is out of line with the other, the linear distance between them is decreased which will result in a lower measured potential, which unless accounted for the instrument will interpret as a lower resistivity (Reynolds, 2011). Because of this, it's important to plan out surveys ahead of time to make sure there aren't any obstacles in the path of the survey line, and generally try to keep the line as straight and as tense as possible. If greater precision is important, a GPS with all the electrode positions preloaded can be used. When planning survey, it also pays to investigate whether or not there are any pipes buried in the study area. Otherwise, if a survey line is placed in parallel with a metal pipe, current may start to pass through the pipe instead of the earth, and voltages between potential electrodes will drop as a result. This is especially true for larger electrode separations (Reynolds, 2011).

2.5 TEM

2.5.1 Basic principles

In the TEM method, a current is sent through an ungrounded transmitter loop (Tx-loop). The artificial current generates a primary magnetic field, in accordance with Ampère's law. When the current is interrupted, the magnetic field rapidly changes. In accordance to Faraday's law of induction this creates a loop of electrical current, also called an eddy current, in a nearby conductor, in this case the ground directly beneath the transmitter loop. Lenz law governs the direction of this current, such that it opposes the change of the magnetic field which generated it. The eddy current will dissipate naturally over time due to the resistance of the earth, converting into heat. This dissipation leads to a decrease in magnetic field strength deeper in the conductor, due to the secondary magnetic field generated by the eddy current weakening, which by the same principles generates further eddy currents. If the size of the conductor is much greater than that of the transmitter, the eddy currents will spread out laterally as well (Reynolds, 2011), as shown in Figure 12.
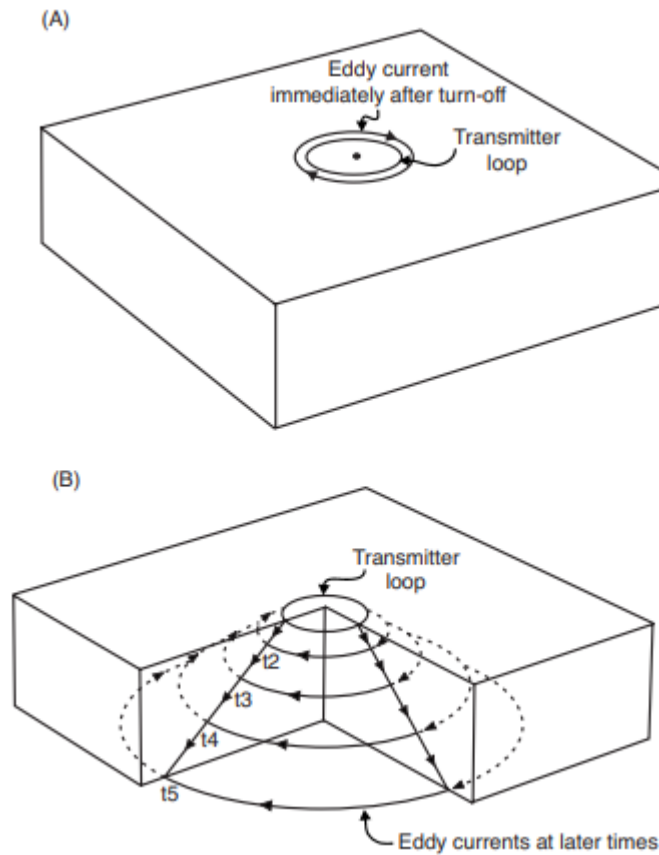

Figure 12. Immediately after the power is removed (a), eddy currents will begin to propagate downwards and outwards (b). Note: this figure is reused with permission from Reynolds (2011). © John Wiley & Sons Inc.

A receiver coil (Rx-loop) is positioned inside the Tx-loop. In theory, the secondary magnetic field is vertical in the receiver loop, thus inducing a voltage in the Rx-coil, which is measured as a function of time. During the first few moments after the primary current is shut off, the current is closer to the surface, and therefore the measured voltage reflects the resistivity of the layers closer to the surface. As time passes, the current flows deeper within the ground, and what's measured reflects deeper layers of the earth. The speed of this propagation is dependent on the resistivity of the earth. This is called a sounding (Christiansen, et al., 2009). The principle of this is shown in Figure 13. Data is measured in time-segments often called gates. These gates have a logarithmically increasing length to reduce signal-to-noise ratio, as the later signals are much weaker. The current direction alternates for each pulse. A pulse typically consists of a 50-200μs ramp up time, 1-40ms on-time, 1-30μs ramp down time, and a 1-40ms off-time for measurements (Christiansen, et al., 2009).
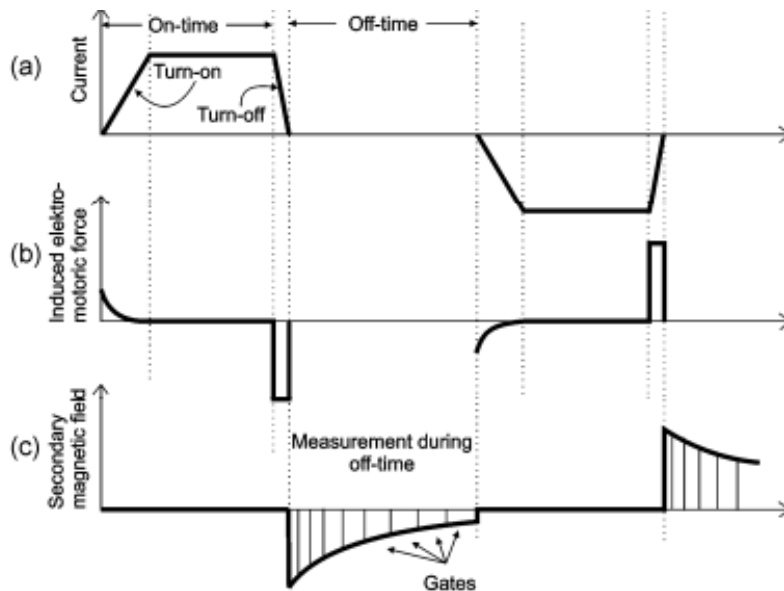

Figure 13. The current in the transmitter loop is shown in (a), with resulting electromotoric force shown in (b), and data recording with the principle of gates is illustrated in (c). Note: this figure is reused with permission from Christiansen, et al. (2009) © Springer Nature.

2.5.2 Current Diffusion

In Figure 14 (a), the current density in a homogenous halfspace with a resistivity of 30Ωm at different times is presented, with darker areas having larger current density. The densities are displayed in such a way that the maximum value at each time gives the same amplitude. In actuality, the density decreases very rapidly with time, and is larger by approximately a factor of 10^6 at 10μs compared to 1000μs. The current propagates symmetrically around the transmitter, and the maximum can be found at a 30-degree angle to the horizontal plane, creating the "smoke-ring" shape as previously seen in Figure 12(a) above. To visualize the contribution to the magnetic field at the surface of the current at each depth at various times, a sensitivity function is employed, as shown in

Figure 14(b). This is created by summarizing the current density and integrating them over thin horizontal slices. As seen, the sensitivity function is quite stable until it reaches a certain depth, from whence it rapidly declines, with later depths having exponentially lower contributions. A reasonably accurate approximation is therefore that transient measurements for a given time is an average of conductivities to this depth, and no deeper. While only strictly true for the case of a homogenous halfspace, these principles remain mostly valid for the assumed real-life case of a layered earth (Christiansen, et al., 2009).
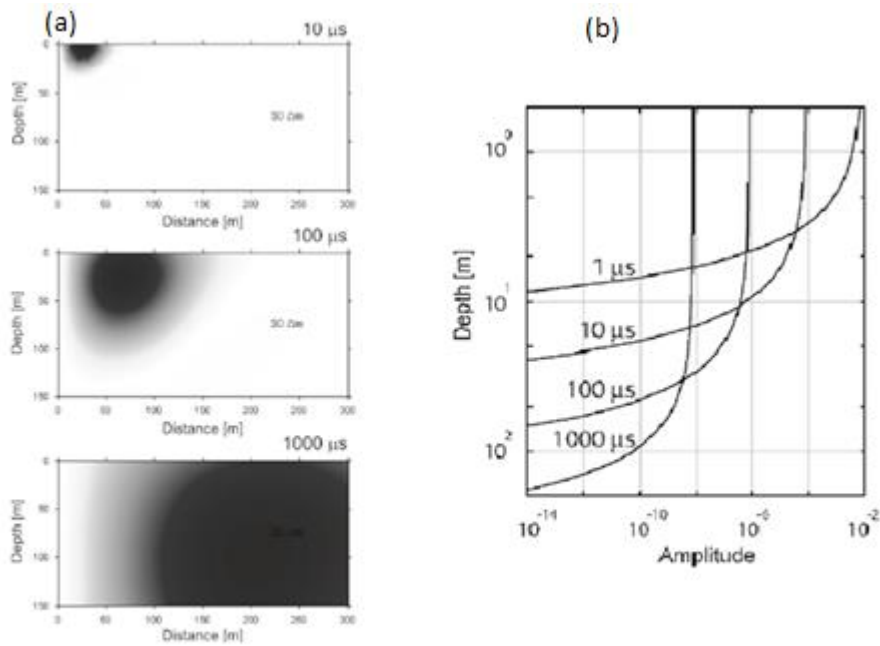
Figure 14. (a) a current travels through a homogenous halfspace, and the resulting sensitivity function in (b) shows the relationship between time, depth, and amplitude of the magnetic field at the surface. Note: this figure is reused with permission from Christiansen, et al. (2009) © Springer Nature.

In Figure 15, two more realistic cases are presented, in (a), a low resistivity layer of 30 Ωm is encapsulated in two higher resistivity layers of 100 Ωm, and in (b) the case is reversed. In (a), the current maximum lingers in the low resistivity layer at later times, shielding the high resistivity layer below, and very rapidly decays in the topmost layer due to diffusion. In (b), the current maximum almost completely skips the higher resistivity layer. Darker areas are the maximum at that point in time, as in Figure 14.

Figure 15. Two different three-layer models. In (a), the current density maximum lingers in the low-density middle layer, whereas in in (b), nearly no c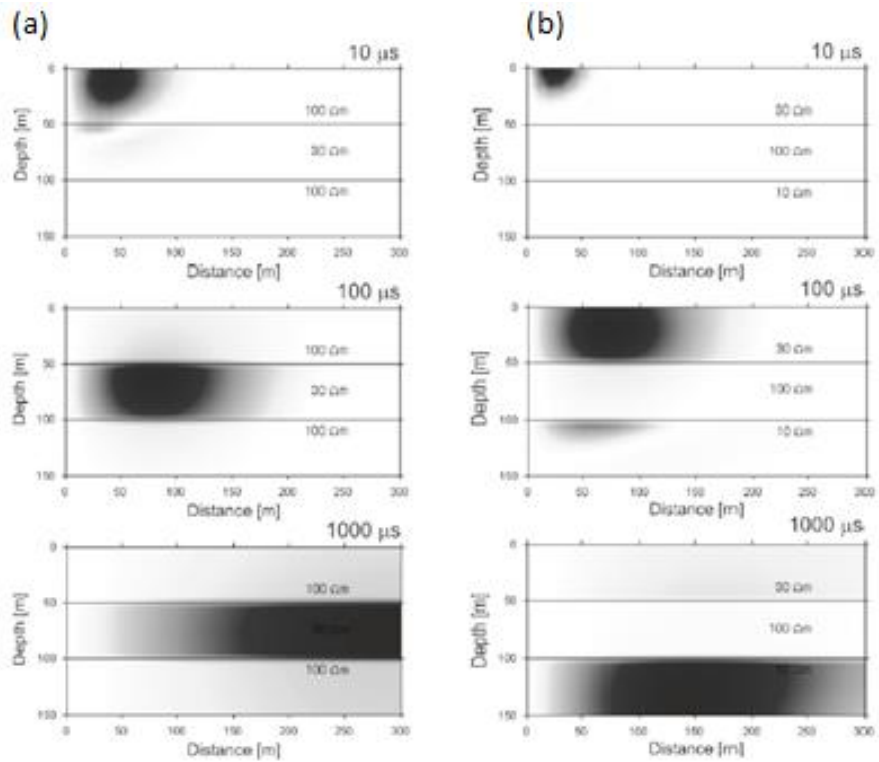urrent is induced in the higher resistivity middle layer. Note: this figure is modified and reused with permission from Christiansen, et al. (2009) © Springer Nature.

2.5.3 Data curves

The decaying secondary magnetic field, *b*, is measured as the induced voltage as a function of time, *db/dt* and graphed in data curves. This plot is quite difficult to interpret and is instead converted into apparent resistivity as a function of time, and by extension depth. In Figure 16(a), several db/dt curves are shown, as well as their corresponding apparent resistivity curves (b), for a homogenous halfspace of varying resistivity, as well as for a two-layered subsurface, where one layer with a resistivity of 100 Ωm and a depth of 40m overlaps another layer with a resistivity of 10 Ωm.. As in the DCIP method, it's important to remember that apparent resistivity is not the same as the true resistivity of the ground (Christiansen, et al., 2009).
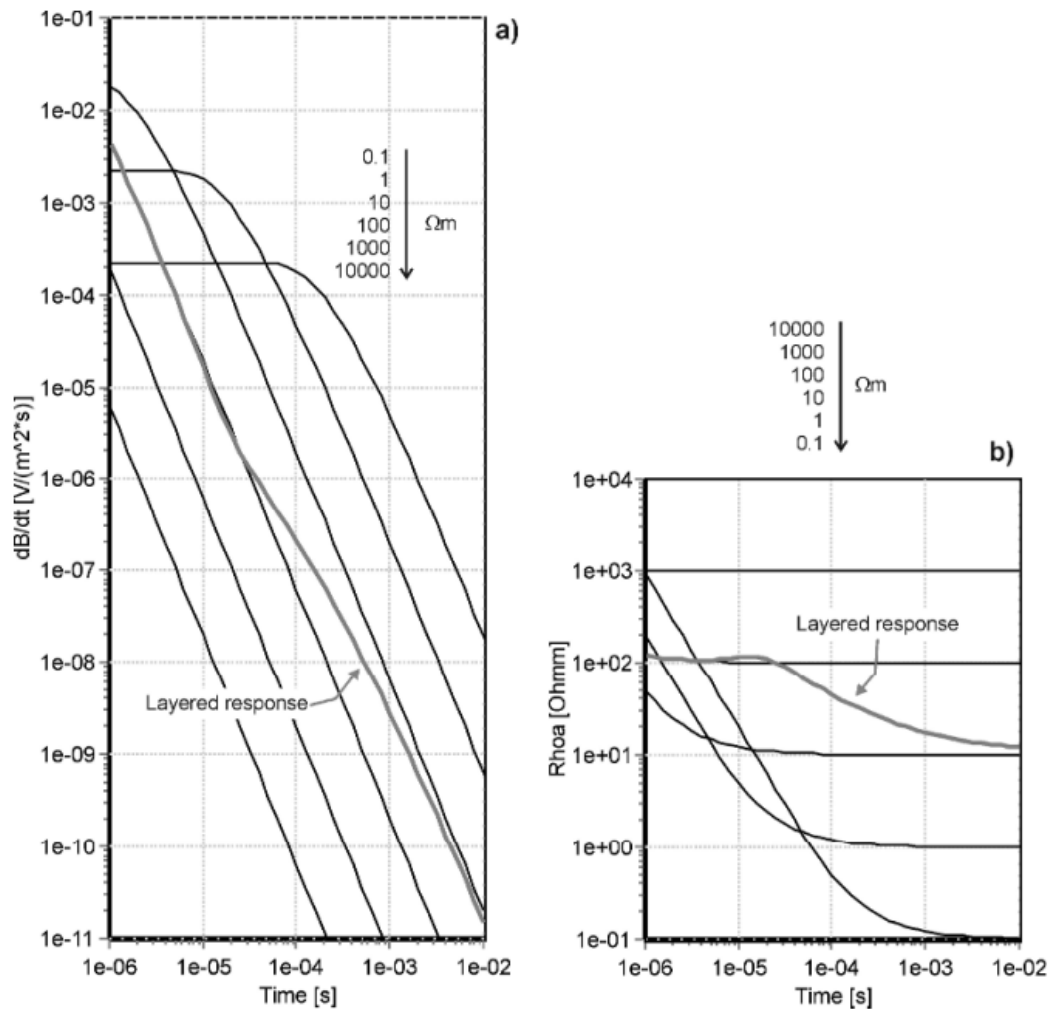

Figure 16. (a) db/dt curves for several halfspaces with different resistivities, with (b) their corresponding apparent resistivity curves. Note: this figure is reused with permission from Christiansen, et al. (2009) © Springer Nature.

21

2.5.4 Noise

Reynolds identifies three categories of error sources in TEM measurements: geometric errors in transmitter-receiver positions and topographic effects, static cultural noise, and dynamic cultural noise (Reynolds, 2011).

TEM is largely insensitive to geometric errors, except in the case of a highly conductive overburden, where the local topography can create severe errors unless certain procedures are followed (Reynolds, 2011).

Static cultural noise stems from things such as pipes, fences, or other conductive utilities present. These features give rise to coupling effects, which is when current is induced in nearby man-made conductors. Coupling is divided into two categories; galvanic coupling and capacitive coupling, based on their generalized electrical circuit diagrams, as shown in Figure 17. Galvanic coupling (a), such as in the case of a nearby power line or animal fences, is characterized by an L-R circuit (L- inductor, R – resistor). Capacitive coupling (b) is instead characterized as an R-L-C circuit (C – capacitor) and can be caused by buried cables. Their respective impact on data curves is also shown in (c) and (d), with capacitive coupling having a more obviously distinguishable effect, whereas the impact of galvanic coupling could easily be missed and interpreted as a lower resistivity layer. It's therefore important to keep a minimum safety distance of 100m to any conductors, with an increased safety distance in areas of higher soil resistivity (Christiansen, et al., 2009).
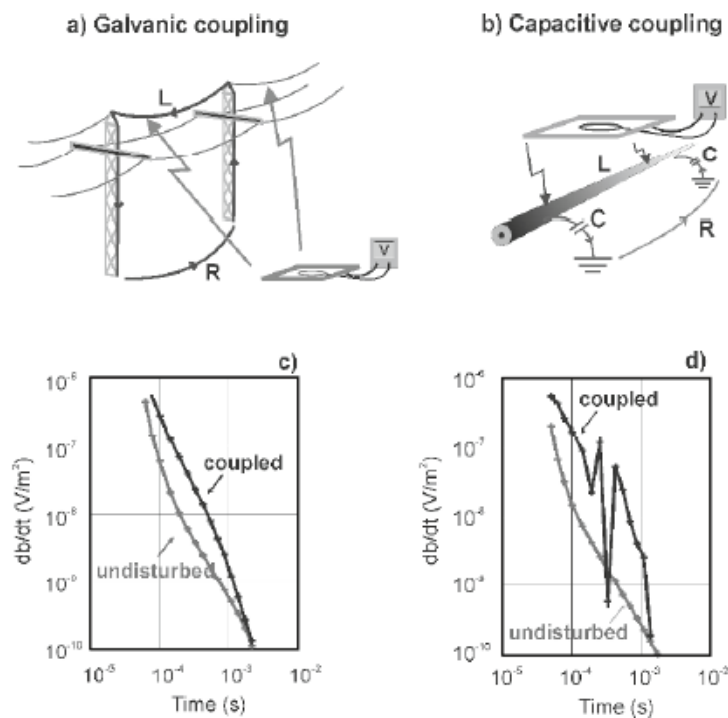

Figure 17. The two types of coupling. The effect of capacitive coupling is harder to overlook than that of galvanic. Note: this figure is reused with permission from Christiansen, et al. (2009) © Springer Nature.

Dynamic cultural noise is caused by sources such as geomagnetic signals, distant lightning discharges, or AC power lines. Power line interference can be removed by notch filtering, a process where interfering frequencies are removed, since its frequency is known (Reynolds, 2011). To reduce the impact of natural noise, TEM measurements employ stacking, or sending out multiple pulses and averaging the result for each gate. Typically, a sounding consists of 1,000-10,000 pulses, or transients. In Figure 18, two soundings of 50 and 5000 transients respectively are shown. Interpreting anything useful from the 50 stacked transients will prove difficult with how irregularly shaped the resulting graph is, but 5000 paints a much clearer picture. The natural background noise is assumed to be gaussian (normally distributed) in strength. When using the log-gating technique, the S/N ratio is proportional to $\sqrt{N}$, or to the square root of the number of signals. As such doubling the number of transients will increase the S/N by a factor of 1.41, with the obvious drawback that soundings will take more time to complete (Christiansen, et al., 2009)
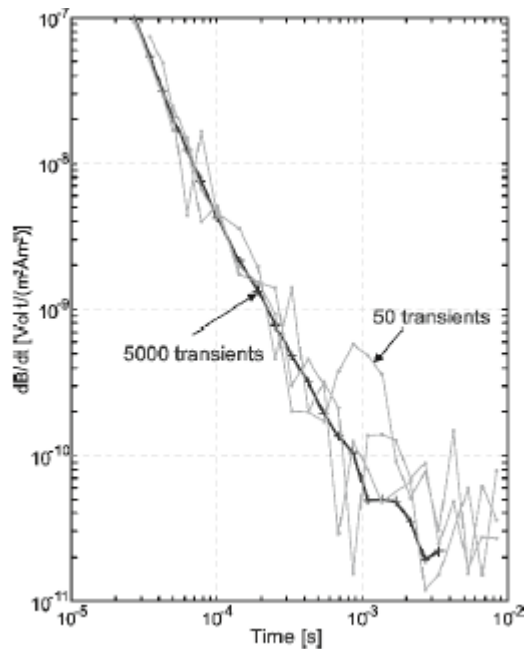
Figure 18. A sounding of 50 transients is compared to one with 5000. The impact of noise is clearly reduced. Note: this figure is reused with permission from Christiansen, et al. (2009) © Springer Nature.

In the topmost layers i.e., at earlier times, it is easy to distinguish the signal from noise, but at later times, the signal might "drown" in noise. Noise strength is expected to have a $t^{\frac{-1}{2}}$ dependency, and the grey noise measurements in Figure 19 seem to conform to this trendline. The earths response curve is expected to have a $t^{\frac{-5}{2}}$ dependency at these later times. When these trendlines get close to intersecting, the S/N ratio very rapidly switches from good to bad as the earth response becomes indistinguishable from noise, as seen in the area where the bottommost black line approaches the grey line. One way to combat this is by increasing the initial signal strength, as shown in the topmost black dotted line. Here, the signal strength was increased by a factor of 10, "lifting" it out of the noisy area (Christiansen, et al., 2009).

Figure 19. Trendlines for noise (grey) and earth response (black). Note: this figure is reused with permission from Christiansen, et al. (2009) © Springer Nature.
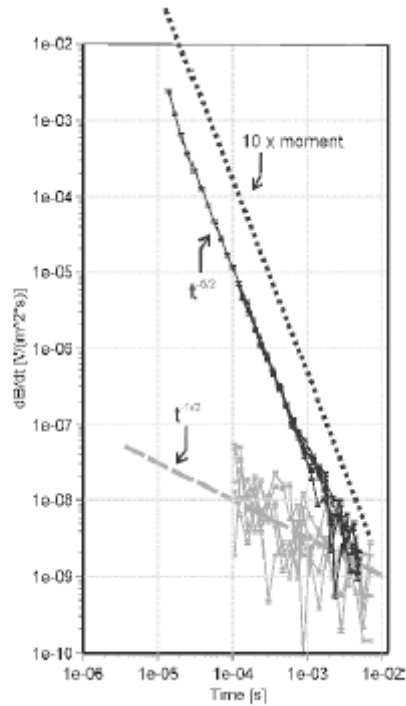
2.5.5 Depth of Investigation

As discussed above, once the signal level passes the level of the background noise, the signal becomes unusable. The mathematical description for penetration depth is presented in equation 3 and is derived from expressions of diffusion time and noise strength.

$$z_d = 0.551 \left(\frac{M}{\sigma V_{noise}} \right)^{\frac{1}{5}}$$
(Eq. 3)

In other words, the depth of penetration (Z_d)is proportional to the ratio of the transmitter strength (M) to the product of average ground conductivity (σ) and background noise level (V), to the power of 1/5. Effective noise level can as mentioned be lowered by stacking, while the conductivity (or resistivity) is dependent on the investigated site. It's interesting to note that to double the depth of investigation, a substantial increase (32 times) of transmitter strength is required (Christiansen, et al., 2009). Considering these factors, it's difficult to give a typical depth of investigation for TEM systems. The system used later in this study, the ABEM WalkTEM (GuidelineGeo), claims a depth of investigation over 800m (ABEM, 2022).

2.5.6 Airborne TEM

Airborne TEM systems exist as a faster, more cost-effective way to survey large areas, such as the helicopter based SkyTEM system used to survey the Alnarp valley by SGU. Several different designs exist, but in the case of the SkyTEM system, a helicopter carries the transmitter and receiver coil, as well as power supply and other components underneath itself on its cargo hook (Christiansen, et al., 2009). The disadvantage is a lower accuracy compared to ground-based systems (Basheer, et al., 2014).

2.6 Inversion modelling

After a measurement has been completed, the data is as mentioned received as apparent resistivity, where the subsurface is assumed to be homogenous, whereas in reality it is of course not. Thus, we are interested in what's known as true resistivity, and converting apparent to true resistivity is known as inversion or solving an inversion problem. This is done via modelling software.

In inversion, a mathematical model is created which gives a response that is near that of the actual measurements. In essence, the model has a set of *model parameters* that are adjusted until the *model response,* which is the synthetic data created in a virtual measurement conducted on the model, is close to that of the actual measured data. The model parameters in this case are the resistivity values we are searching for, and the measured data is the apparent resistivity values, or in the case of IP, the apparent IP values (Loke, 2004).

The model is based on the *finite element method*, which is commonly used for many types of engineering problems, such as modelling heat flow or various forces in structural mechanics. The finite element method is a numerical model for solving partial differential equations, which are the basis for describing many physical phenomena, and works by dividing the studied area up into a number of smaller sections, *finite elements.* Together, these finite elements are referred to as a mesh. It is then possible to assume a linear variation in the studied variable across each element, given that a small enough element size is used, even though the variation over the whole area is nonlinear. The result is then assembled into a larger solution for the whole area. This process is iterative, and the model will be continuously modified until the difference between the model response and the observed data is below a certain threshold. This optimization method is known as the least squares' method (Johansson, 2018).

2.7 Interpretation

2.7.1 Resistivity

When interpreting a resistivity distribution as representing a stratigraphy or a water occurrence, it is important to realize the multitude of possible interpretations. For any given denomination, such as sand or clay, a wide range of resistivity values is possible. In Figure 20 (Palacky, 1988), some values for resistivity for a variety of soil types and rocks are given.

IMAGE REMOVED IN ELECTRONIC VERSION DUE TO COPYRIGHT

Figure 20. Resistivity values for a selection of soil and rock types. The large intervals and overlap between different materials makes interpretation based solely on resistivity difficult. Note: this figure is taken from Palacky (1988).

The wide variety of possible resistivities for a given substance can be attributed to several factors. As discussed, the majority of electrical flow in a soil is conducted via the ionic fluids in the pore system. With this in mind, it's easy to understand that the resistivity is dependent on the porosity, ionic content in present water, and pore saturation. Conductivity will increase as ionic concentration increases, and thus produce lower resistivity. If little or no pore fluid is present current would be forced to flow through the rock itself, which is highly resistive, if not metallic. This explains why solid, unsaturated rocks are low conductive. In fact, completely dry sediments of any size are very resistive. Tortuosity, meaning how interconnected the pore system is and how complex this system is, will also play a part. With higher tortuosity the current will have to travel a longer path, resulting in higher resistance (GPG, 2021a).

Considering the wide overlap between ranges, direct current measurements cannot be used to say for certain which materials are present in the soil. It is therefore important to have some prior knowledge of the site, such as local geology, to conduct a good interpretation (Reynolds, 2011). Luckily anyone who drills a well in Sweden is bound by law to send a variety of data to SGU, including lithological logs, which is available for anyone to view (SGU, 2021).

Not much information is available specifically about the resistivity of the materials found in the Alnarp valley. The SkyTEM survey shows that resistivity varies between 1-100 Ohm/m (Erlström, 2021) in the middle and southeastern parts of the Alnarp valley for most depths. Typically, solid limestone has a quite high resistivity, as seen in Figure 20, but this may not be the case in our area. One study (Klitten & Olsen, 1995) which examined geophysical properties of the Copenhagen limestone found resistivities roughly in the 50-250 Ohm*m range, although this drilling was conducted out at sea.

Deeper in the fractured bedrock, time, pressure and higher temperatures have led to a greater ionic content of the groundwater. In areas where groundwater is heavily exploited, this deeper water can be pulled upwards (Vrba, 2002). As we know, a higher ionic content means greater conductivity. Since most of our surveys take place around Grevietäkten where groundwater is extracted, we may see quite low resistivity in the bottommost, fully saturated Alnarp sediments than in other coarse sediments that may appear closer to the surface, that may or may not be saturated with water albeit with a lower ionic content. Similarly, the weathered limestone itself may be saturated with ionic water in its cracks, providing a very easy path for electrical current to take. Saturated sediments near the surface are expected to have a lower ionic content due to being recharged by rainwater.

Generally, the resistivity of the saturated sediments that make up the Alnarp sediments are likely to be lower than that of solid bedrock, but higher than that of the clayey materials on top (Kirsch, 2006), although it may be difficult to make this distinction here.

2.7.2 Induced polarization

Induced polarization can be a great help when dealing with resistivity profiles where the suspected lithology has much overlap in resistivity. A number of factors affects chargeability. A major cause of the aforementioned grain polarization is sulfide mineralization. Thus, soils with large amounts of minerals are very chargeable. Similarly, greater quantities of clay present will lead to greater chargeability. As was the case with resistivity, greater pore-water salinity, and tortuosity lead to a larger induced polarity response (GPG, 2021b). Induced polarization values for some minerals and rocks are presented in Figure 21.
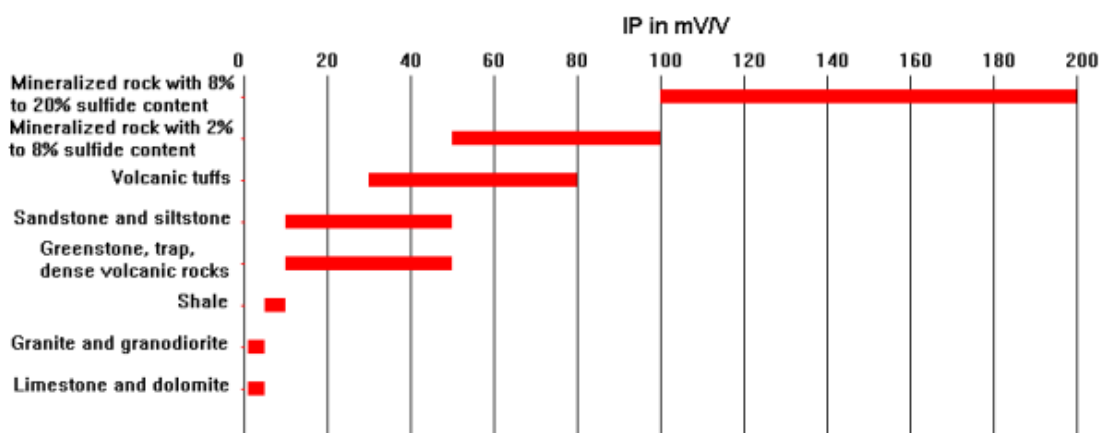

Figure 21. Induced polarization values in mV/V for some rocks and minerals. Note: this figure is reused with permission from Loke (2004) © Dr M.H.Loke.

3 Methodology

3.1 Pre-study

The pre-study phase consisted of investigating various potential measuring sites. The reasons for selecting the various sites are presented together with an overview of the site in Chapter 4. Early on it was decided to focus the study around the Grevietäkten area, where groundwater is extracted for the city of Malmö. It was also decided to examine at least one area far outside this area, to identify any differences. Some areas were selected in order to "fill in the gaps" in the existing SkyTEM survey using DCIP, others were chosen in order to have all three survey methods (SkyTEM, DCIP, TEM) available in the same area, to integrate information and study any differences. The distance to nearby boreholes for helping the interpretation was also considered.

First, the result of the SkyTEM survey was studied using the 3D visualization software Geoscene3D to see if any interesting survey areas could be found. These areas were examined further in softwares such as Google maps, to try and determine if there were any local features that would prevent us from carrying out our investigation. Once an area was deemed suitable, the local landowners were contacted via phone to get permission. To do this, the identity of the landowners was learned by using Lantmäteriets webpage *Vem äger Fastigheten* (Lantmäteriet, 2022). Then, contact information was acquired using websites such as *mrkoll.se* (Mrkoll, 2022) or *hitta.se* (Hitta, 2022).

3.2 Fieldwork procedure - DCIP

DCIP measurements were carried out during a two-week period starting the 19th of April 2021 and concluding the 30th of April. The instrument used was the ABEM Terrameter LS2 (GuidelineGeo). Multi-core cables with a length of 100 meters and a spacing of 5 meters were utilized, along with stainless steel electrodes, crocodile clips, connectors, and other miscellaneous equipment such as rubber hammers for driving electrodes into the earth. The system also requires an external power source in the form of a battery. In order to collect topography data, a Topcon RTK-GNSS system was used, consisting of a receiver antenna connected wirelessly to a tablet for operating and data storage. The topographic data process collection essentially consisted of walking along the survey line, stopping at each electrode and logging its location with the GNSS.

3.3 Data processing and inversion - DCIP

Via the software *Terrameter Ls Toolbox,* data from the instrument was transferred from the instrument and combined with topographical data recorded by the Topcon GNSS in a .dat text file format, in a fashion that the modelling software could read. This procedure simply consisted of creating data columns pairing the topographical values with the x-distance of the measurement line with the 5 m spacing between data points. In some cases, the topographical data was altered slightly after visual inspection by removing redundant GPS loggings of a single electrode, or in a few cases interpolating missing data.

Before inversion may begin, data processing is often necessary to remove bad data points (Reynolds, 2011). Bad data points are categorized into two types, systematic noise, and random noise. Systematic noise stems from issues such as poor ground contact including dirty electrodes, or forgetting to attach an electrode entirely, attaching the cable backwards and other such manual errors. As mentioned, these bad points are often easy to spot on pseudosections. Random noise arises from wider phenomena which will affect all points, such as telluric currents (Loke, 2004). It may also be necessary to convert output data from the instrument to a format which modelling software can read, and to add topography data if they were recorded separately, as in our case.

The inversion software used in this project, RES2DINV comes with a feature to help remove bad data points. This is done by first running an inversion, and then switching to the 'RMS error statistics option', where data points are displayed in bar charts, where points with high root mean square errors are easily singled out. This error is a measure of the percentage difference between the logarithms of the measured apparent resistivity values, and the ones calculated during the inversion process. The user can adjust the maximum allowed error, and points with greater error than acceptable can be removed (Loke, 2004).

RES2DINV is designed to be as automatic as possible, to allow the intended users to use the program without much knowledge about geophysical inversion theory. Therefore, it comes with a set of default parameters which will usually provide adequate results. These parameters can be changed for greater accuracy if the user so decides. For example, if the subsurface is suspected to be 'blocky' with sharp resistivity boundaries, the user can choose to depart from the conventional least squares method, and instead use the blocky inversion method, which may provide better results in this scenario. The user can also decide on which method to use when including the impact of the section topography on the finite element mesh (Loke, 2004).

The parameter settings used within RES2DINV is listed in the appendix.

3.4 Fieldwork procedure - TEM

TEM measurements were heavily delayed for multiple reasons, and ended up being carried out starting the 15th of November, and concluding on the 19th of November. The instrument used was the ABEM WalkTEM. This system comes with two receiving antennas, to be used simultaneously for a better vertical resistivity reading. The RC-5 receiver is a piece of rigid plastic measuring 0.59x0.59m, while the RC-200 receiver measures is a wire loop, measuring 10x10m when deployed. The transmitter is also a wire loop, measuring 40x40m. Other equipment includes the power source, a dampening resistor for the transmitter, along with various connecting cables (GuidelineGeo, 2023).

The dual antenna system is designed to get good results both at shallow and at large depths. The small RC-5 antenna reads the early and shallow data while the RC-200 reads the late and deeper data. There is also some overlap in data between the two.

One site was examined per day, and on every site between 4-8 measurements were carried out, depending on the local conditions. At some sites, where the ground was difficult to walk or where tall crops prevented us from seeing our equipment in the distance, the work progressed quite slowly. In other locations, conditions were much more optimal and allowed for quicker work and thus more data collected.

A typical day included finding measurement points via GNSS, marking them via wooden poles, and then setting up the equipment at each point. Figure 22 shows a schematic of the system setup, with the two receiving antennas encapsulated by the transmitting loop, and the instrument placed outside. A measuring tape and plastic stakes were used to mark the four corners of the outer receiver and the transmitter. Something not depicted here is that the cables connecting the antennas to the instrument should always intersect the outmost antenna and transmitting loop at a right angle, and no loops in the antennas should be left, all to minimize interference by their resulting electromagnetic fields.
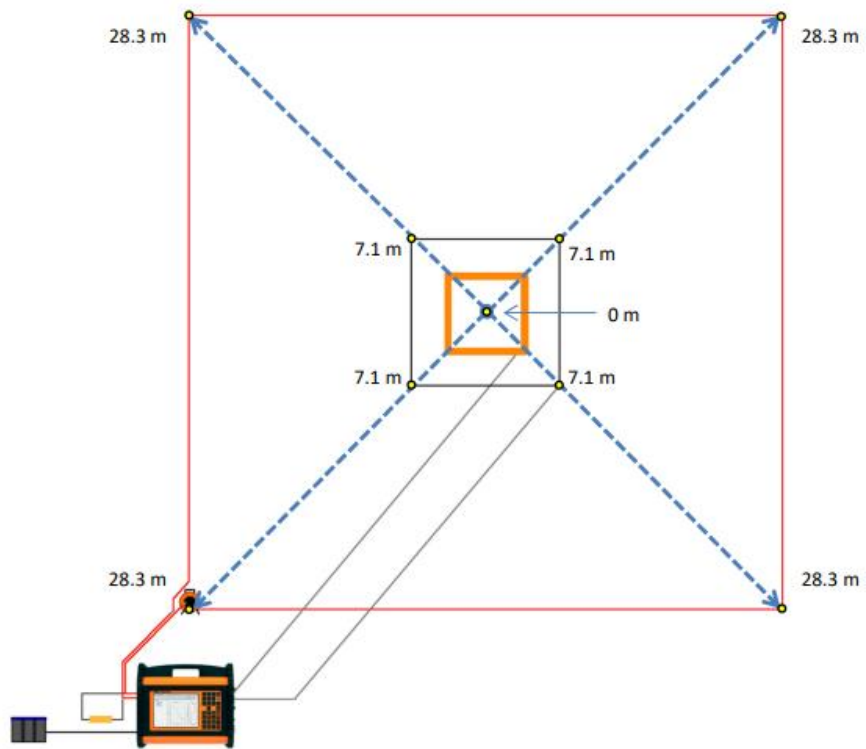
Figure 22. Abem TEM field setup schematic. Note: this figure is reused with permission from ABEM (u.d.) © GuidelineGeo.

3.5 Data processing and inversion - TEM

The inversion of TEM data was carried out in SPIA. Four data input channels are used in total, the low moment together with the high moment of the small and the large receivers, respectively. The measured stacked apparent resitivities (Ohm*m) is graphed and can be used to inspect the input data of the four channels visually.

There are a few visuals that can be used to assess the data quality directly, as stated within the SPIA manual. If a gate substantially differs in value to the previous and next gates, this might consist of noisy data, and the data of a single channel must follow a "swift curve". The two channels corresponding to the low and high moment should show segments of continuous and overlapping data. The low and the high moment channels should also overlap between the small and large receivers (AGS, 2022).

A default standard deviation value of the stacked data was set to 5%. The uncertainty of individual data points can also be changed, for example those corresponding to great depths, as the influence of noise is assumed to increase.

Data points, each showing a gate, can be inspected and removed which was the case for most of the stations. Due to the overlap of data, this could be done without loss of gates for the inversion. Instead, gates were prioritized based on its origin. Early gates of a low moment (LW) channel represent data of better quality than that of high moments (HM). Late gates of the low moment channels are however less trustworthy and here the early gates of the high moment channels were prioritized. Often, the segment of the late gates of a low moment channel deviated from the segment of high moment data, thus this segment of gates was removed. Additionally, very late HM data points if sign of large misfit, could be removed to improve the final data residual but with the cost of a lower depth of investigation (DOI). The DOI however was in most cases sufficiently high at each site, to reach the expected bedrock level and beyond, thus no valuable data was lost through this action.

The inversion can vary its smoothness, i.e., the factor that the resistivity of two adjacent layers can vary. A normal smoothness of 2 was used, meaning that each next layer cannot vary more than a factor 2 (AGS, 2022).

Two different inversions are produced, a smooth and a layered. The difference is graphical, and for the smooth inversion there are 20 created layers with a fixed thickness that are automatically log-scaled between the boundaries so that the real thickness increases with depth. This procedure thus models shallow layers more detailed than deep. The layered inversion has no constrictions on the layer thicknesses. The resulting resistivity approximation show large variations between the smooth and layered models (AGS, 2022).

Residuals are given in the output, with a value below 1 of the root mean square error (RMSE), corresponding with a fit of the inversion model to the input data within the standard deviation (AGS, 2022).

At measurement stations where the data of the low and high moment showed a constant offset in apparent resistivities (Ohm*m), a residual below 1 could not be achieved.

4 Results and interpretation

When the results were examined, a trend was noted regarding the IP distributions, namely that every profile had very low and uniform chargeability values, varying roughly between 1-10 mV/v. These low values show that the geological materials are generally non-polarizable in the investigated areas, which made interpreting the results very difficult. It was therefore decided not to bring them into consideration when performing our interpretations. As a result, only ERT (DC) will be presented, as well as our TEM measurements and SkyTEM where applicable. Resistivity profiles were generated by importing all available data into the software GeoScene3D, applying a uniform color scale. Where ERT was used, a higher resolution profile with its own color scale is also included, which comes directly from Res2DINV.

The bedrock boundaries that are marked in our resulting profiles are based on SGU's soil depth map (SGU, 2023a). For each profile, a soil map showing the lithology of the topsoil that our profiles run over is also presented. These are based on SGU's topsoil map (SGU, 2023b), and a legend to complement them is present below in Table 1.

Table 1. Legend of the topsoils presented in soil maps in each profile. The soil types are translated from Swedish, and the original wording in Swedish is also included. The table is sorted based on geological age.

Symbol	Soil type
	Peat (torv)
	Peat (torv)
	Postglacial sand (postglacial sand)
	Fine glacial clay (glacialfinlera)
	Glacial coarse silt-fine sand (Glacial grovsilt-finsand)
	Glacial sediment, sand (isälvssediment, sand)
	Glacial sediments (isälvssediment)
	Fine clay till (moränfinlera)
	Clayey tilll (Lerig morän)
	Rough clay till (morängrovlera)

Where available, nearby boreholes are also shown together in the profiles. The approximate orthogonal distance to the profile in meters is shown underneath. In Table 2, a legend for reading these boreholes is presented. Additionally, a table is also available for each profile presenting their lithology.

Table 2. Legend for reading the boreholes that appear in most profiles.

■	Peat
■	Clayey moraine
■	Moraine
■	Clay with sand
■	Clay with silt
■	Clay
■	Fine sand, silt with clay
■	Silt
■	Fine sand, silt
■	Sand with clay
■	Sand
■	Sand, gravel
■	Sand to block
■	Gravel with clay
■	Gravel
■	Stone, block
■	Sandstone, carbonate rich
■	Limestone, quartz rich
■	Limestone, unspecified
■	Bedrock, unspecified

The profile locations are presented in Figure 23. The approximate extent of the Alnarp valley is shown in purple. For orientations sake, the two metropolitan areas in the northwest of the profile are Malmö and Lund. The profiles have been given names based on a nearby settlement. After each profile's name in the headlines below, the start and end direction in which the profiles were measured is indicated, so SW-NE means the profile begins in the southwest and ends in the northeast. In an image such as Figure 27, the start is always at the zero-meter mark, in the left of the picture.
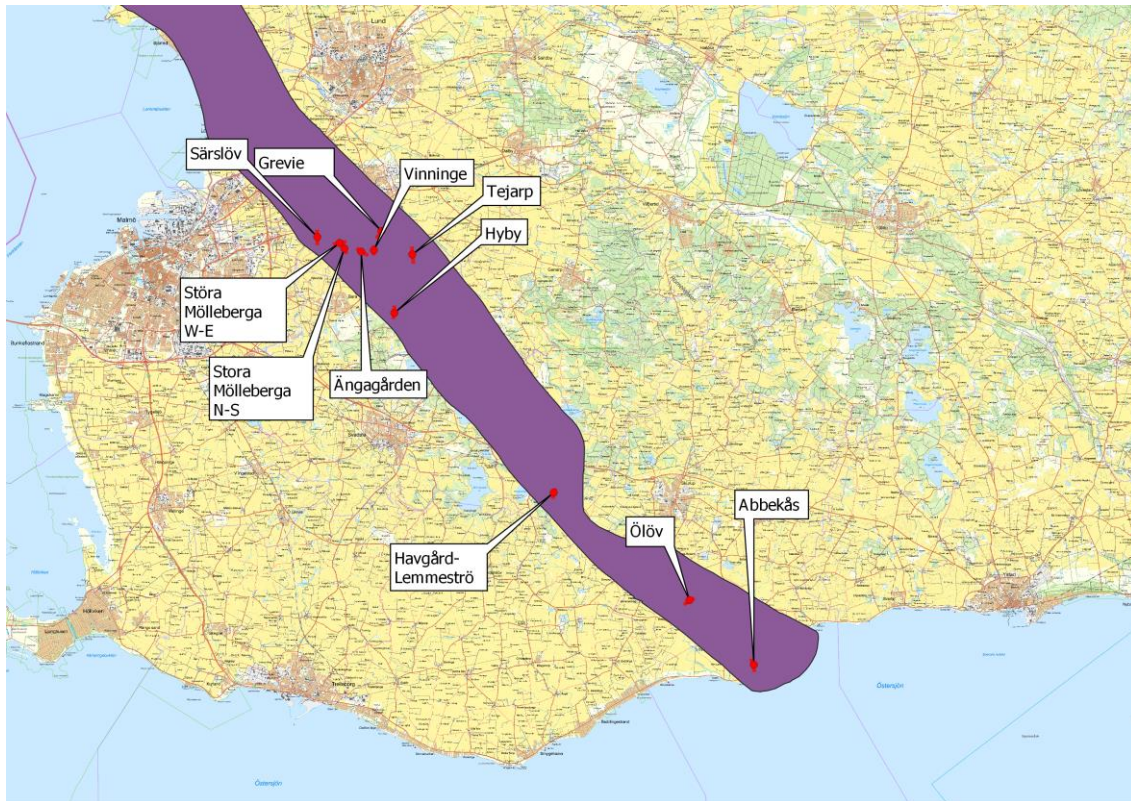

Figure 23. Each profile's geographical location. The purple indicates the approximate location and extent of the Alnarp valley.

4.1 Profile 1: Grevie (SW-NE)

Description

Close to this profile, there are several borehole logs available that show the predominant stratigraphy presented in Table 3. The upper layers are dominated by sand deposits across the first (southern) half of the profile, and to the north the surface materials are instead clayey till. Vertically it then changes to a clayey till, and sometimes very thin layers of clay. What is classified as clay dominates in the bore-holes closest to the southmost part of the profiles. The boreholes closest to the south also show a 12 m thick gravel layer. The groundwater level was found 8m below the ground in 1966 (SGU, 2023c).

The profile was chosen as a complementary measurement of 5 m electrode spacing ERT to measurements previously done by VA SYD and following the same approximate line.

As seen in Figure 24, the ERT line follows the SkyTEM profile with a slight offset. TEM soundings were carried out starting from the southern end. During the field day, four soundings were performed, localized to the middle of the ERT profile.
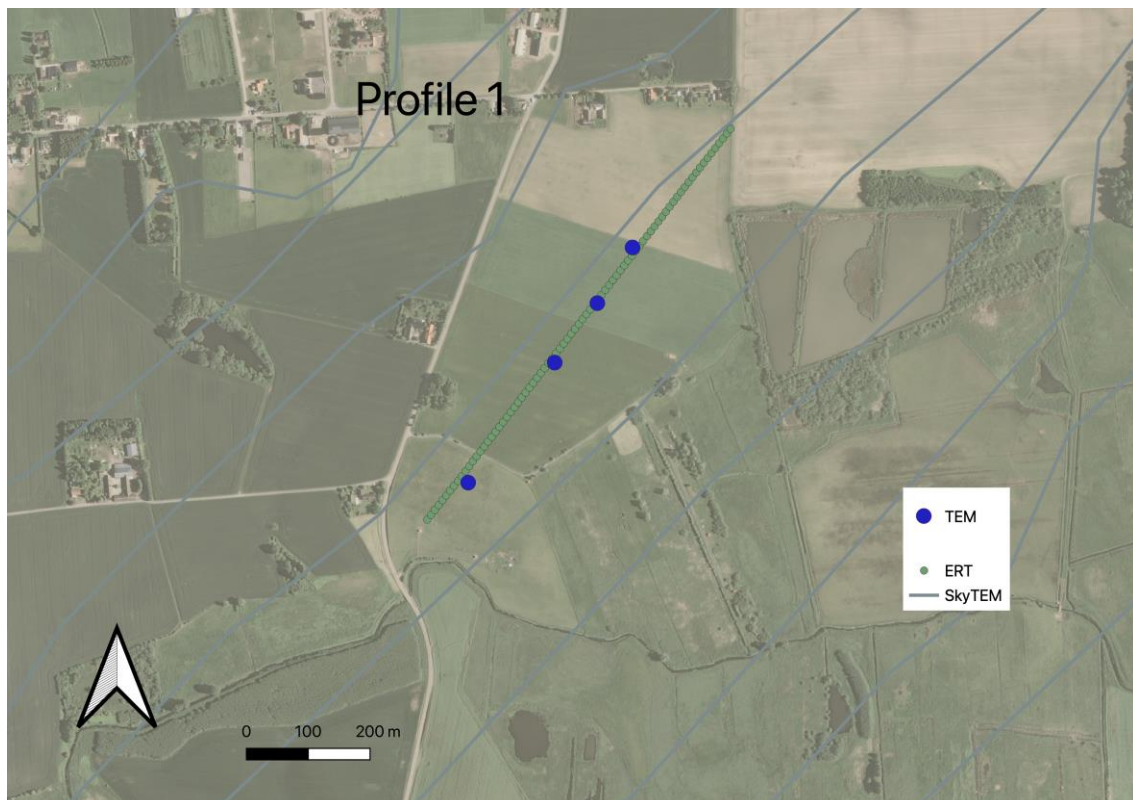
Figure 24. Map of survey location 1 including TEM points in blue, SkyTEM lines in grey, and the 5m spacing of the ERT represented by green dots. In this case, borehole locations are not presented due to security reasons.

Figure 25. Soil map of the area near profile 1 with approximate ERT profile location in red. For more information, refer to Table 1.

Table 3. The lithology of the two closest boreholes. In this case, we were not able to show the borehole locations on the map due to security reasons.

Level	0-16.5 m	16.5-36 m	36 – 42.2	42.2 – 71.1
Lithology (200m from 300 m mark)	Sand and clay	Till with thin coarse silt layer	Silt to thin clay	Coarse silts to sand
Level	0-5	5 – (30 to 40)	40 to bedrock at 75 to 80 m	At 45 m depth at central profile
Lithology (south)	sand	Till or clayey till and thin clay	Sand and gravel	Clay (1m thickness)

Results profile 1: Grevie

Field description

Contact resistances were generally good on this survey, except for one electrode that crossed a small gravel road.

Resulting profiles

Figure 26. Higher resolution ERT Profile, including mean residual error percentage.

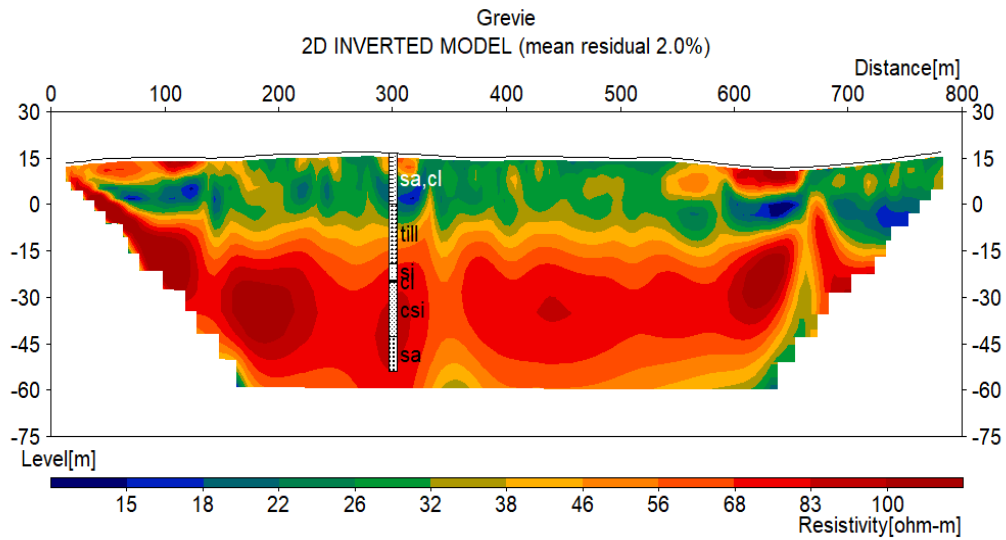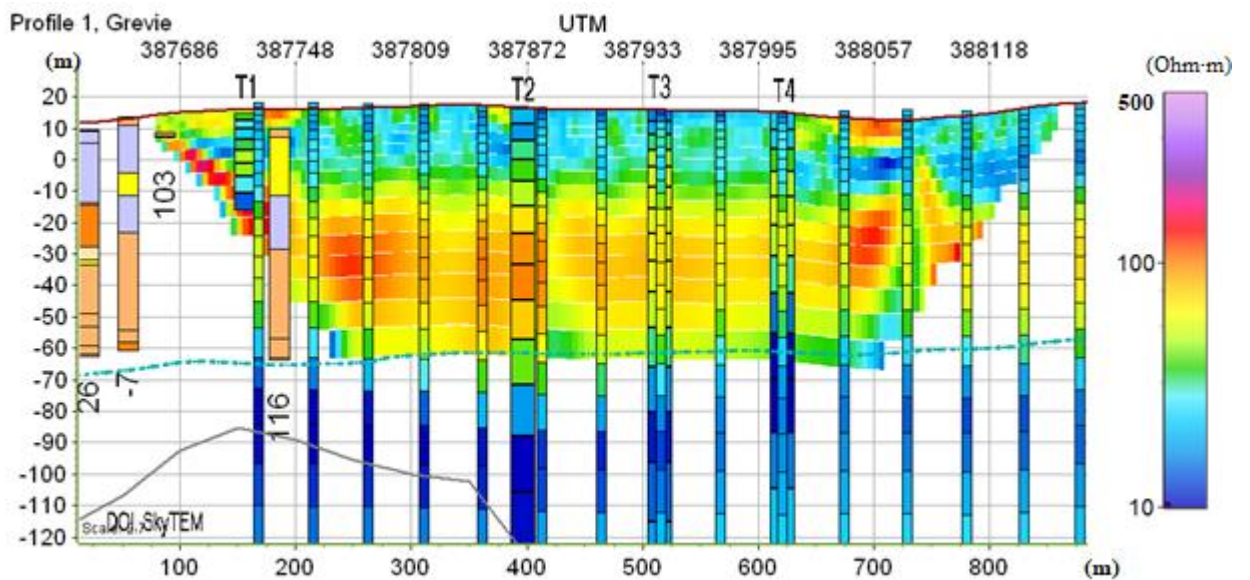Figure 27. The ERT, TEM and available SKYTEM soundings are presented. SKYTEM soundings are offset by up to 70 meters. Also shown are local boreholes together with their distance to the ERT profile. Colour scale shows resistivity values between 10 and 500 Ohm·m.

Interpretation

The three geophysical methods agree on the general vertical distribution of resistivities. Comparing with the boreholes shown in Table 3, the two main lithological units are a clay or clayey till that overlies units of mainly sand, with appearance of fine sand as well as gravel. This agrees well with the expected general lithology of the area, as presented previously in chapter 2.

Looking at the near surface, soil resistivities vary roughly between 20 and 40 Ohm·m, coinciding well with boundaries of the sand and clay layers, followed by clayey till that appears in boreholes. Shallow areas (5-10m depth) of higher resistivities appear around the 200 and 700 m marks along the ERT profile. These deposits are interpreted as sand agreeing with the presence of thin sand layers in the boreholes. SkyTEM data around those locations appear to miss these small variations in resistivity due to lower resolution, and likely due to the laterally constrained inversion that tends to smooth lateral variations. Ground TEM measurement T1 shows reliable results only in the first 25 meters from the surface. At the upmost layer of T1 a small increase in resistivity is observed reflecting the interpreted sand deposit. The same correlation is however not observed between the upmost layer of T2 and the ERT. v

T2 around 50 m depth show the highest resistivities that is also captured by the SkyTEM data between the 300 and 450 m marks. This is interpreted as the existence of higher resistive lithology covering a larger area also orthogonal to the ERT profile. The highest resistivities observed in the ERT profile at the first 300 m as well as around 700- to 800 m is not captured by the SkyTEM. An interpretation can be that lithology of higher resistivities vary more locally hence captured by the ERT but not SkyTEM. It should also be noted that there is a higher horizontal distance between the ERT and SkyTEM lines southward. As for the quick change between higher and lower resistivities seen in the ERT at around 730 m in the sand layer, it is likely the SkyTEM shows more of an average value within these changes. Similarly, the slightly lower resistivity seen in the ERT around 400 m in the sand layer could indicate a relatively local change laterally, as it is not observed in the TEM. Near the bedrock a layer of around 20 Ohm·me appears again in all methods. It is possible that this is a layer of clayey till from previous ice ages, as discussed in chapter 2.1. It could also simply be a smoothing effect of the inversion at this low-resolution depth.

As for the very low resistivity shown within the bedrock, this survey is very close to Grevietäkten, where groundwater is extracted. This can lead to intrusion of water with high ionic content, as discussed in chapter 2.7.1. If the local bedrock is quite fractured, it could explain these results.

To summarize, the clayey till has resistivities in the range between 20 and 40 Ohm·m while the sandy sediments generally reach up to 100 Ohm·m. Locally the ERT however shows values higher than 100 Ohm·m and since gravel is present in a close borehole to the southwest this may reflect variations to coarser grains.

More detailed results would have been achieved, if time would have allowed for a ground TEM measurement made closer to the 750 m trying to capture the rapid change in resistivity observed in the ERT.

4.2 Profile 2: Vinninge (S-N)

Description

The profile is located just south of profile 1. Apart from a thick unit of coarse sediments, a possible clay layer was observed as a low resistive layer in the SkyTEM data. Limited to the south and disappearing to the north of the profile. This layer could limit the total thickness of coarse sediments at depths below the Dalby till in the first 40 m.

A borehole present at 450 m south of the profile is described in Table 4. Further comparison can be done using the boreholes close to profile 1.The groundwater level at this well was found 19 m below the ground in 1972 (SGU, 2023c). Local topsoil consists of clayey till, sand, and fine clay (Figure 29).
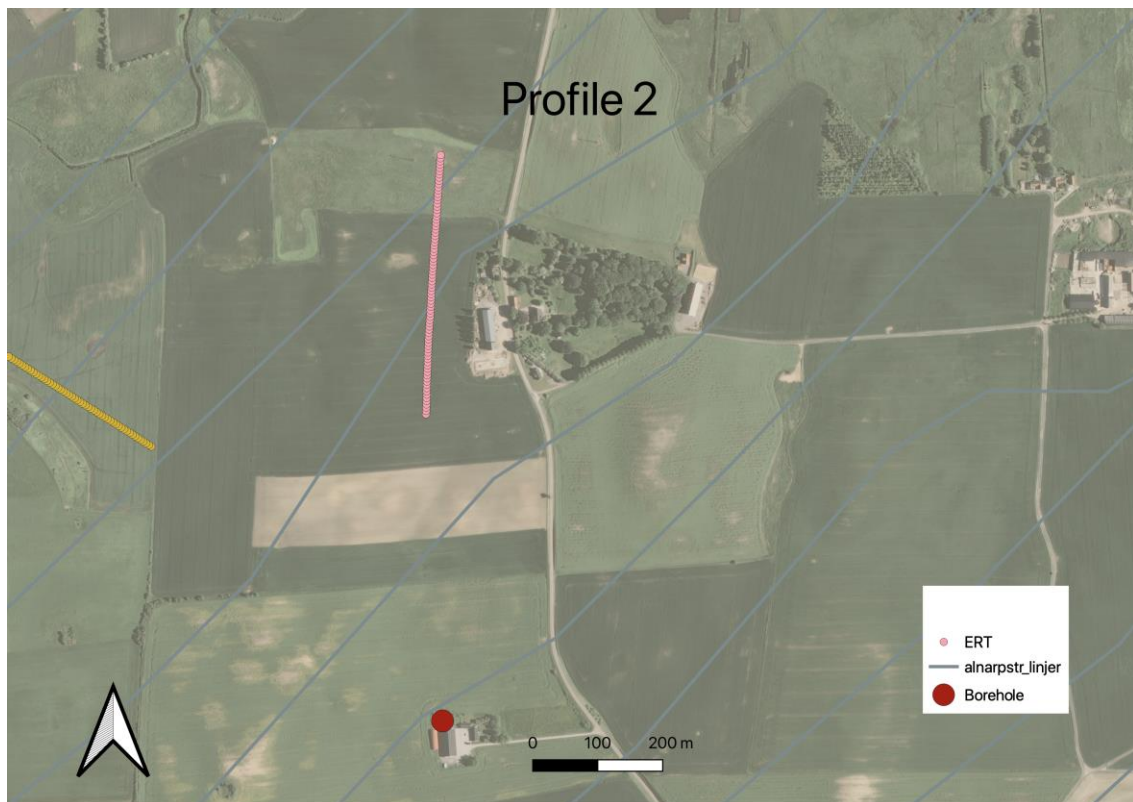
Figure 28. Map of survey location 2, including ERT profile in pink, nearby borehole(s) and SkyTEM.
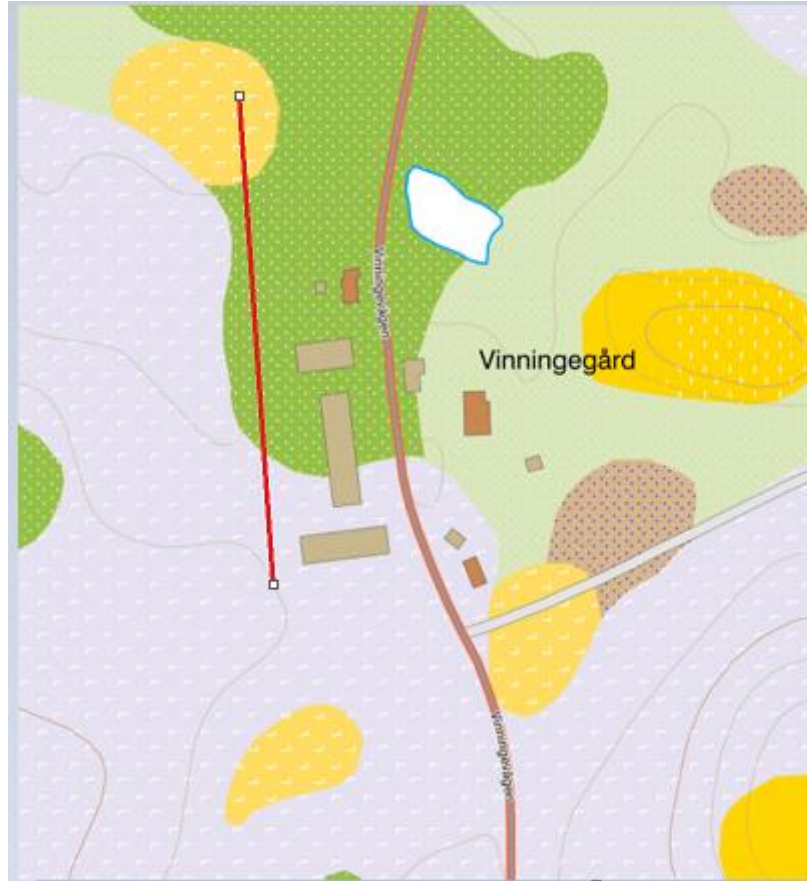
Figure 29. Soil map with approximate survey location in red. For more information, refer to Table 1.

Table 4. The lithology of the closest borehole, approximately 450m south of the starting point of the ERT profile.

Level	0-11 m	11 – 18 m	18 – 38 m	38 – 45 m	45 – 47 m	47 – 90 m	90 -
Lithology	Till clay	Clay	Till clay	Sand	Till clay	Sand and silt	Limestone

Results profile 2: Vinninge

Field description

This profile is located just south of profile 1. Contact resistance was generally good.

Resulting profiles
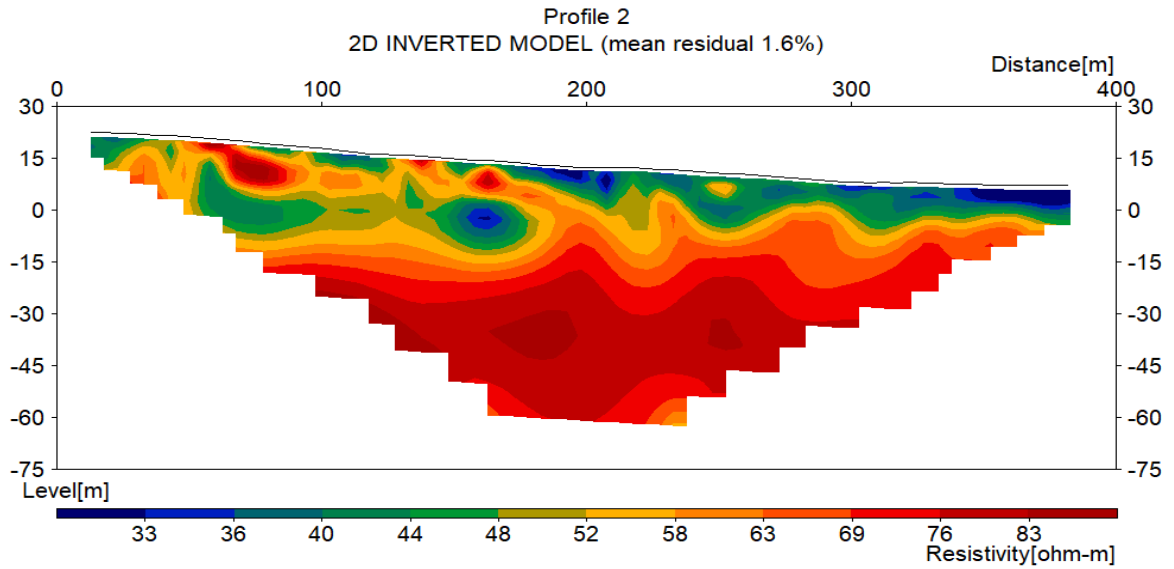
Figure 30. Higher resolution ERT Profile, including mean residual error percentage.
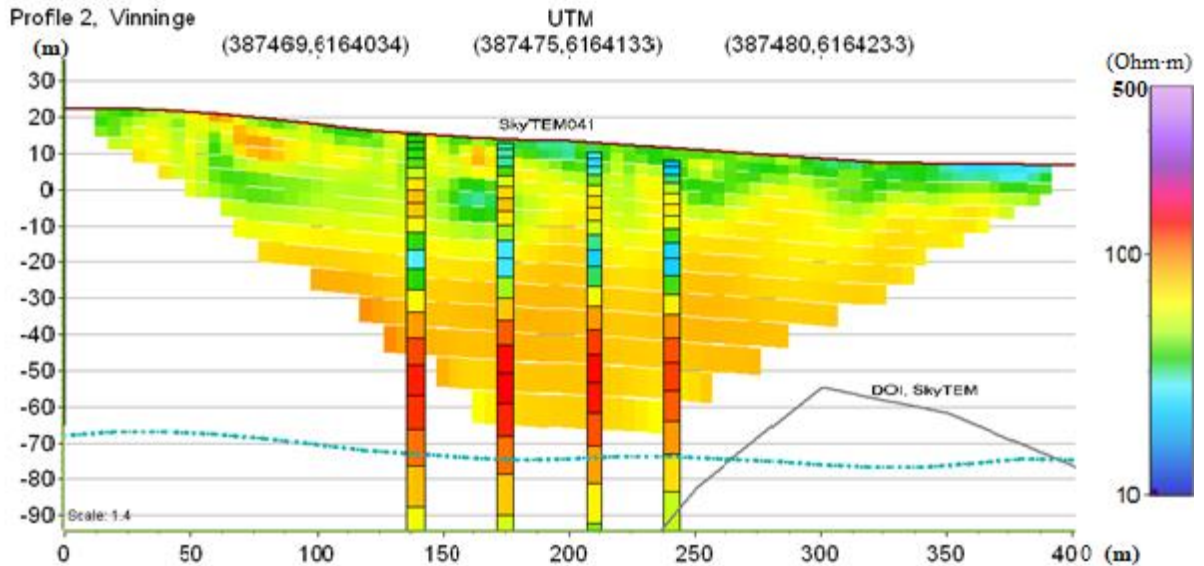
Figure 31. ERT profile shown together with local SKYTEM survey soundings. No boreholes in this area were close enough to include. Colour scale shows resistivity values between 10 and 500 Ohm·m.

The ERT profile seems to show a lower resistivity layer with a thickness varying between 10 to 30 metres across the whole area, followed by a higher resistivity layer. However, the sequence of resistivity changes seen in the SkyTEM soundings are not directly visible in the ERT. Firstly, the low resistive section in the SkyTEM soundings at 30 m to 40 m below ground level with resistivities in the range of 15-20 Ohm·m is absent in the ERT. Secondly, the upper 30 m seem to show somewhat opposite variations in resistivity between the ERT and SkyTEM.

Interpreting these results is quite difficult. The SkyTEM shows a lower resistivity layer at around 40m depth, that does not appear in the ERT profile. This coincides roughly with the clay till layer in the nearby borehole. On the other hand, the ERT inversion has a very low mean residual error, i.e., it's a very good fit to data. An ERT measurement should also have a higher resolution especially at such a shallow depth, and the error of the SkyTEM measurement is unknown to us. After this consideration, the ERT results are considered more reliable.

The topmost 40 meters or so varies in resistivity in a range of about 30-70 Ohm·m. Shallow patches of resistivities up to 100 Ohm·m, visible in the ERT around 75 m and 160 m, are interpreted as sandy areas within the till deposit. The deeper, higher resistivity layer of around 80 Ohm·m is interpreted as fully saturated sand and silt, the aquifer. If the thin layer of clay is present in the area, it does not appear in terms of a resistivity response. Either way, this layer is thin enough that the sand above it is most likely in contact with the deeper sand and silt. There is a patch of low resistivity topsoil in the north part of the profile. This coincides with the patch of postglacial fine clay shown in the soil map. The profile slopes downward in this direction, and west of the northernmost part lies a small pond. This could also be attributed to the soil having higher degrees of saturation.

The bedrock doesn't have the same abrupt shift to a very low resistivity here as in profile 1, despite being quite close nearby. Instead, it seems to show a gradual shift to lower resistivity, and while SkyTEM is not great at picking up these sharp local boundaries, it does capture it in this case.

4.3 Profile 3: Stora Mölleberga (W-E)

Description

The topsoil in this area varies greatly. The profile extends first over glaciofluvial sand, then a shorter section over clayey till and then over coarse silt to fine sand as depicted in Figure 33. Shallow 20 to 30 m of sediments are shown to be either a till-clay, or a sandier till depending on the location the of borehole. The closest borehole is located 60 m from the 220 m mark, as presented in Table 9 shows that besides from the clay till and till extending to a total depth of less than 40 m, the sediments are coarse silt to sand down to the bedrock. This profile thus could give a direct read of resistivity values for beds of saturated coarse silt to sand. Groundwater level is expected to be close to the surface especially around the 500 m mark, as the small pond appears in a slight depression and a river is running north of the profiles. Measured values from 1966 place the groundwater level between 6 and 8m depth (SGU, 2023c).

This profile cuts through wide gaps in the SkyTEM profiles, which are the results of nearby powerlines, and was meant to investigate if the low resistive layer around 40 m depth, appearing in SkyTEM profiles north and south at the western section, is present. Unfortunately, due to a lack of time in the field, the profile was not extended as far as we would have liked.

Additionally, TEM soundings were carried out along the ERT line, especially chosen due to the absence of SkyTEM. While the ERT line reaches somewhat close to the powerline towards the west at merely 150 m distance at one point, it was assumed that this distance would be sufficient.
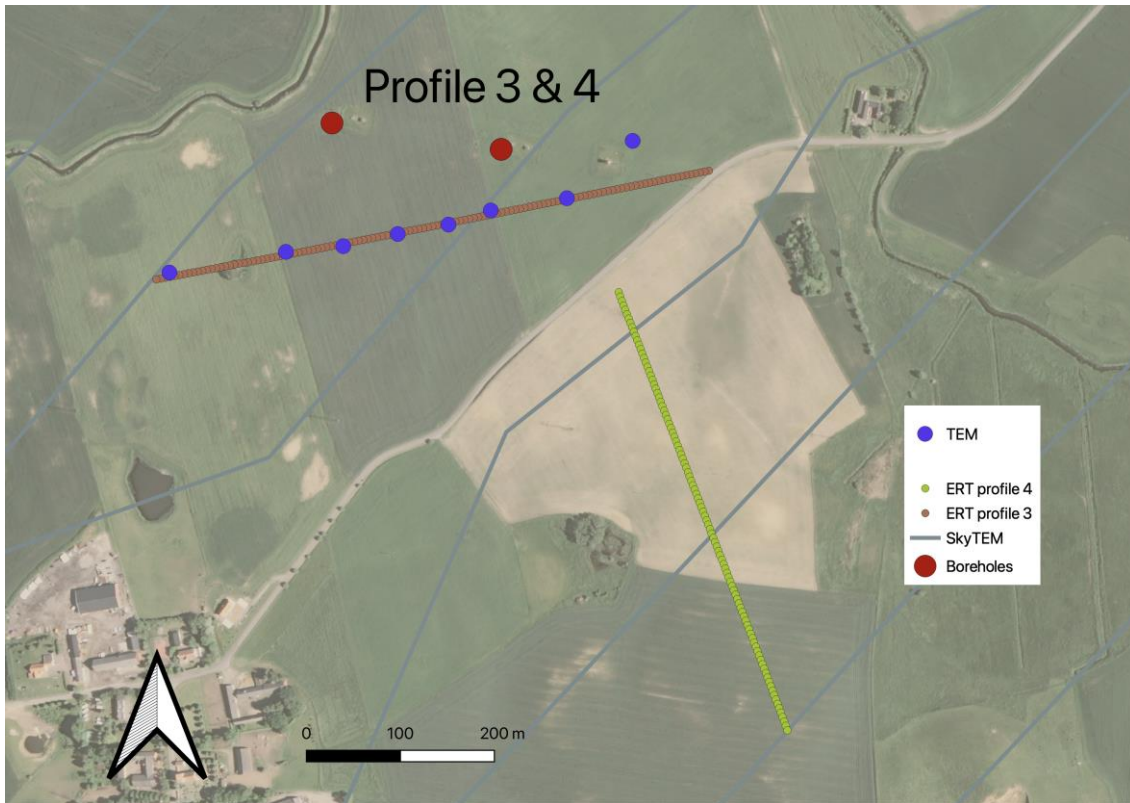
Figure 32. Map of survey location 3, including ERT, nearby borehole(s) and SkyTEM. Profile 3 in orange, 600m in the W-E direction, and profile 4 in red, 500m in the N-S direction. TEM points are placed along profile 3.
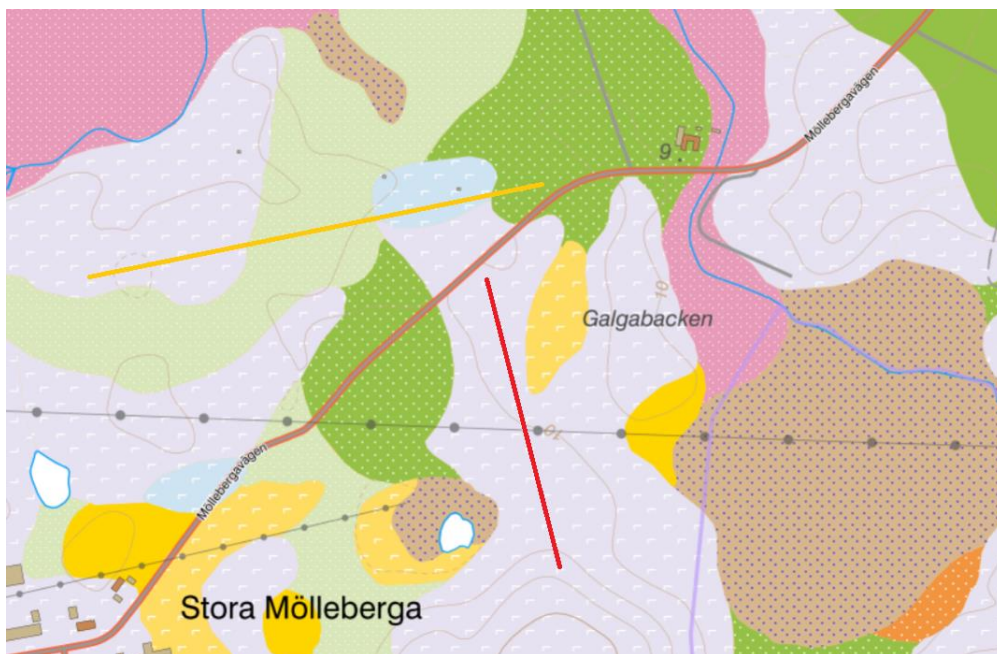
Figure 33. Soil map for the two profiles at Stora Mölleberga. Profile 3 in orange, and 4 in red. For more information, refer to Table 1.

Table 5. The lithology of the two closest boreholes.

Level	0 – 20.4 m	20.4 – 38.5 m	38.5 – 73.4 m	

Lithology (60 m N of 210 m mark)	Till clay	Till	Coarse silt and sand with possible appearing gravel at the bottom	
Level	0 – 34.6 m	34.6 – 37.2	37.2 -71 m	71 m -
120 m N of 400 m mark	Sand and till	Till clay	Coarse silt and sand	Limestone

Results profile 3: Stora Mölleberga

Field description

At approximately 120 meters along the profile, four meters to the north a draining well was situated with an expected pipe in a southerly direction, thus intersecting the survey line. Similarly, at approximately 200m another draining well was situated 2 meters north. Near the 400-meter mark, a small surface water was crossed with the electrodes placed on both sides.

On measuring with the last two cables, bad contact with several electrodes resulted from a very dry soil. Exceeded set limit for contact resistance was thus accepted for a number of these electrodes.

Local topsoil consists of sandy till, rough silt – fine sand, and clayey till.

Resulting profiles

Figure 34. Higher resolution ERT Profile, including mean residual error percentage

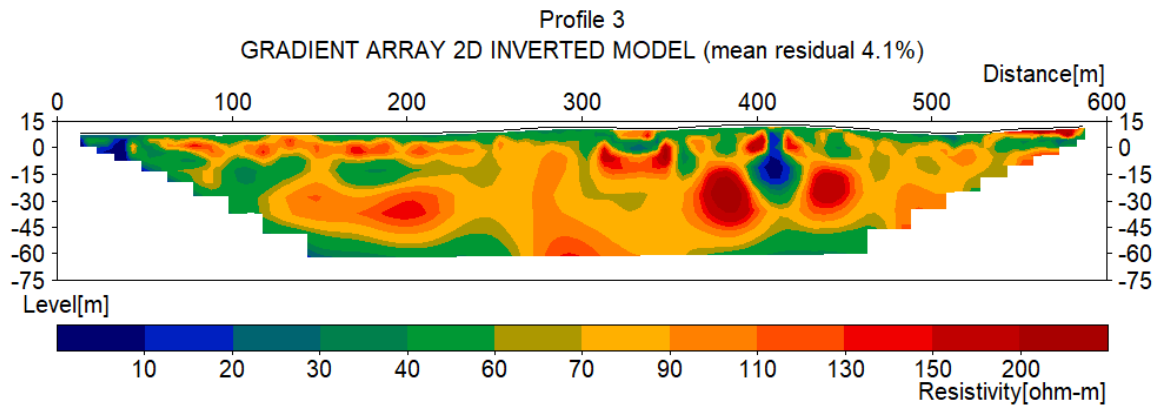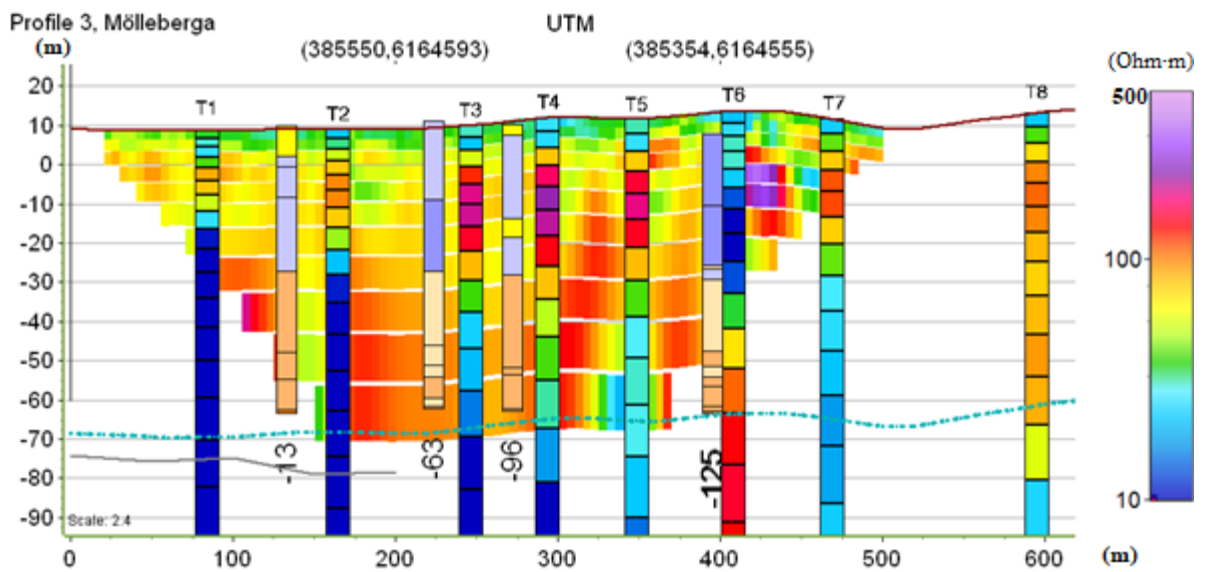Figure 35. ERT profile shown together with TEM survey result and several local boreholes. Colour scale shows resistivity values between 10 and 500 Ohm·m.

Interpretation

Another result that is quite tough to interpret. ERT and TEM results conflict with each other nearly everywhere. TEM soundings show very low resistivity at deeper depths, possibly due to interference from the nearby powerline. This view is supported further by the fact that this effect seems to abate in the eastward direction as the distance between powerline and profile increases. It also shows some patches of very high resistivity in T3-T5 that ERT doesn't pick up at all. The TEM data in this area is therefore seen as untrustworthy. The pond at the 400m mark creates a disturbance in the ERT results, most likely contributing to the rather high mean residual of 4%.

The borehole 60m north of the 210-metre mark (Table 5) has a clayey till in the first 20 metres. The other borehole also shows till, which may or may not be clayey in nature. The first 20 meters has a resistivity ranging from about 40-90 Ohm·m. This fits in with the similar interpretation of tillclay till in profile 2. Patches of high resistivity appear beneath this layer and could be interpreted as sandier areas judging by the sand and till present in the northern borehole. The saturated Alnarp sediments show resistivity values between 40 and 90 Ohm·m for the most part. The TEM data is to be considered untrustworthy in this case, so not much can be said about the bedrock.

The ERT resistivity profile show values for the saturated coarse silts and sand to be in the range of 50 to 150 Ohm·m. The anomaly at the 400 m mark shows the area with the small pond with resistivities down to below 10 Ohm·m locally, surrounded by patches of much greater resistivity. It can also be seen in T6, meaning it is not some quirk of the inversion. This could possibly be due to something buried here, a pipeline or some other highly conductive object.

4.4 Profile 4: Stora Mölleberga (N-S)

Description

The surface soil is marked as clayey till over the entire length of the profile, with proximity to a small region marked with clay at the northern end (Figure 33). A well at 600 m SE shows a groundwater level of 30 m depth in 1970 (SGU, 2023c).

Table 6. The lithology of the closest borehole.

Level borehole (120 m north)	0 – 27 m	27 – 70 m
Lithology	Clay and till clay	Coarse silt and sand with appearing gravel at the bottom

Results profile 4: Stora Mölleberga

Field description

A power line crosses cable 2 at electrode 13 (cable 1 to the north). A well was observed 30 m from the joint between cable 1 and 2 at the eastern side of the survey line.

Contrary to the previous profile, the ground had a relatively low contact resistance due to rainfall the previous night.

Resulting profiles

Initial data had to be corrected with bad data points removed in the Res2DInv software to reduce the inversion residual error from around 16% to 3.8%. These bad data points where all located around the 400 m mark (Figure 36) where an anomaly was observed also in the pseudosection.

After data processing, resistivities for this profile show normally observed values. The circular anomaly seen in the pseudosection now has a resistivity up to 400 Ohm·m. This anomaly is thought to be the reason why the mean residual error is significantly higher for this profile.
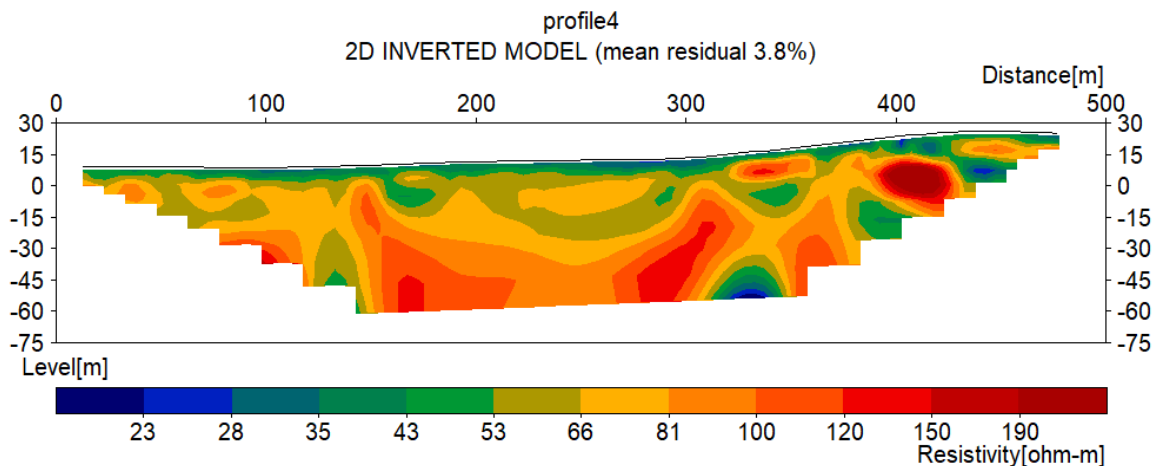

Figure 36. Higher resolution ERT Profile, including mean residual error percentage.
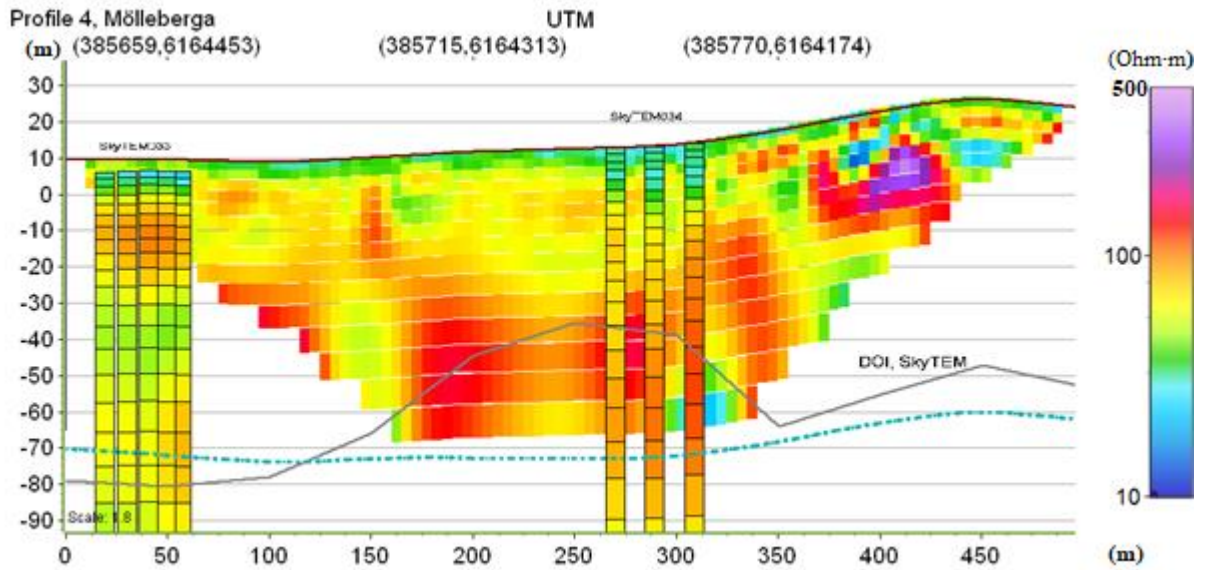
Figure 37, ERT profile shown together with available SKYTEM survey result. Notice the gap created by a present powerline starting at 50 meters, as well as the relatively high resistivity in the anomaly at 400 meters. Colour scale shows resistivity values between 10 and 500 Ohm·m.

Interpretation

The resistivity in the section of SkyTEM033, presented in Figure 37, intercepting the survey show good correlation with the borehole to the north as shown in Table 6. The first 30m shows resistivity values in a range of about 35-65 Ohm·m, corresponding with the clay and clayey till found nearby. A shift to coarser sediments with resistivities of up to 200 Ohm·m can be seen deeper below. No clear resistivity change is seen from the sand to the bedrock elevation, although most of the bedrock is beyond the depth of investigation of the SkyTEM. A patch of low resistivity material is visible in the ERT. This may represent a very local patch of clay or similar or may simply be a result of the data processing. In general, the SkyTEM and ERT data in this area seems to agree, a low resistivity layer followed by a higher resistivity one. There are lateral variations in resistivity that can be seen both in our ERT measurement and in SkyTEM 034. This could be variations in the thickness of the clay till and coarse sand deposits. The anomaly at the 400m mark is tough to interpret. Measuring well over 50 meters across, it's too large to be a boulder. What could cause an anomaly such as this is unknown to the authors.

51

4.5 Profile 5: Ängagården (W-E)

Description

The surface soil in this profile is dominated by clayey till, crossing into two patches of silt – fine sand, as seen in Figure 38.

Looking at the SkyTEM profiles (Figure 39), this ERT survey could shine some light on the transition between lines 38 to 39. For line 39, a deeper low resistivity area is observed close to the surface. This difference is more pronounced further along the lines. The ERT profile could thus help either confirming its location or deducing if it is caused by any noise.

Apart from the borehole located 600 m from the south-eastern end that was previously presented for profile 2 (Table 2), the boreholes in Table 7 are used as reference material. Considering all close boreholes, it is not clear how the geologic layers vary over the area. To the NE, thin clay layers are present at varying levels between 35 to 55 m depth, whereas no clay is recorded 500 m to the SW.

The groundwater level was measured in 1970 to a depth of 31 m (SGU, 2023c).
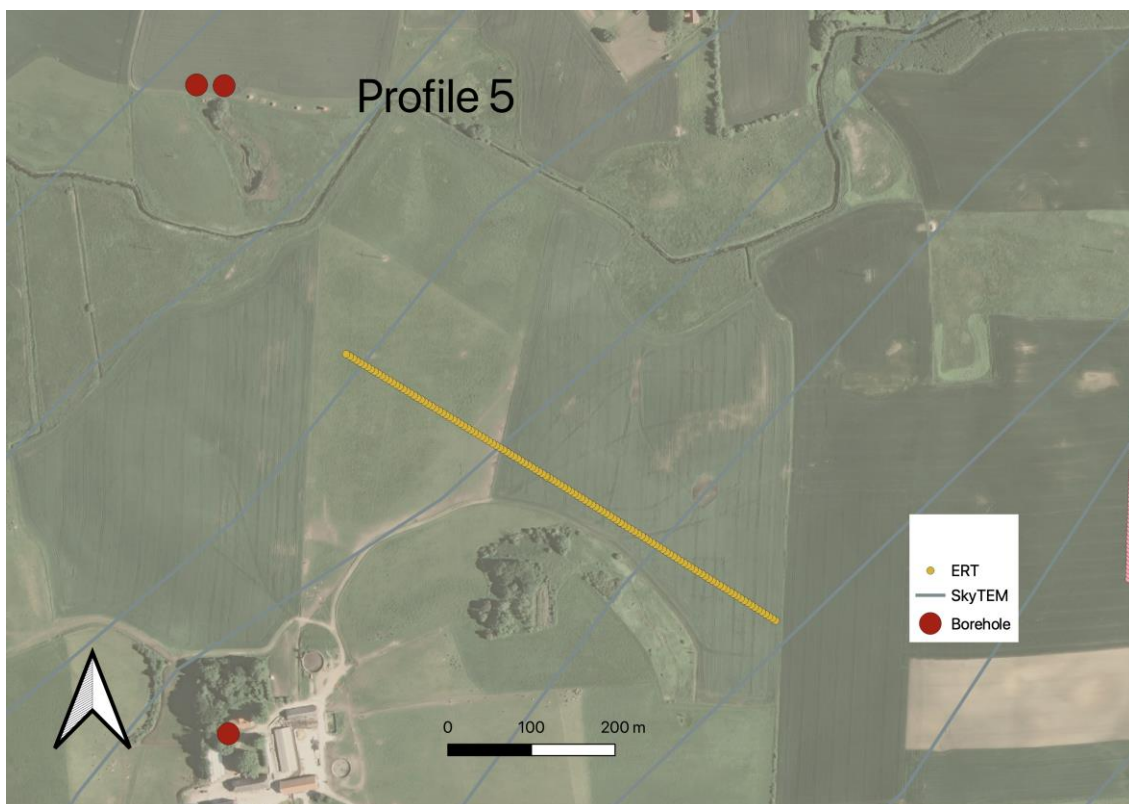
Figure 38. Map of survey location 5, including ERT, nearby borehole(s) and SkyTEM.

Figure 39. Soil map for profile 5, with the approximate survey location in yellow. For more information, refer to Table 1.

Table 7. The lithology of the two closest nearby boreholes.

Level	0 – 40 m	40 – 45 m	45 – 56 m	56 – 70 m
Lithology (320 m from N-W end point)	Till clay and clay	Sand and gravel	Clay	Sand, gravel with appearance of till clay
Level	0 – 2.6 m	2.6 – 63.0	63.0 - 94 m	94 m -
Lithology (450 m S from cable 5)	Fine sand	Till clay	Sand and gravel	Sandy limestone

Results profile 5: Ängagården

Field description

The in-field scouting revealed an electrical fence that had to be considered when choosing the start of the profile. A safety distance of approximately 50 m was held to this electric fence, with regards to possible noise. A disturbance and possible source of error is that along cable 3 the safety distance to the electric fence was unfortunately reduced to around 30 m. In the planning phase, many alternative profile directions where considered. To make use of the intersecting SkyTEM data and trying to cover the local variations in the geology of interest, the profile was placed in a SE-NW direction. The profile extends 600 m as beyond that, planted crops prevented further extension of the line, as agreed upon with the farmer.

Resulting profiles

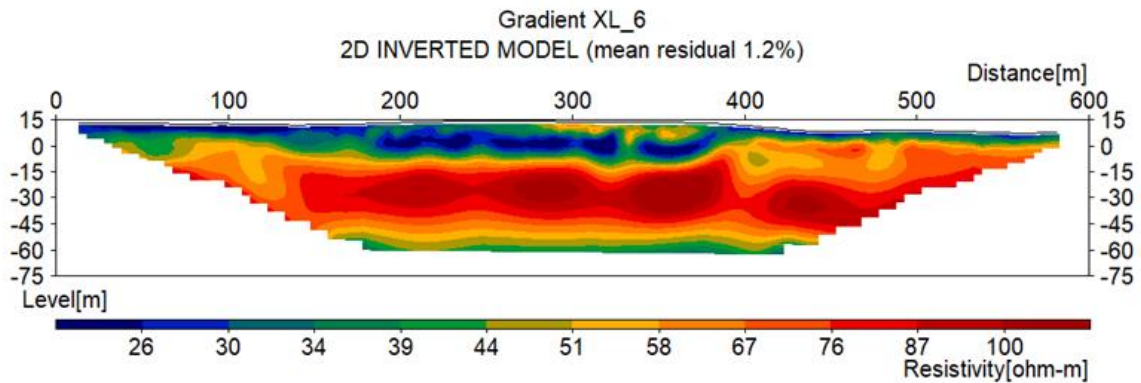Figure 40. Higher resolution ERT Profile, including mean residual error percentage.
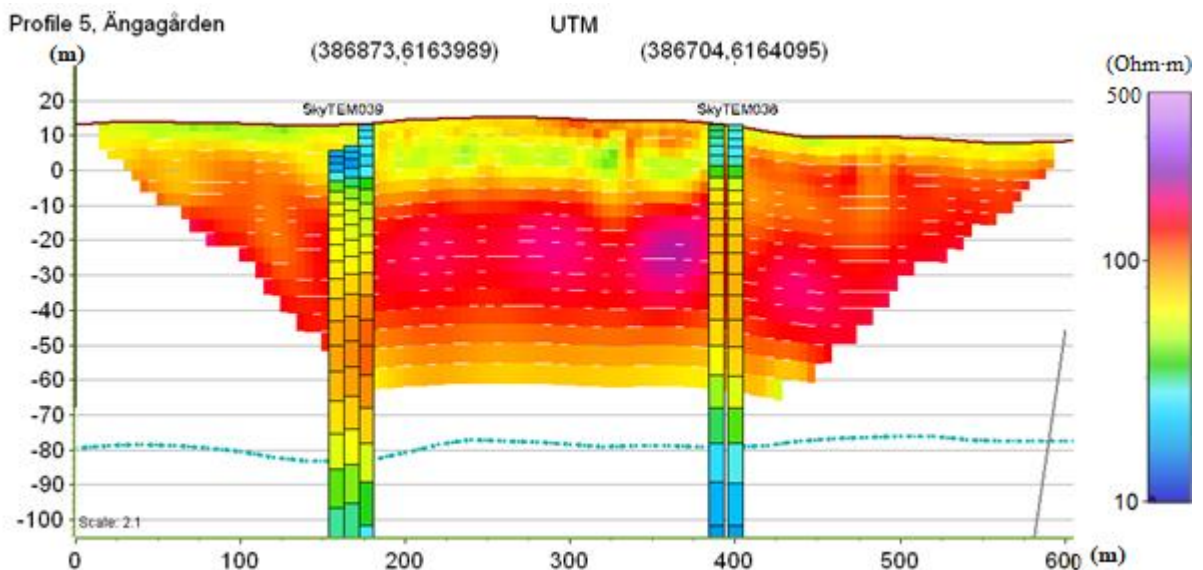

Figure 41. ERT profile shown together with local SKYTEM soundings. No boreholes were close enough to include. Colour scale shows resistivity values between 10 and 500 Ohm·m.

Interpretation

Near the surface, we see the expected lower resistivity of the clayey till and clay layers seen in one of the nearby boreholes (Table 5). We also see a patch of higher resistivity near the 300m mark that the SkyTEM measurement does not pick up. This could be explained by the sand as reported in the first 2.6m of the other borehole of Table 5. The low resistivity layer thins at around the 400-meter mark, near SkyTEM line 038. This shift explains why the low resistivity layer in this area is thicker in SkyTEM line 039. According to local boreholes the clay/clay till should extend down to a depth of around 60 meters in this area, but after around 20 meters we start to see resistivity values of around 100-150 Ohm·m, which are higher than what we have previously interpreted as clay/till clay, for example in profile 1. Perhaps the range for these clayey soils are greater than we thought, or the notations in the borehole logs are not quite accurate and the till is coarser than we are led to believe.

At a depth of around 45 meters patches of even higher resistivity are visible. One of the local boreholes has sand and gravel at this depth, which may be what we are seeing here. These patches may also be the reason for SkyTEM 38 showing higher resistivities than SkyTEM 39 at this depth. At a depth of around 60 meters, a transition to a lower resistivity layer is visible. This layer has a thickness of around 30 meters, correlating well with the aquifer sand and gravel layer in the southern borehole. DCIP is unable to penetrate in it entirety but shows resistivities in the 40-60 Ohm·m range. The bedrock is visible at a depth of around 95 meters. The outright clay layer appearing at 45 meters below surface in one nearby borehole is not discernible, despite its relative thickness of nearly ten meters.

4.6 Profile 6: Tejarp (S-N)

Description

This profile was selected to help characterizing the geology of a section of the eastern Alnarp valley where no boreholes are present. Instead, comparisons can be made to a nearby borehole, approximately 1km to the west.

The SkyTEM profiles intersect this profile in three locations, allowing a direct comparison between all three methods at these locations.

The surface soil consists of mostly coarse clay till with an occurrence of peat in the northern half of the profile (Figure 43).
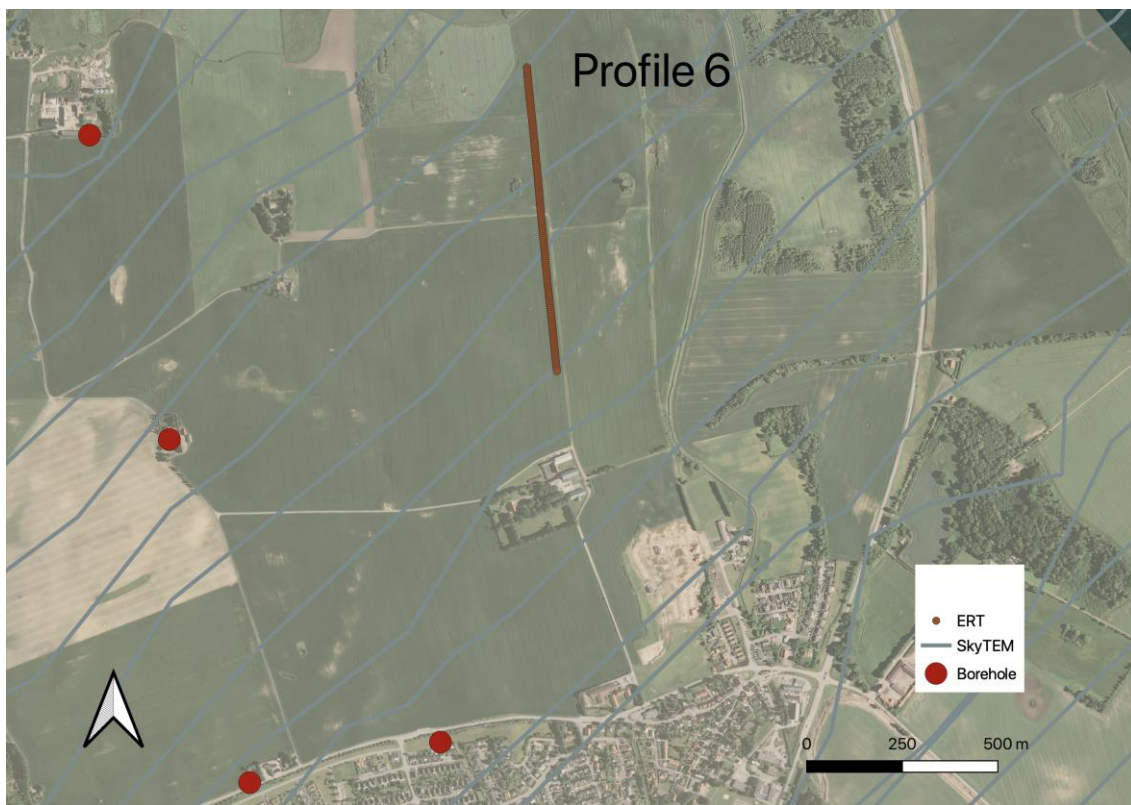
Figure 42. Map of survey location 5, including ERT, nearby borehole(s) and SkyTEM.

Figure 43. Soil map for profile 6, with the approximate survey location in yellow. For more information, refer to Table 1.

The borehole to the west of the southern end shows that two mighty coarse-grained layers exist within the stratigraphy, with a confining unit of clay separating them (Table 6). Both boreholes indicate that the Alnarp sediments are thick and confined. Bedrock is at approximately 80 meters depth. Well data from 1940 mark the groundwater level at 20 m depth (SGU, 2023c).

An additional borehole to the south of the profile shows clay extending 25 m from the surface with sand and gravel continuing downwards (Table 6).

Table 8. The lithology of the two closest boreholes.

Level	4 – 10 m	10 – 52 m	52 – 72 m	72 – 86.5 m	86.5 – 93.5	93.5 m -
Lithology (1 km west of S end)	Clay	Sand and gravel, fining downwards	Clay mixed sand	Fine sand	Gravel	Sandy limestone
Level	7.6 – 12 m	12 – 14	14 – 31.5 m	31.5 – 68.5 m	68.5 – 79 m	79 m -
Lithology (1km west of N end)	Clay	Gravel and sand	Clay	Sand	Gravel	Limestone

Results profile 6: Tejarp

Field description

Together with the farmer it was decided to place the profile along one of the "truck tracks" which was also close to the planned location of the line. The survey was also parallel to a gravel paved small road which facilitated the work. The profile begins at the northern end slightly south of the powerline. Generally, electrode contact resistances were low. There is a small but constant elevation increase towards the south of the profile.
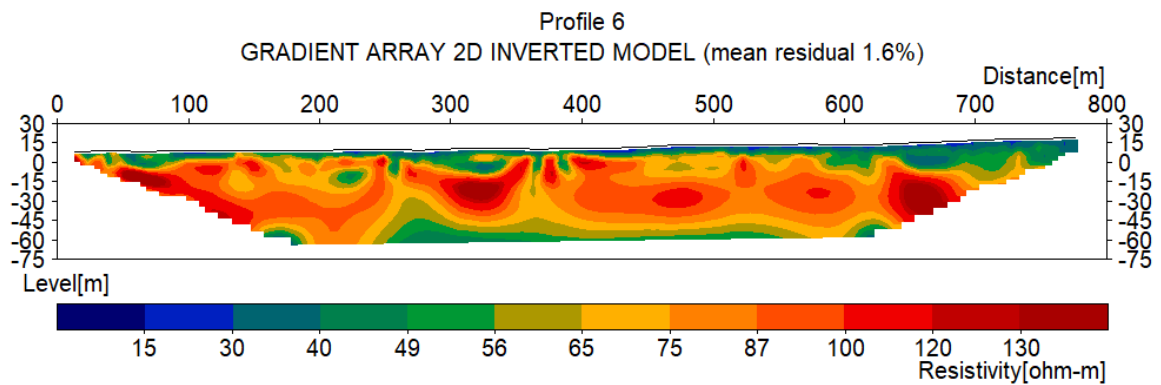
Resulting profiles

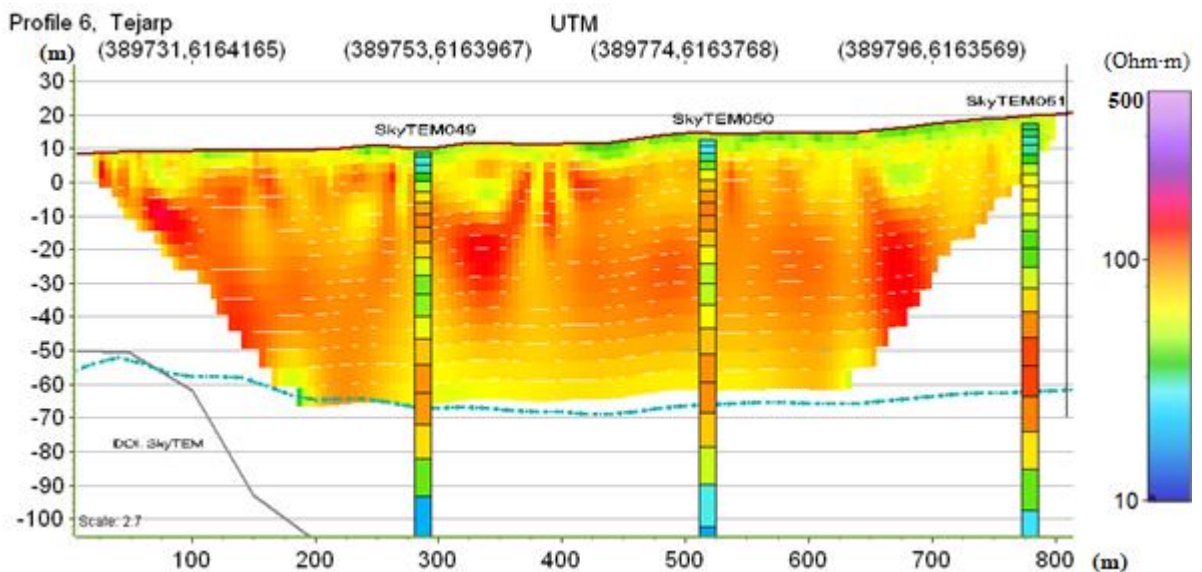Figure 44. Higher resolution ERT Profile, including mean residual error percentage.

Figure 45. ERT profile shown together with local SKYTEM soundings. No local boreholes to include. Colour scale shows resistivity values between 10 and 500 Ohm·m.

Interpretation

This 800 m profile intersect three SkyTEM profiles. From the south to the north the bedrock elevation varies from 75 m to 82 m. Interestingly the resistivity varies greatly between that of the SkyTEM and the ERT and is almost reversed in some places. Near the bedrock for example, SkyTEM shows higher resistivity than the ERT. At depths of 40 to 50m the SkyTEM instead shows much lower resistivity than the ERT. Boreholes does not indicate a major change in grain size at these levels however, both recording sand through these depths.

The surface soil consisting of peat to the north shows low resistivities, 30 to 50 Ohm·m. Other low resistivity patches near the surface could represent clayey areas. The surface clayey till varies in thickness and compared to the boreholes it is relatively thin, mostly less than 10 m. Both nearby boreholes contain gravel which could explain the patches of high resistivity material seen throughout the middle depths of the profile. Interestingly however, resistivity decreases as the bedrock is approached, despite both boreholes indicating gravel closest to the bedrock, and although both boreholes are quite far away, gravel appearing near the bedrock both to the north and south of the profile could indicate it being present here as well. Something similar is observed in Profile 5 and to a lesser extent in Profile 3, with the bottommost gravelly sediments showing quite low resistivities. It seems that if the sediments are part of the aquifer layer and thus saturated with water, there is sometimes little correlation between coarseness and resistivity. In these cases, there is a correlation between depth and lower resistivity.

4.7 Profile 7: Särslöv (N-S)

Description

This location was partly chosen because the ERT could possibly reach the bedrock. The selected profile crosses three SKYTEM profiles with a gap at the southern end that is close to a powerline. It was also selected to investigate if a clay layer present in a borehole further west is present here. In preparations as well as in the initial in-field visual scouting, a small pond was missed which led to the decision to slightly change the direction of the profile after the third cable was already placed.

Additionally, it was decided to carry out a TEM survey to get further possibilities to compare the geophysical methods as the SkyTEM intersects were sparse.

The topsoil, as depicted in Figure 47, is predominantly coarse clayey till over the entire profile.
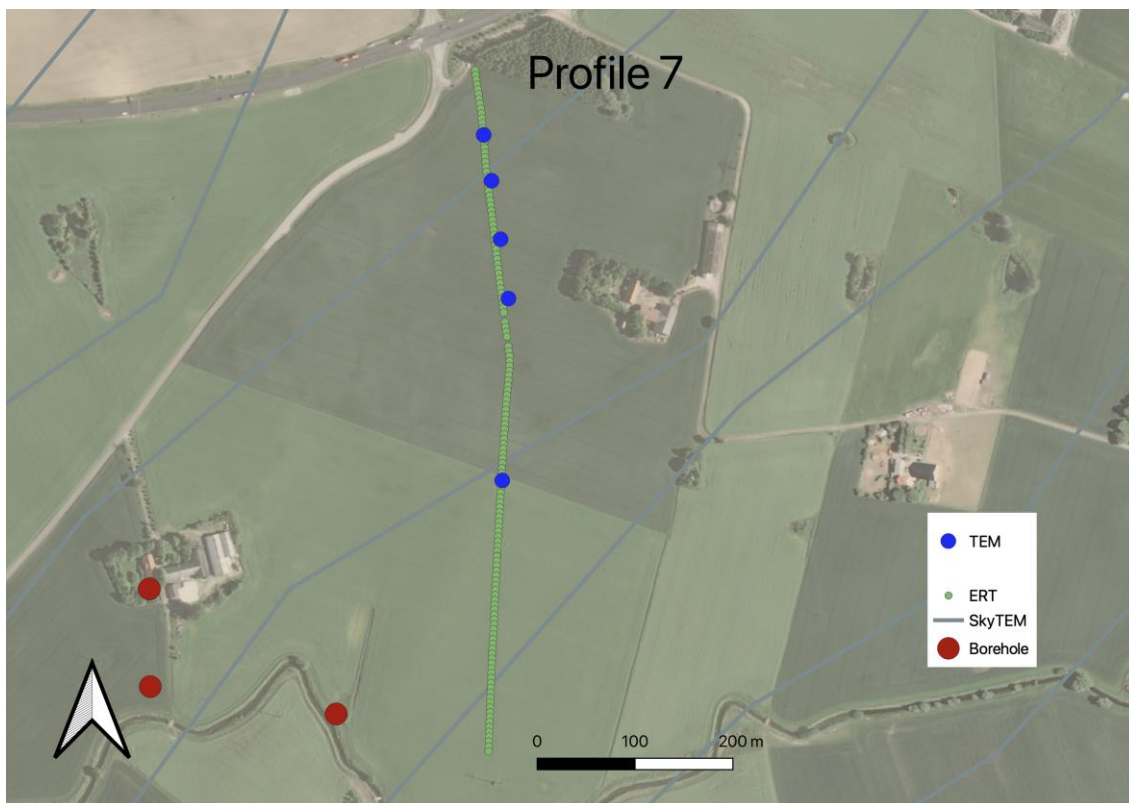

Figure 46. Map of survey location 7, including ERT, TEM, nearby borehole(s) and SkyTEM.
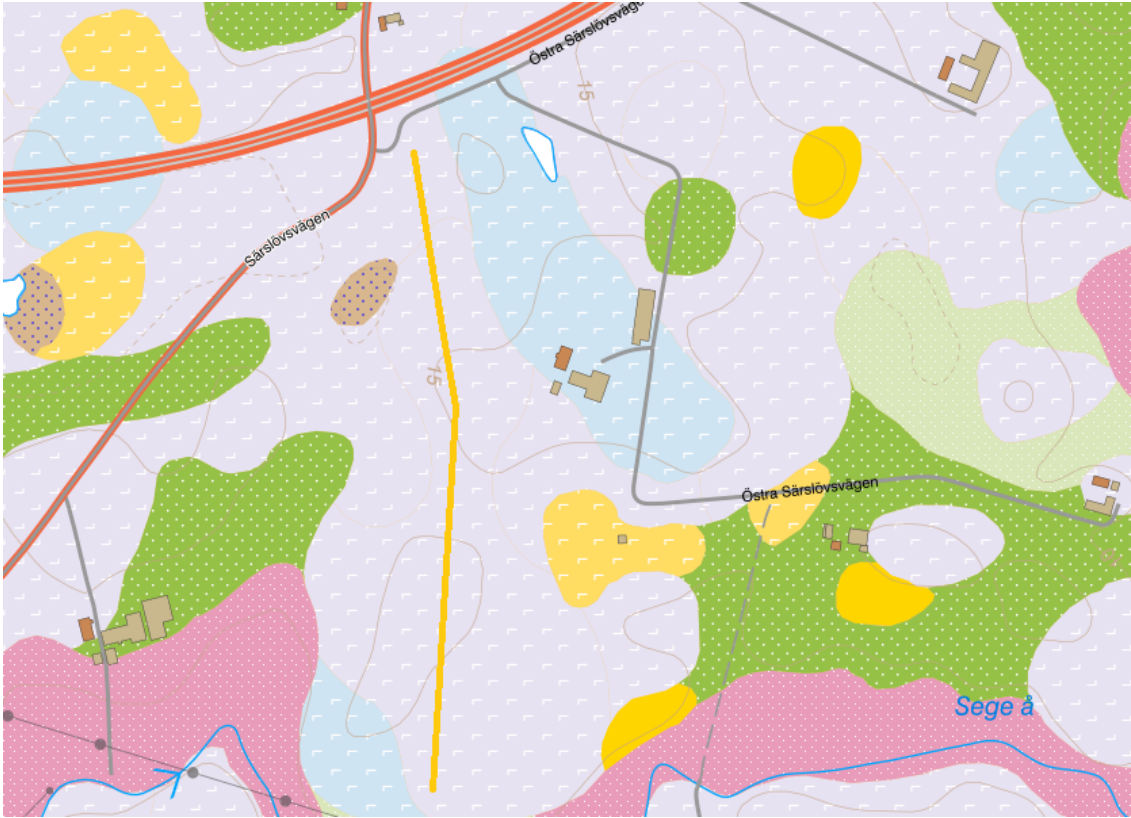
Figure 47. Soil map for Särslöv, with approximate survey location in yellow. For more information, refer to Table 1.

Available boreholes, at 500 m to the north as well as one at 150 m from southern end (Table 7) suggest a bedrock elevation of around 70 m depth. From the bedrock upwards, both boreholes show layers described as sand to coarse silt somewhat clayey with a thickness of about 30 m. However, another borehole 350 m west of the profile shows a 10 m thick clay layer from 50 to 60 m depth. The top 30 to 40 m is expected to be the clayey till. The borehole at 150 m south does not denote the till as clayey for depths of 18 to 43 m. Groundwater at the closest well to the southern end was measured in 1966 to a depth of 5.5 m (SGU, 2023c).

Boreholes south of the profile show a relatively thick layer of clay and a similar thickness of a low resistive section is shown in the SkyTEM profiles (Figure 46). As these profiles show this low resistive layer thinning out to the north-east and as no clay was classified in the borehole to the north it could be assumed that this represents the extent of the clay layer. Thus, over the profile the depth of the water bearing layers varies due to the varying thickness of the clay.

Table 9. The lithology of the closest borehole.

Level (150 m south of profile's south end)	0-18.3	18.3-43.3	43.3-72.3	72.3 -
Lithology	Till clay	Till	Coarse silt to sand	Limestone

61

The borehole presented in Table 7 is located 150 m from the southern end. The borehole 300 m from the northern end shows the same principial stratigraphy. Exceptions are that the surface till is not noted to be clayey while the possibly water bearing sediments of coarse silt is noted as somewhat clayey.

Results profile 7: Särslöv

Field description

After measurements with the first few cables had been done, a small pond was observed in the path of the straight survey line. Cables 4 and onwards thus were re-directed. Electrode contacts were good owing to the clayey till.
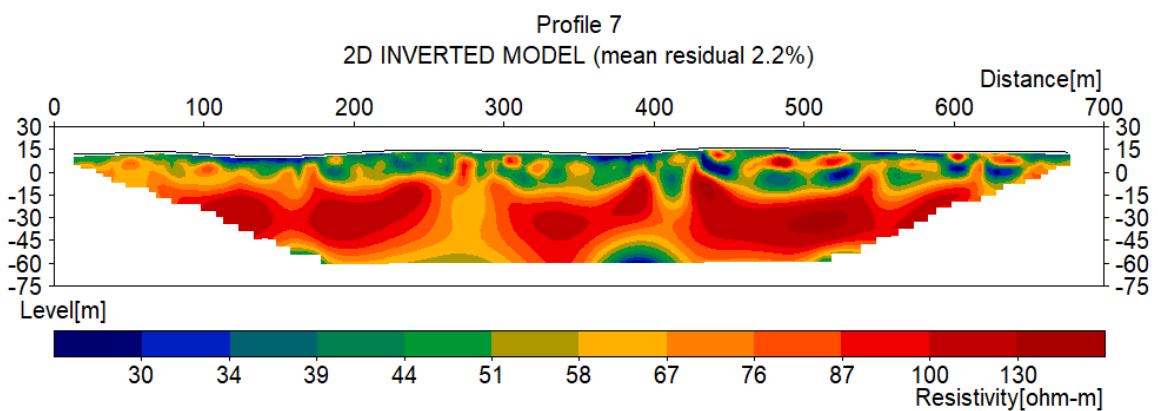
Resulting profiles

Figure 48. Higher resolution ERT Profile, including mean residual error percentage
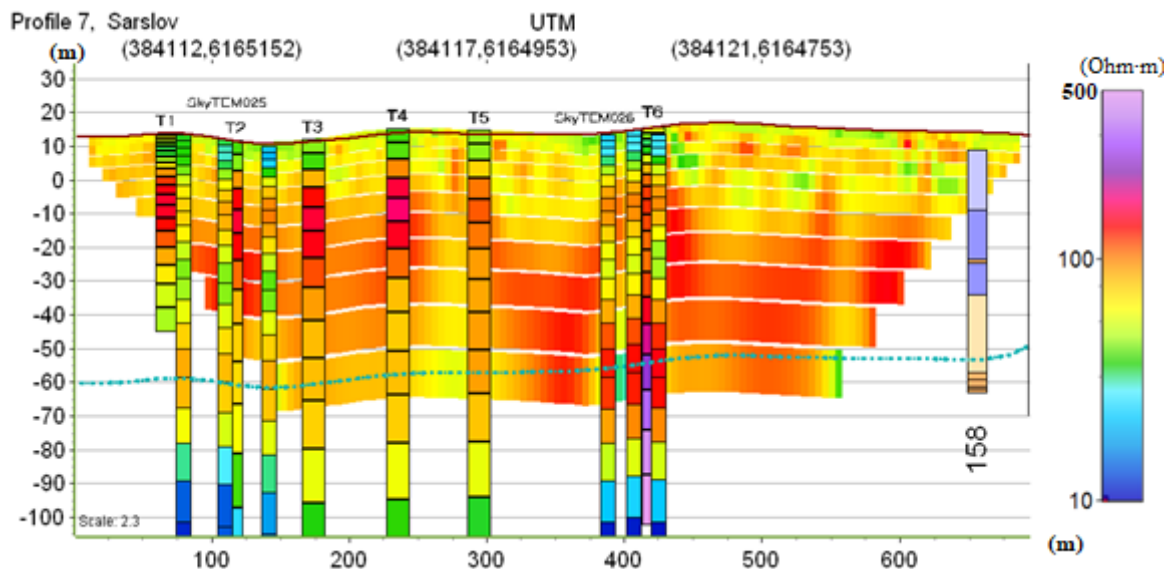
Figure 49. SkyTEM soundings up to 50 m from the ERT profile included. Colour scale shows resistivity between 10 to 500 Ohm·m. No boreholes close enough to include.

Near the surface, all three methods agree on a low resistivity layer of varying depth near the surface. The topsoil is noted as clayey till, and the first 18 meters of the nearby borehole presented in Table 9 is also noted as such, agreeing with the results. Resistivities here range roughly from 30 to 70 Ohm·m across all methods. With the shift to what is noted as till in Table 7, we see an increase in resistivities across all methods. This shift is especially visible in Figure 48, with resistivities up 130 Ohm·m. At depths of 43-73 meters, the more water bearing sediments of coarse silt and sand can be found. The shift to these materials is not clearly visible.

In the south of the profile, T1 and SkyTEM detect a low resistivity layer at a depth of around 40 meters, near the edge of the ERT profile. This appears again at the 400m mark. As it does not coincide with the height of the clay layer found in the borehole to the west, this is unlikely to be what we are seeing. It's possible that this is because of lateral smoothing in the SkyTEM inversion. TEM results also correlate well with ERT results across the profile, leading us to trust these two more.

As hoped, the ERT managed to penetrate down to the expected bedrock elevation. There is however not any visible transition between soil and bedrock in terms of resistivity, as there for example was in profile 1. It is possible that the bedrock is less fractured here. There is however a reduction of resistivity further beyond the bedrock surface visible in the TEM results.

4.8 Profile 8: Hyby (S-N)

Description

In this area, situated just south of the main studied area around Grevietäkten, bedrock elevation is unusually deep at around 117 meters. Further, there are two thick possible aquifer layers, separated by a thin layer of clay, as shown in Table 10. This area was chosen to examine whether there is a difference in resistivity between the two layers owing to water saturation, i.e., whether the clay layer is acting as an aquiclude in this case. The closest borehole is 200 m to the south of the profile (Table 10) and will be used as the main comparison with the geophysical results. Topsoil along the profile consists mainly of clayey till, but a patch of sandy deposits is crossed near the middle of the profile, as seen in Figure 51. Soil. The groundwater level below surface was measured in Hyby, 1.5 km away, between 1970 to 1986 and varied roughly between 5 and 8 m (SGU, 2023c). ERT and the SkyTEM only overlaps in the north end of the profile.

Figure 50. Map of survey location 8, including ERT, nearby borehole(s) and SkyTEM.
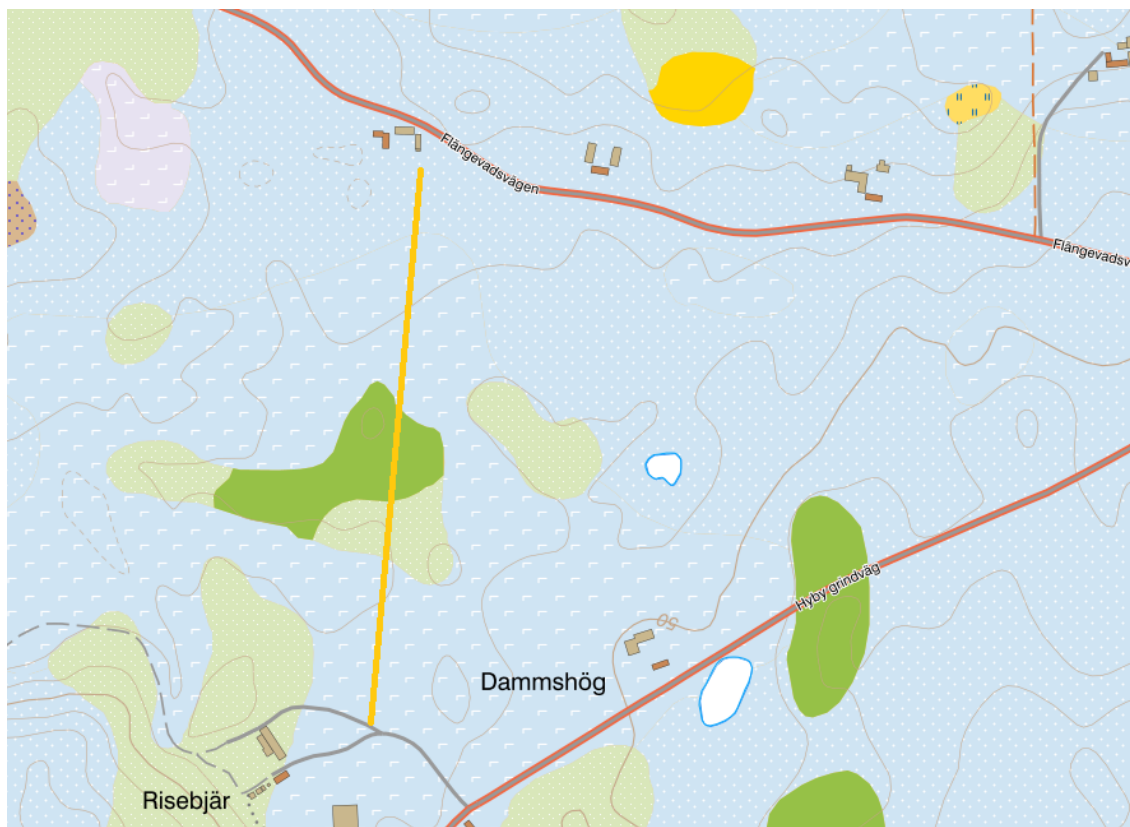
Figure 51. Soil map for hyby, with approximate profile location in yellow. For more information, refer to Table 1.

Table 10, lithology of the closest nearby borehole.

Level (m)	0-47	47-79	79-82	82-117	117
Lithology (200m south of profile's south end))	Till	Sand to coarse silt	Clay	Coarse silt to sand	limestone

Results profile 8: Hyby

Field description

The profile is situated with a surface slope to the west leading to a small depression where a small pond is located after the 150 m distance.

On this site several bad electrode contacts appeared with contact resistances of 600-900 Ohm. One electrode had a resistance of over 1 k Ohm and had to be force used.

Resulting profiles
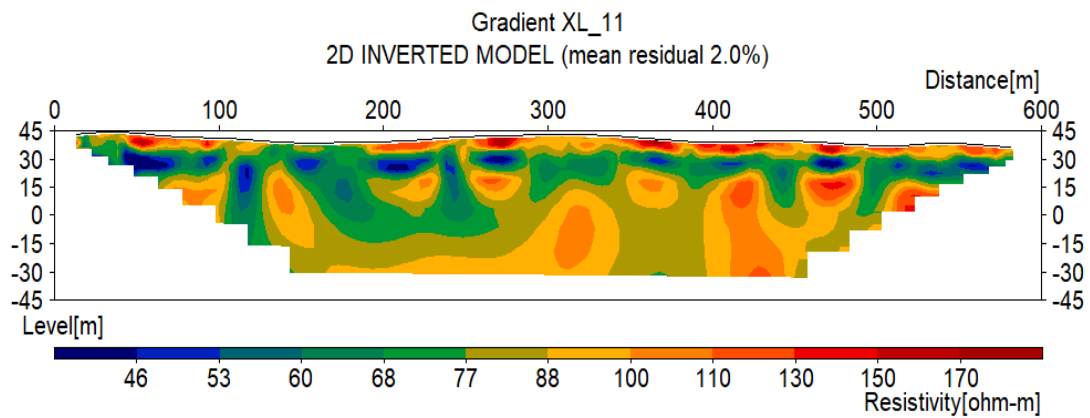
Figure 52. Higher resolution ERT Profile, including mean residual error percentage.
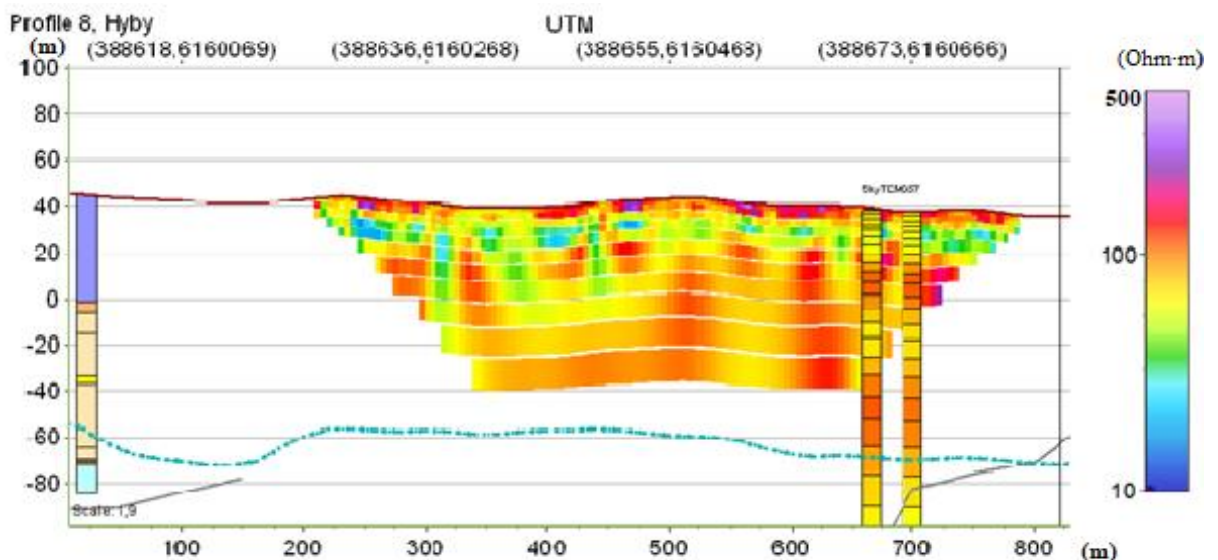
Figure 53. SkyTEM soundings up to 70 m from the ERT profile included. Borehole at 117m SE included. Colour scale shows resistivities between 25 to 250 Ohm·m.

66

Interpretation

Near the surface, resistivities vary with patches of up to 200 Ohm·m found throughout, explaining the issue with high contact resistance in some electrodes. The difference in surface soil, at 200 to 350 m of the ERT section covering fine sands to sands is not revealed in terms of a resistivity change. The till which is present in a nearby borehole (Table 10) in the first 45 meters is likely clayey or silty in nature considering its quite low resistivity.

Unfortunately, the DCIP was unable to penetrate deep enough to properly compare the two layers, only penetrating some distance through the shallower. SkyTEM shows a possible high resistivity layer close to the bottom. In this case, combining DCIP and TEM would have been helpful. Nevertheless, this first layer has resistivities of about 60-100 Ohm·m, which when compared to previous profiles is not an uncommon range for water-bearing aquifer sediments.

4.9 Profile 9: Abbekås (S-N)

Description

At this location there is an immediate borehole 60 m from the middle of the profile (Table 11), as well as one just south of the southern end point. There is not much variation between them, but the southern borehole marks no clay till over the bedrock and instead shows sand in the Skivarpsströmmen. The area thus has a mighty thickness of sand and coarse silt with an upper and thick confining unit of clay till. The groundwater level was measured to a shallow depth of 3.5 m in 1985 (SGU, 2023c). With the proximity to the sea, the groundwater meets the seawater at most just 500 m south.
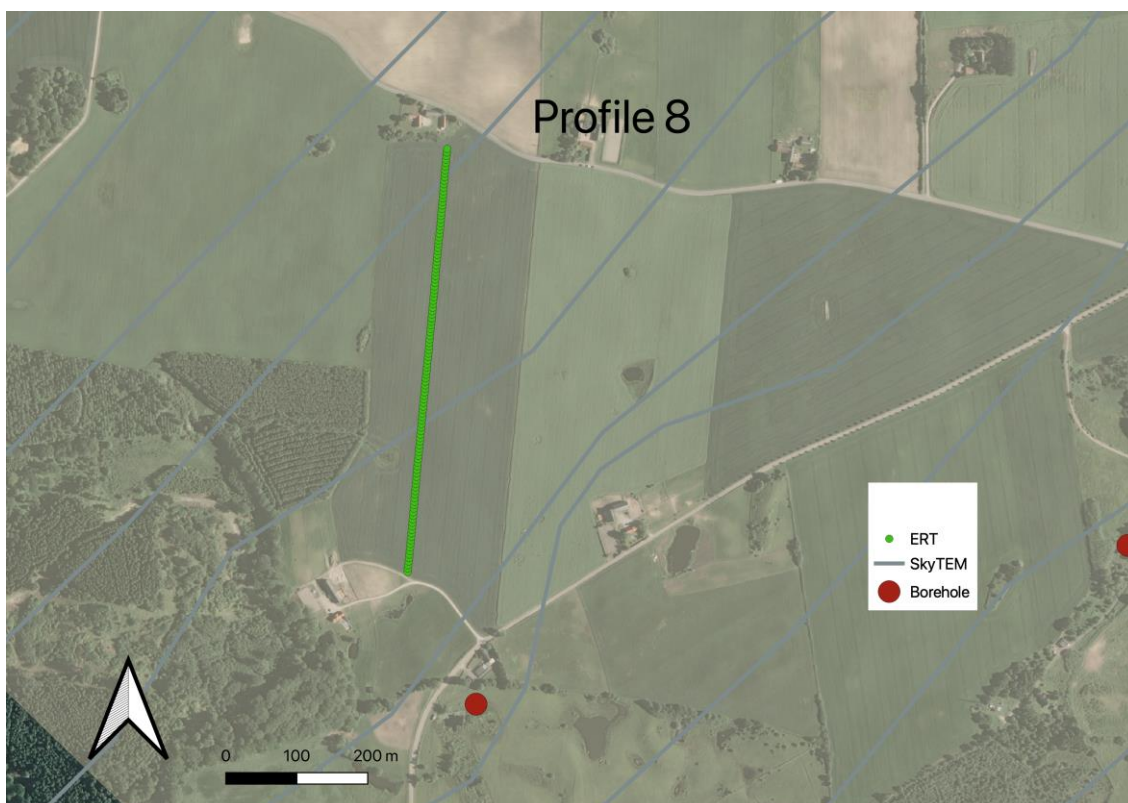
Figure 54. Map of survey location 9, including ERT, nearby borehole(s) and SkyTEM.

Figure 55. Soil map for abbekås, with approximate survey location in black. For more information, refer to Table 1.

Table 11. Lithology of the closest nearby borehole.

Level (m)	0-45	45-74	74-76	76
Lithology (60m from middle of profile)	Clay till	Sand to coarse silt	Clay till	Limestone

Results profile 9: Abbekås

Resulting profiles

A low mean residual was achieved for the ERT inversion. The resistivity profile shows fairly constant horizontal and vertical variations from start to end. Values for the sediments range between 25 and 70 Ohm·m.
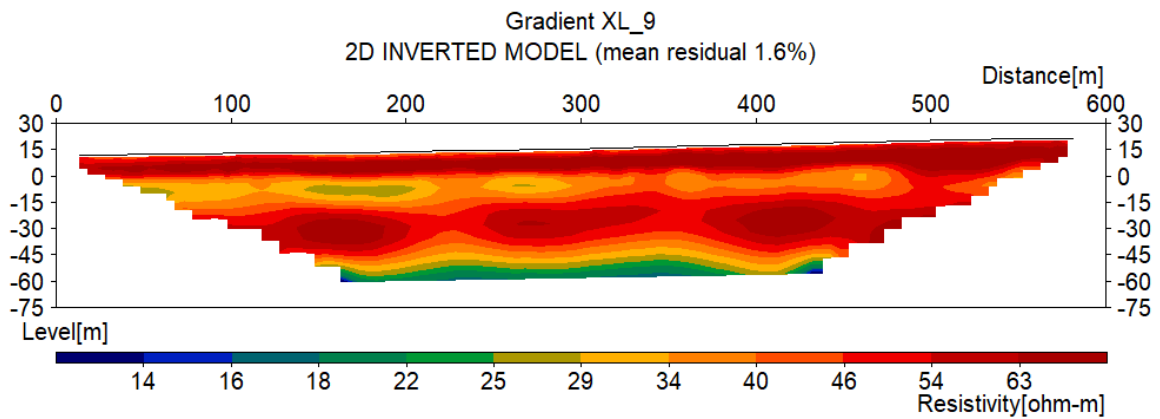
Figure 56, Higher resolution ERT Profile, including mean residual error percentage
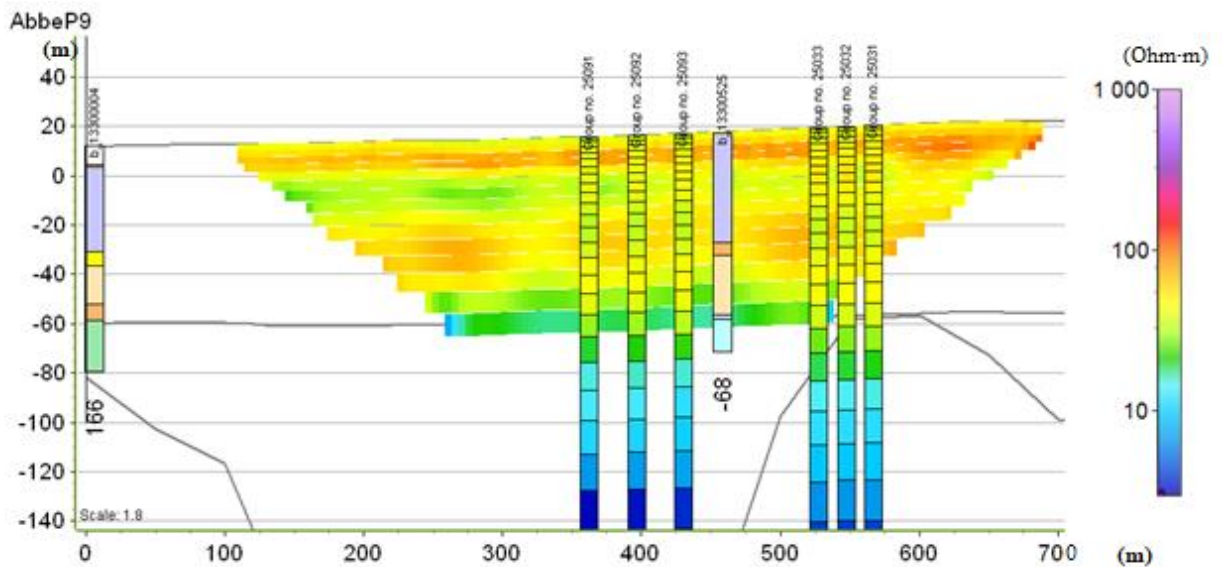
Figure 57. SkyTEM soundings up to 50 m from the ERT profile included. Boreholes included with projection distance to ERT shown beneath. Colour scale shows resistivity between 3 to 1000 Ohm·m.

The borehole 60 m from the 370 m mark gives a very close comparison with the ERT profile and in this location the bedrock can also be studied.

While the ERT shows distinct layering in terms of resistivity changes, the borehole notes only clay till to the depth of 45 m. A possible interpretation is therefore that this clayey till varies in its composition with a higher clay content roughly between 10 and 30 m depth compared to the top 10 m with resistivities up to 60 Ohm·m. Up to date ground water level observations places the water table at 3 to 4 m depth which means most of the observable cross section is saturated and thus lower resistivities should be expected even if parts of the till is in fact sandier in nature.

At the time of measuring the weather had been warm and dry so a drier topsoil could be why there is a big difference in observed resistivity between the ERT and the SkyTEM data in the shallower portion

Interestingly, the SkyTEM data indicate a slightly lower resistivity at 30 to 40 m depth, which coincides with the clear increase observed in the ERT.

The clear change to a much lower resistive layer occurs at depths agreeing with the border to the limestone. This profile is situated very close to the coast, so the low resistivities of the bedrock are likely a result of saltwater intrusion.

4.10 Profile 10: Ölöv (S-N)

Description

At this southern transect of the Alnarp valley, there is a great shift in SkyTEM data between the SW and NE side. Similarly, the two boreholes presented in Table 12 differ greatly in both depth and layering. The closest of these boreholes is about 700m away from the profile location as shown in Figure 58, while the other one is further southeast. The aim of this survey location was to investigate the geology of the north-eastern side.
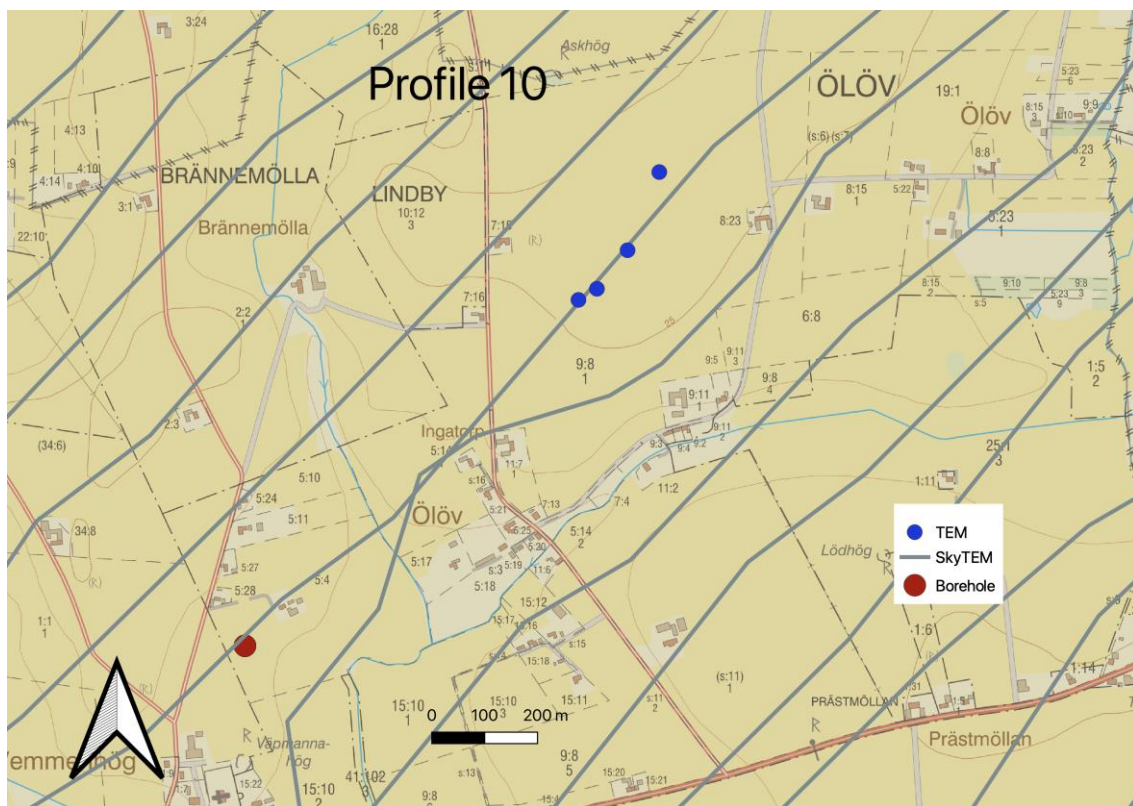
Figure 58. Map of survey location 9, including ERT, nearby borehole(s) and SkyTEM.
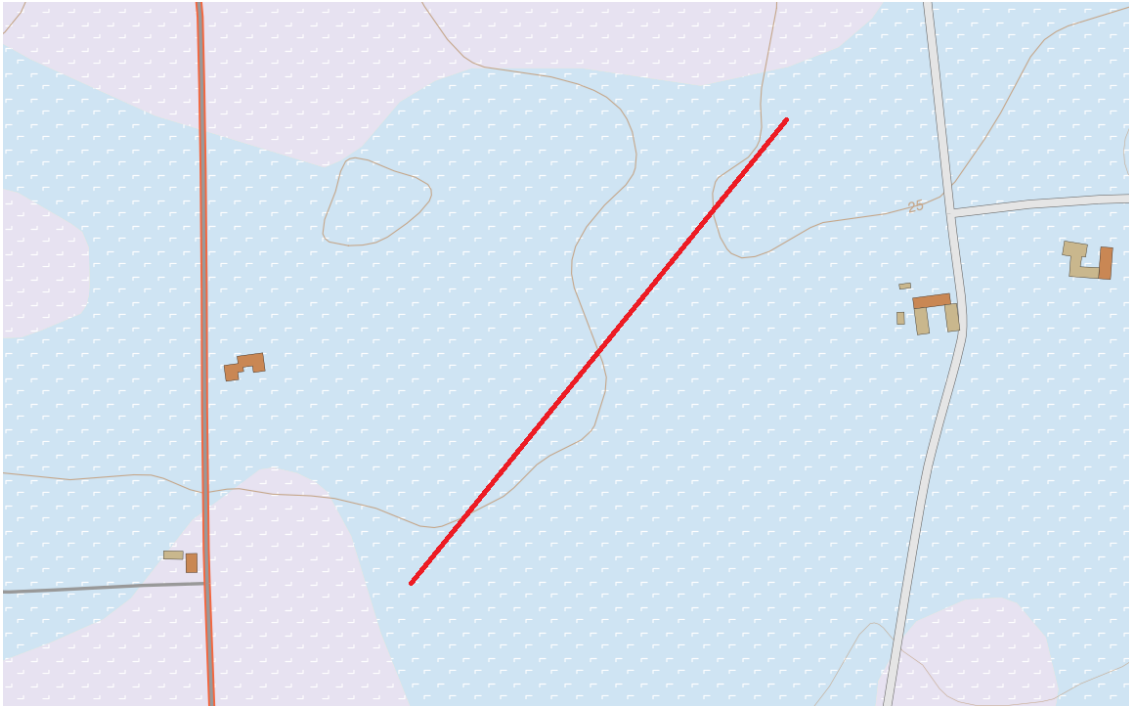
Figure 59. Soil map för ölöv, with approximate profile location in red. For more information, refer to Table 1.

Table 12. The lithology of the two closest nearby boreholes.

(700 m SW) Level (m)	0-10	10-37	37-46	46-81			
Lithology	Gravel	Clay till	Clay	Gravel and sands			
(1.3 km SE) Level (m)	0-6	6-42		42-60	60-74	74-80	80-111
Lithology	Sand and gravel	Clay till and till, with layers of sands		Coarse silt, sand and gravel	Clay and clay till	Sand, gravel and stone	Clay till

Results profile 10: Ölöv

Resulting profile
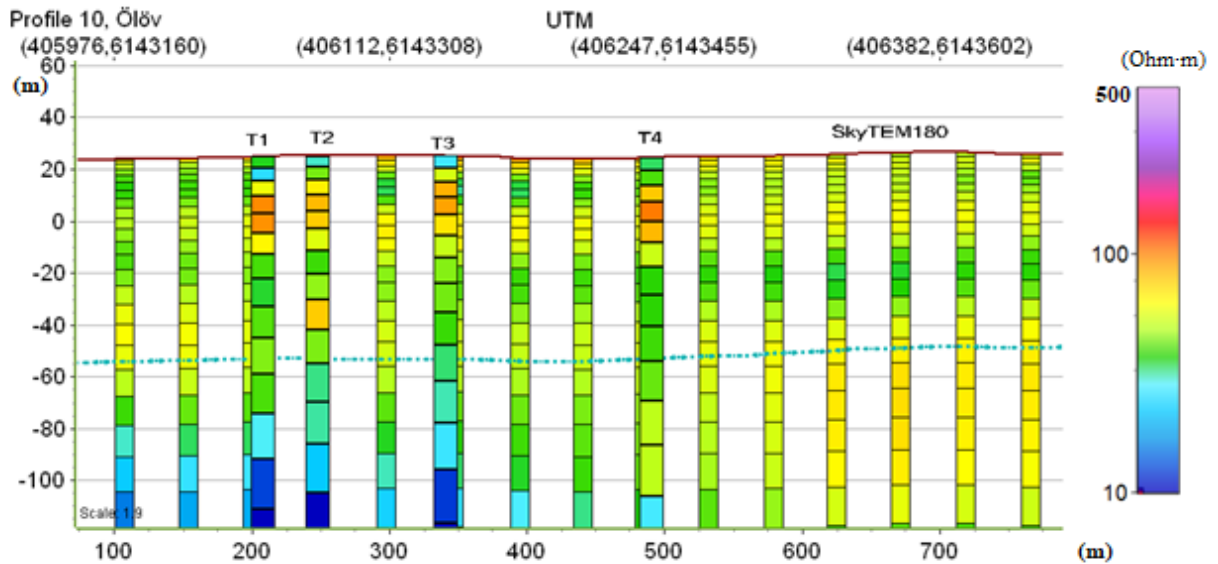
Figure 60. TEM soundings marked T1 to T4 with a wider profile of SkyTEM soundings. SkyTEM soundings included up to 50 m orthogonally from the imaginary line through which the TEM measurements are placed. Color scale shows resistivities between 10 to 500 Ohm·m.

Interpretation

The TEM and SkyTEM show similar results, but there are some differences. TEM picks up a low resistivity layer at the surface, followed by a higher resistivity layer of around 20m thickness, while the SkyTEM shows two layers of higher resistivity, with one of lower in between. At around 35 meters depth, both methods agree on the start of a lower resistivity layer, although the thickness of this differs between methods and it can be due to different resolution. At the bedrock boundary in T1-T3, we see another decrease in resistivity going as low as 10 Ohm·m. We see something similar in T4, but bedrock resistance is greater here. This agrees with the SkyTEM also showing a greater bedrock resistivity in this direction.

The upper low resistivity layer in the TEM results coincides with what we see in the local soil map (Figure 59), till with a high clay content. The borehole lithology in Table 11 has gravel near the surface in both instances, which is likely not present here. This large, immediate difference between the soil map/results and the boreholes makes us question how reliable the boreholes are in this instance. Clayey till with layers of sand appears in the southeastern borehole and may be present here judging by the distinct layering of high/low resistivity layers appearing in both SkyTEM and TEM, with a possible sand layer appearing at around 20 meters depth in the TEM. The coarser Alnarp sediments are expected to appear at a depth of roughly 40 meters judging by nearby boreholes, and they show resistivities ranging between around 40 to 80 Ohm·m. We see a lower bedrock resistivity in the first half of the profile in both TEM and SkyTEM. It is perhaps possible that the bedrock is more fractured and weathered here.

73

4.11 Profile 11: Havgård - Lemmeströ (S-N)

Description

This area is located where Alnarpsströmmen narrows significantly compared to both NW and SE. The thickness of the sediments is also much higher, with the bedrock at a depth of more than 110 m.

Available boreholes are sparse, but the borehole to the north (Table 13) at the chosen location shows a stratigraphy deviating from those at nearby profiles to the NW. With a thick and deep clay layer above the Alnarp sediments, the thickness of the aquifer is reduced.

Looking at nearby SkyTEM results, the main change in resistivity is usually between the clayey till near the surface and the underlying Alnarp sediments, and then another shift near the bedrock boundary. In this case (Figure 63), an another low resistivity layer is visible in most of the soundings in profile 11a, and in the first, southern parts of 11b, at depths of about 40 to 70 meters, not quite agreeing with the clay present in Table 13 at 65-85m. It was decided to investigate with TEM at this site to see if the clay layer extends southwards. Topsoil along the profile consists exclusively of clay as shown in Figure 62.
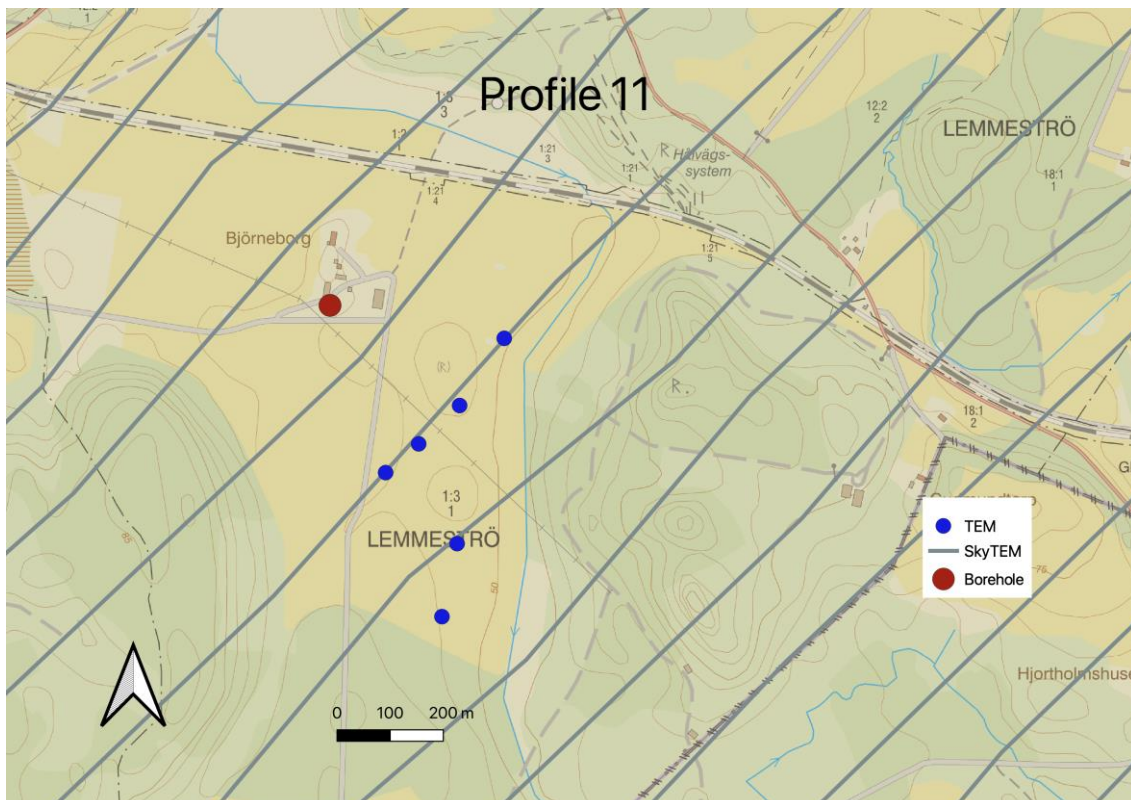
Figure 61. Map of survey location 9, including TEM, nearby borehole(s) and SkyTEM.

74

Figure 62. Soil map for Havgård-Lemmeströ. For more information, refer to Table 1.

Table 13. The lithology of the borehole 280 m from T2 and T3 intersecting line as shown in figure 60 and 61.

Level	0-45	45-65	65-86	86-120
Lithology	Clay and clay till	Fine sand to sand	Clay	Fine sand, sand and gravel

Results profile 11: Lemmesterö-Havgård

Resulting profiles
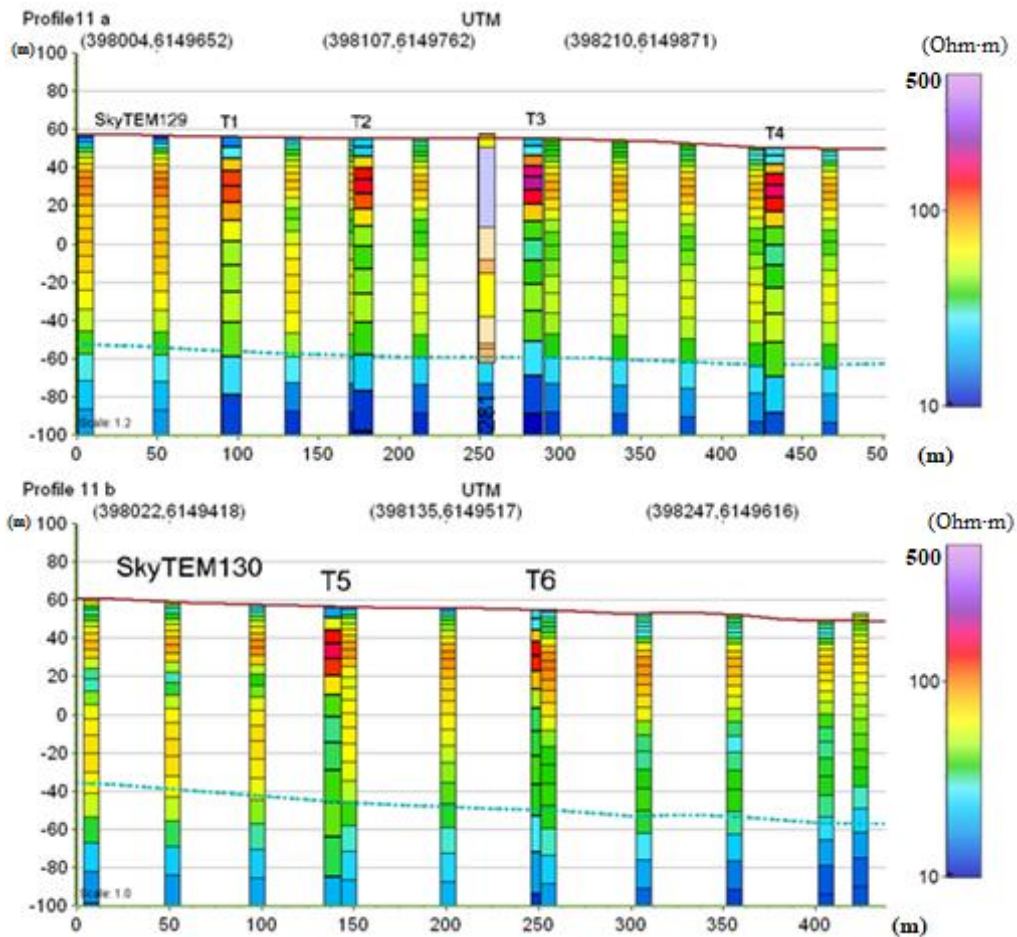
Figure 63. TEM soundings marked T1 through T4 in (a), and T5 through T6 in (b). SkyTEM soundings marked with belonging profile number and included up to 50 m from the imaginary line through which the TEM measurements are placed. Bore-hole 281 m north of profile 11a. Colour scale shows resistivities between 10 to 500 Ohm·m.

Compared to the SkyTEM, the ground TEM shows a higher gradient in resistivity between the topsoil clay and underlying layer, which is visible starting from a depth of around 20m at about 200 Ohm·m, up to 300 Ohm·m in T3. What material makes up this layer is unknown. The available borehole (Table 13) has clay and till clay at this depth. As it is at a consistent depth and seen throughout the entirety of both profiles, it's not likely that this is a coarser part of the till, instead it is most likely its own layer made up of some coarser material such as gravel or sand. The fine sand to sand layer may be present just below this depth and could act as a confined aquifer of its own, confined by the till above and the possible thick clay below. The thick layer of clay at 65-86m depth may or may not be present; there is a decrease in resistivity here in the TEM measurements, but it coincides with the decrease in resistivity towards the bottommost water-bearing sediments and the bedrock. The Alnarp sediments show resistivity values ranging between 40 and 80, and low bedrock resistivities of around 10-20 Ohm·m, indicating a very fractured bedrock.

5 Discussion

5.1 Pre-study and Fieldwork

Finding suitable survey locations was quite difficult. They had to be interesting from a geological standpoint in some way, somewhat close to a borehole to aid in interpretation, not too close to some source of noise, and so on. Once a location was found, permission from the landowner was also needed, which was not always granted. Some farmers were concerned that the findings of our study could have an impact on their usage of fertilizers if a water protection zone was declared, for example. Others simply did not reply to emails or answer our telephone calls. The time for the pre-study phase was also limited. These factors combined led to some survey locations not being ideal; they are sometimes too far away from boreholes, or some source of disturbance was overlooked. We also seriously underestimated the time required to carry out measurements. In some instances, we had planned to complete two profiles of 600-800 meters in a single day. However, already after the first day, this turned out to be impossible. Just completing a single 800-meter survey, with three people, took nearly ten hours, and although the time was reduced as we gained experience with the system, surveys had to be shortened.

The original aim was to conduct measurements exactly along previously designed profiles. However, in many cases the conditions on-site did not allow this as crops growing in the field would have been trampled, or there turned out to be something in the way. It would have also been quite time consuming and difficult to follow these profiles exactly when using DCIP, as each insertion point for a stake would have had to been found and marked first using GPS, and conducting measurements already turned out to be more time-consuming than planned. Instead, we often relied on existing tractor trails, which allowed us both to keep a relatively straight line without difficulty and to not trample more crops than necessary. The original aim was also to conduct all measurements with both methods in the same three-week period, which unfortunately was not possible due to several reasons, including a broken TEM component which had to be replaced.

5.2 Comparison between the different methods

One of the aims of the study was to look at how the different methods compare to one another in terms of results, strengths, and weaknesses. Something to keep in mind is that the ERT and TEM measurements were not carried out at the same time, and indeed not even in the same season. ERT was carried out in April, and TEM in November. What effect a reduced temperature and wetter conditions during the TEM measurements could have had is not fully known, but it could be expected that the wetter topsoil during TEM measurements would lead to lower resistivity values near the surface. Perhaps this could explain why TEM picks up a lower resistivity layer near the surface while ERT doesn't in Profile 7, for example. The weather conditions during the SkyTEM measurements are not known.

In terms of results, the DCIP and TEM methods produced resistivity values roughly in an interval of 10-150, with some outliers. This can be compared to the range of around 10-100 that the SkyTEM shows in most of the valley, as discussed in chapter 2.7.1. In profiles with both methods and no disturbances, ERT and TEM show very similar results.

SkyTEM fails to pick up local variations in resistivity in several profiles compared to the other methods, both in places where the resistivity is locally very high and in places where the layering is seemingly more complex. Nevertheless, SkyTEM does provide a somewhat accurate picture in the most common case in the area i.e., a low-resistivity till clay layer near the surface on top of a higher-resistivity coarse sediment layer, on top of a low-resistivity bedrock. One pattern that can be observed is that it sometimes detects a low resistivity layer at depths where DCIP or TEM, which should be more accurate, does not detect one. Such layers are visible in profiles 2, 6 and 7. The reason for this is unknown, but it could be due to smoothing and lateral constrain in the inversion process of the SkyTEM data. If one was to look exclusively at the SkyTEM data in such an instance, you may interpret this as a layer of clay, an aquiclude. This is one of the drawbacks of the method, any interpretation made from it risks being flawed and differing from ones made with more accurate data. Its main benefit is of course the sheer amount of data being gathered. The data from this SkyTEM survey covers 5200 km (Brolin, 2021), a staggering amount of data compared to the maximum of 800 meters we were able to survey in one day.

The other methods have their strengths and drawbacks as well. While DCIP fails to penetrate to the very bottom of the aquifer in many of our surveys, the high-resolution 2D image generated is a very helpful tool for interpretation. TEM has great depth penetration but is only 1D, and is very vulnerable to interference by nearby powerlines etc. Compared to DCIP, the amount of data acquired per time spent is also low; we found that one full day of TEM measurements could produce around 6 data points, compared to a 6-800m profile with DCIP, specifically while using the multiple-gradient array configuration, as other configurations may take longer to gather this amount of data. DCIP also collects induced polarization data, and while this turned out to be of no help for this thesis, it can be of great help in other studies, and since it gathers both resistivity and induced polarization data simultaneously, there is no drawback to using it.

One upside of TEM is that it does not suffer DCIP's problems with too high contact resistance. There were only a few instances of trouble with this during this study, but in some areas with dry, highly resistive topsoil one can imagine carrying out DCIP measurements to be very difficult. It is also considerably less physically demanding to carry out TEM measurements, if one doesn't have access to an offroad vehicle of some sort, as the equipment is not as heavy to lug around by hand and there is a lot less backtracking involved. Both methods have a low impact on the soil, but TEM has even less as there is nothing inserted into it.

We assess that TEM is more useful as a quick, cost-effective, pre-study method of investigation in most cases, where only one or two data points are necessary. According to our study, the resistivity measurement is very similar to DCIP results. For more detailed investigation, DCIP offers superior resolution and much greater amounts of data. The exception is when one wants to investigate something at depths of about 60 meters or above, at which the resolution of DCIP is poor, or fails to penetrate entirely. They also complement each other nicely in situations where one is interested in both deeper and more shallow parts, especially since the results are outputted in Ohm·m in both cases and thus can be directly compared. There is also the possibility of doing a mutually constrained inversion (MCI), where data from both ERT and TEM are used together in an inversion to generate a mutual model, although ideally then both measurement types should be carried out closer together timewise so that the data are more comparative (Christiansen, et al., 2007).

5.3 Discussion of results

In terms of inversion, the mean residual percentages of our ERT profiles, at least after some data processing, range from around 1 percent to 4 percent in some cases. After discussions with our supervisor, it was agreed that this can be considered as good, reliable results although 4 percent is a bit on the high side.

As previously mentioned, IP values generally ranged between 1-10 mv/V with very little correlation to the present materials. This combined with a lack of information regarding interpreting within this range prompted us to not take IP values into consideration.

One aim of the thesis was to characterize the aquifer and the overlaying soils in terms of resistivity, as far as this is possible. As a preamble, this section relies heavily on the interpretations being correct, which they very well may not be. Geophysical methods are a helpful tool for interpreting what lies beneath our feet, but the only way to know for sure is by drilling down and looking. Resistivity ranges can overlap heavily, and the boreholes we used as an aid when interpreting was sometimes up to a kilometer away. In areas with two nearby boreholes, they often contradict one another, showing how the layering may change over "short" distances, and making interpretation more difficult. Borehole logs are not necessarily accurate either, what one geologist has specified as clayey till another might call till, for example. Nevertheless, some values and the reasoning behind them are presented below.

Layers of clay are found in many of our profiles, and as expected they often appear close to the surface. They are expected to have quite low resistivity. Reynolds (2011) suggests

a range of about 1-100 Ohm·m, or 50-150 if very dry. In this examination, the materials that were interpreted as clay fell in a range of around 10-40 Ohm·m, suggesting a wetter clay.

The till found in the area was often described as clayey, suggesting a lower resistivity material. Reynolds suggests a range of 10 – 5000, a quite wide range owing to the many different varieties (Reynolds, 2011). What was found in this study often fell in a range of about 30-80 Ohm·m. One outlier to this is profile 5, in which suspected clayey till reaches upwards of 150 Ohm·m. The reason for this is unknown, but it may simply be due to local geology differing from that of nearby boreholes. A transition from lower resistivity to higher with depth is often seen. The principal geology of the area as discussed in chapter 2.1 points to a till of higher clay content near the surface, and one with coarser grain sizes at depth, which correlates well with this pattern.

In nearly every profile the bedrock, consisting of limestone, shows quite low resistivity values. One suggested range for limestone can be found in chapter 2.7.1, suggesting 1000-100 000 Ohm·m, which is far away from our results that suggest a range of about 10-100 Ohm·m in the studied area. As previously discussed, this could be the result of a very fractured bedrock combined with groundwater pumping in the area causing the water of higher ionic content to move upwards. Interestingly, the results of profiles near Grevie look quite similar in terms of bedrock resistivity to the profiles close to the coast, for example Abbekås, where the ionic (salty) water of the ocean infiltrating into the aquifer is the likely culprit. This supports the theory that these results are due to a higher ionic content as well. However, Profile 11 has a similarly low bedrock resistivity despite being quite far away from Grevietäkten, or any other major water-extracting area. It's possible that these results then are exclusively a result of heavy weathering and fractioning. One other possible explanation is density. Water of a higher ionic content is denser than freshwater. This denser water could then, over time, sink towards the bedrock, where ionic concentrations could rise, although the authors were unable to find a source to support this theory.

Gravel is found throughout the profiles, appearing both in patches closer to the surface and as part of the saturated Alnarp sediments. In Profile 5, patches of what we interpreted as sand and gravel has resistivities of around 300-400 Ohm·m. These patches are found surrounded by till clay and are thus not a part of the Alnarp sediments. Reynolds (2011) offers two resistivity values for gravel, 100 for fully saturated and 1400 when dry. If our interpretation is correct, the gravel found here should be partly saturated. Gravel also appears as part of the Alnarp sediments, often mixed with sand, and is difficult to get a read on by itself. The Alnarp sediments will be clumped together and discussed in their own segment.

Sand appears mainly as part of the Alnarp sediments, but on occasion appears in layers by itself, often just below or at the surface. In profile 1, a few patches of what we interpreted as sand appear just below the surface, with resistivities of around 100 Ohm·m. A similar interpretation is done in profile 3. One source (Zandz, 2022) puts moderately wetted sand in a range of 60-130 Ohm·m.

The Alnarp sediments, consisting of coarse silt, sand and gravel saturated with water, generally range between 40 and 100 Ohm·m. With their higher resistivities, they are usually distinguishable from the overlaying clayey till. The principal geology of the area tells us that local till gets coarser with depth, and indeed it is often more difficult to distinguish between these coarser tills and the Alnarp sediments. In some instances, a clear decrease in resistivity is observed as the bedrock is approached, correlating with

parts or the entirety of the assumed thickness of the Alnarp sediments. This can be observed in profiles 5, 6 and 9, and to a lesser extent in several other profiles. In other cases, they appear as a homogenous layer, as in profiles 1 or 2. Other times they appear patchier. In any case, it is difficult to interpret a thickness of these sediments by resistivity alone, although an approximation can often be made.

These results are presented in Table 14. There is quite a lot of overlap between our interpretated ranges, as is often the case with resistivity ranges.

Table 14, interpreted resistivities of the most prominent materials of the Alnarp valley.

Material, interpeted	Resistivity (Ohm·m)
Alnarp sediments	40-100
Clay	10-40
Gravel	300-400
Limestone	10-100
Sand	100
Till	30-80

6 Conclusions and recommendations

In conclusion, this geophysical survey in the Alnarp valley demonstrated the usefulness of ERT, TEM, and SkyTEM in understanding the subsurface. Each method contributed unique information, and when used in combination, they provided a more comprehensive picture of the geological structures. The obtained results and interpretations can serve as a foundation for future studies and hydrogeological investigations in the region. ERT and TEM showed similar results in profiles without disturbances. TEM's advantage was its depth penetration, while ERT offered high-resolution 2D images for interpretation. Both methods complemented each other, especially when studying both shallow and deeper subsurface features. The principal geology of the area as described in past studies, as well as local boreholes indicated the presence of clay, till, limestone, gravel, and sand in the studied area. The interpreted resistivity ranges for these materials were generally in agreement with existing literature, with the exception of limestone, but local variations and overlapping ranges made interpretation challenging. The Alnarp sediments, consisting of coarse silt, sand, and gravel, appeared with resistivity values ranging from 40-100 Ohm·m.

The authors would like to finish this report by providing some possible improvements to our study, and provide some recommendations for potential future studies. One possible improvement could be to visit a potential site in person beforehand to look for issues not visible on a map. Like previously mentioned, occasionally there were issues in the field that could have been avoided by more careful planning with better information beforehand. Looking back, it would have been an interesting addition to include one or more profiles outside of the Alnarp valley and comparing them to the ones inside, to see if it is possible to perceive the Alnarp sediments using exclusively resistivity. This could be useful to define the extent of the Alnarp valley more sharply, as in some areas around the edges there are few boreholes available. A more careful selection of sites, closer to available boreholes, would also have been appropriate in some cases.

If carrying out a similar study such as ours, using both DCIP and TEM, one should also strive to carry them out as close as possible timewise to one another, to try and mitigate wetter or drier weather, as well as yearly groundwater variations, from having an impact on results. Preferably this should be done in spring or early autumn when the weather is pleasant. Doing fieldwork in November was not a very enjoyable experience for the authors. As discussed in the previous chapter, the fact that the limestone bedrock has such a low resistivity was unexpected. Some possibilities as to why this is were discussed, but without more data it's impossible to tell for sure. A possible future study might then involve examining the weathering and the water chemistry of the water around Grevietäkten.

7 References

ABEM, 2010. *Instruction Manual Terrameter SAS 4000 / SAS 1000.* :GuidelineGeo.

ABEM, 2022. *ABEM WalkTEM 2.* [Online]
Available at: https://www.guidelinegeo.com/product/abem-walktem-2/
[Accessed 19 4 2023].

ABEM, n.d. *ABEM WalkTem User's Guide.* :GuidelineGeo.

Adcoc, J., 2020. *Avoiding common problems and improving results in resistivity surveys.*
[Online]
Available at: https://www.youtube.com/watch?v=sGRzzgJDIwY
[Accessed 25 12 2023].

AGS, 2022. *Getting started with SPIA TEM.* [Online]
Available at: https://wiki.ags-cloud.dk/wiki/S_SPIATEMManual
[Accessed 28 12 2022].

Barmen, G., 1992. *On the Combination of Isotope Hydrogeology with Regional Flow and
Transport Modelling,* Lund: Department of Engineering Geology, Lund Institute of Geology.

Basheer, A. A. et al., 2014. Relevance of AEM and TEM to Detect the Groundwater Aquifer at
Faiyum Oasis Area, Faiyum, Egypt. *International Journal of Geosciences.*

Binley, A. & Kemna, A., 2005. DC Resistivity and Induced Polarization Methods. In:
Hydrogeophysics. :Springer, pp. 129-156.

Brolin, C., 2021. *Resistivitetssektioner längs flygmätningslinjer, Sydvästskåne,* : SGU.

Brolin, C. & Dahlqvist, P., 2020. *Bearbetning av helikopterburen TEM-data,* : SGU.

Christiansen, A. V., Auken, E., Foged, N. & Sørensen, K. I., 2007. Mutually and laterally
constrained inversion of CVES and TEM data: a case study. In: *Near surface geophysics.*
Aarhus: , pp. 115-123.

Christiansen, A. V., Auken, E. & Sørensen, K., 2009. The transient electromagnetic method. In:
Groundwater Geophysics. :Springer, pp. 179-226.

Dahlin, T. & Zhou, B., 2006. Multiple-gradient array measurements for multi-channel 2D
resistivity imaging. *Near Surface Geophysics,* p. 114.

Daily, W., Ramirez, A. L., Binley, A. & LaBrecque, D., 2005. Electrical Resistance Tomography -
Theory and Practice. In: D. K. Butler, ed. *Near-Surface Geophysics.* :Society of Exploration
Geophysicists, pp. 525-550.

Erlström, T., 2021. *Grundvattenbildning i Alnarpsströmmen. Numerisk modellering av
grundvattenbildning och akvifersförhållanden.,* Lund: LTH, Teknisk Geologi.

GPG, 2021a. *Electrical Conductivity.* [Online]
Available at:
https://gpg.geosci.xyz/content/physical_properties/physical_properties_conductivity.html
[Accessed 5 3 2023].

GPG, 2021b. *Chargeability.* [Online]
Available at:
https://gpg.geosci.xyz/content/physical_properties/induced_polarization_physical_properties
_duplicate.html
[Accessed 5 3 2023].

Greggio, N. et al., 2018. High-Resolution Electrical Resistivity Tomography (ERT) to
Characterize the Spatial Extension of Freshwater Lenses in a Salinized Coastal Aquifer. *Water.*

GuidelineGeo, 2023. [Online]
Available at: https://www.guidelinegeo.com/product/abem-terrameter-ls-2/
[Accessed 7 3 2023].

Gustafsson, O., 1978. *Beskrivning till hydrogeologiska kartblader trelleborg NO/Malmö SO.*
Stockholm: SGu.

Gustafsson, O., Thunholm, B., Gustafsson, M. & Rurling, S., 2005. *Beskrivning till kartan över
grundvattnet i Skåne län,* Uppsala:

Hitta, 2022. [Online]
Available at: https://www.hitta.se/
[Accessed 18 2 2022].

Johansson, A., 2018. *Structural effects on externally induced building vibrations,* Lund: Division
of Structural Mechanics, faculty of Engineering.

Johansson, M., Widing, S., Leander, B. & Persson, K., 2006. *Groundwater model, Mike She, of
the salt water distribution in Alnarpsströmmen, southern Sweden.* Cagliari-Chia Laguna, Italy,

Johnson, T., 2007. Battling Seawater Intrusion in the Central & West Coast Basins. *Technical
bulletin 13.*

Kirsch, R., 2006. *Groundwater Geophysics - A Tool for Hydrogeology.* :Springer.

Klitten, K. & Olsen, H., 1995. *Geophysical log-stratigraphy of the Kobenhan Limestone.*
Copenhagen, Bulletin of the Danish Geotechnical Society.

Landberg, J. & Hartzén, L., 1987. *Geotekniska och geohydrologiska erfarenheter från
grundläggning på kritkalksten.* no. 4 ed. :Väg och vattenbyggaren.

Lantmäteriet, 2022. [Online]
Available at: https://www.lantmateriet.se/sv/Fastigheter/vem-ager-fastigheten/
[Accessed 28 2 2022].

Leksunim, 2018. *Alnarpsdalen i sydvästra Skåne med Alnarpsströmmen och Skivarpsströmmen.*
[Online]
Available at: https://commons.wikimedia.org/w/index.php?curid=73021462
[Accessed 3 4 2022].

Liljegren, R. & Björkman, L., 2004.
https://web.archive.org/web/20060209051446/http:/www.geol.lu.se/netu/virtex/Tornquistzonen.html. [Online]
[Accessed 9 4 2021].

Loke, D. M., 2004. *Tutorial : 2-D and 3-D electrical imaging surveys,* : University of Alberta.

Lowrie, W. & Fichtner, A., 1997. *Fundamentals of Geophysics.* :William Lowrie.

Malmö stad, 2021. [Online]
Available at: https://malmo.miljobarometern.se/vatten/grund-och-dricksvatten/grundvattenuttag/

McNeill, J., 1980. *Technical Note TN-5 - Electrical conductivity of soils and rocks,* : Geonics.

Miller, U., 1977. *Pleistocene deposits of the Alnarp valley, southern Sweden. Microfossils and their stratigraphical application.* Lund: Lund University.

Milsom, J. & Eriksen, A., 2011. *Field Geophysics.* :John Wiley & Sons Inc.

Mrkoll, 2022. [Online]
Available at: https://mrkoll.se/
[Accessed 3 3 2021].

Olson Engineering, 2023. *Electrical Resistivity Tomography.* [Online]
Available at: https://olsonengineering.com/methods/geophysical-methods/electrical-resistivity/2d-er-tomography-ert-profiling/
[Accessed 10 3 2023].

Olsson, P.-I., 2016. *Advances in time–domain induced polarization tomography.* Lund: Department of Biomedical Engineering, Lund University.

Palacky, G., 1988. Resistivity characteristics of geological targets. In: *Electromagnetic methods in applied geophysics.* :Society of Exploration Geophysicists, pp. 52-129.

Reynolds, J. M., 2011. *An Introduction to Applied and Enviromental Geophysics.* :John Wiley & Sons Inc.

Ringberg, B., 1980. *Beskrinving till jordartskartan 2C Malmö SO.* Uppsala: SGU.

Ringberg, B., 1987. *Beskrivning till Jordartskartan Malmö NO,* Uppsala: SGU.

ScienceDirect, 2023. [Online]
Available at: https://www.sciencedirect.com/topics/earth-and-planetary-sciences/confined-aquifer
[Accessed 1 3 2023].

SGU, 2021. [Online]
Available at: https://www.sgu.se/grundvatten/brunnar-och-dricksvatten/brunnsarkivet/
[Accessed 7 4 2021].

SGU, 2023a. [Online]
Available at: https://apps.sgu.se/kartvisare/kartvisare-jorddjup.html
[Accessed 17 4 2023].

SGU, 2023b. [Online]
Available at: https://apps.sgu.se/kartvisare/kartvisare-jordarter-25-100.html
[Accessed 17 4 2023].

SGU, 2023c. *Grundvattenkartvisare.* [Online]
Available at: https://www.sgu.se/produkter-och-
tjanster/kartor/kartvisaren/grundvattenkartvisare/
[Accessed 17 4 2023].

Slater, L. D. & Lesmes, D., 2008. *The Induced Polarization Method,* : Department of
Geosciences, University of Missouri-Kansas City.

Soupios, P. et al., 2007. Use of Engineering Geophysics to Investigate a Site for a Building
Foundation. *Journal of Geophysics and Engineering.*

Sydvästskånes grundvattenkommitté, 2021. [Online]
Available at: http://www.ssgk.se/kommitten/
[Accessed 10 02 2021].

U.S EPA, 2016. [Online]
Available at: https://archive.epa.gov/esd/archive-
geophysics/web/html/resistivity_methods.html#:~:text=Apparent%20resistivity%20is%20defi
ned%20as,arrangement%20and%20spacing%20of%20electrodes.
[Accessed 3 4 2023].

UBC, EOAS, 2021. [Online]
Available at: https://www.eoas.ubc.ca/ubcgif/iag/foundations/properties/2physprop-iag.htm
[Accessed 10 03 2021].

VA SYD, 2021. *Bulltofta vattenverk.* [Online]
Available at: https://www.vasyd.se/Artiklar/Dricksvatten/Bulltofta-vattenverk
[Accessed 22 03 2021].

VASYD, 2008. *Vattenskyddsområde för VA SYDs vattentäkt vid Grevie.* [Online]
Available at: https://docplayer.se/18850457-Vattenskyddsomrade-for-va-syds-vattentakt-vid-
grevie.html
[Accessed 10 10 2021].

Vattenbyggnadsbyrån, 1969. *Samarbetskommittén För Alnarpsströmmen - Utredning,* :
Samarbetskommitén för Alnaprsströmmen.

Vrba, J., 2002. Chapter 5. The impact of aquifer intensive use on groundwater quality. In:
*Commission on Groundwater Protection of the International Association of Hydrogeologists
(IAH).* Prague

Zandz, 2022. *Soil resistivity.* [Online]
Available at: https://zandz.com/en/soil-resistivity/
[Accessed 10 03 2023].

A. Appendix

7.1.1 Res2DINV settings.

Inversion settings

Initial damping factor (0.01 to 1.00)

0.1500

Minimum damping factor (0.001 to 0.75)

0.0200

Local optimization option (0=No, 1=Yes)

1

Convergence limit for relative change in RMS error in percent (0.1 to 20)

1.0000

Minimum change in RMS error for line search in percent (0.5 to 100)

0.5000

Number of iterations (1 to 30)

20

Vertical to horizontal flatness filter ratio (0.25 to 4.0)

0.25000

Model for increase in thickness of layers(0=default 10%, 1=default 25%, 2=user defined)

2

Number of nodes between adjacent electrodes (2 or 4)

2

Flatness filter type, Include smoothing of model resistivity (0=model changes only,1=directly on model)

1

Reduce number of topographical data points? (0=No,1=Yes. Recommend leave at 0)

0

Carry out topography modeling? (0=No,1=Yes)

1

Type of topography trend removal (0=Average,1=Least-squares,2=End to end)

0

Type of Jacobian matrix calculation (0=Quasi-Newton, 1=Gauss-Newton, 2=Mixed)

1

A

Increase of damping factor with depth (1.0 to 2.0)

1.0500

Type of topographical modeling (0=None, 1=No longer supported so do not use, 2=uniform distorted FEM, 3=underwater, 4=damped FEM, 5=FEM with inverse Swartz-Christoffel)

4

Robust data constrain? (0=No, 1=Yes)

1

Cutoff factor for data constrain (0.0001 to 0.1))

0.0500

Robust model constrain? (0=No, 1=Yes)

1

Cutoff factor for model constrain (0.0001 to 1.0)

0.0050

Allow number of model parameters to exceed data points? (0=No, 1=Yes)

1

Use extended model? (0=No, 1=Yes)

0

Reduce effect of side blocks? (0=No, 1=Slight, 2=Severe, 3=Very Severe)

1

Type of mesh (0=Normal,1=Fine,2=Finest)

2

Optimise damping factor? (0=No, 1=Yes)

1

Time-lapse inversion constrain (0=None,1&2=Smooth,3=Robust)

3

Type of time-lapse inversion method (0=Simultaneous,1=Sequential)

0

Thickness of first layer (0.25 to 1.0)

0.5000

Factor to increase thickness layer with depth (1.0 to 1.25)

1.1000

USE FINITE ELEMENT METHOD (YES=1,NO=0)

1

WIDTH OF BLOCKS (1=NORMAL WIDTH, 2=DOUBLE, 3=TRIPLE, 4=QUADRAPLE, 5=QUINTIPLE)

1

MAKE SURE BLOCKS HAVE THE SAME WIDTH (YES=1,NO=0)

1

RMS CONVERGENCE LIMIT (IN PERCENT)

0.100

USE LOGARITHM OF APPARENT RESISTIVITY (0=USE LOG OF APPARENT RESISTIVITY, 1=USE RESISTANCE VALUES, 2=USE APPARENT RESISTIVITY)

0

TYPE OF IP INVERSION METHOD (0=CONCURRENT,1=SEQUENTIAL)

0

PROCEED AUTOMATICALLY FOR SEQUENTIAL METHOD (1=YES,0=NO)

0

IP DAMPING FACTOR (0.01 to 1.0)

1.000

USE AUTOMATIC IP DAMPING FACTOR (YES=1,NO=0)

0

CUTOFF FACTOR FOR BOREHOLE DATA (0.0005 to 0.02)

0.00010

TYPE OF CROSS-BOREHOLE MODEL (0=normal,1=halfsize)

0

LIMIT RESISTIVITY VALUES(0=No,1=Yes)

1

Upper limit factor (10-50)

50.000

Lower limit factor (0.02 to 0.1)

0.020

Type of reference resistivity (0=average,1=first iteration)

0

Model refinement (1.0=Normal,0.5=Half-width cells)

0.50

Combined Combined Marquardt and Occam inversion (0=Not used,1=used)

0

Type of optimisation method (0=Gauss-Newton,2=Incomplete GN)

2

Convergence limit for Incomplete Gauss-Newton method (0.005 to 0.05)

0.005

Use data compression with Incomplete Gauss-Newton (0=No,1=Yes)

0

Use reference model in inversion (0=No,1=Yes)

1

C

Damping factor for reference model (0.0 to 0.3)

0.01000

Use fast method to calculate Jacobian matrix. (0=No,1=Yes)

0

Use higher damping for first layer? (0=No,1=Yes)

1

Extra damping factor for first layer (1.0 to 100.0)

5.00000

Type of finite-element method (0=Triangular,1=Trapezoidal elements)

1

Factor to increase model depth range (1.0 to 5.0)

1.050

Reduce model variations near borehole (0=No, 1=Yes)

0

Factor to control the degree variations near the boreholes are reduced (2 to 100)

5.0

Factor to control variation of borehole damping factor with distance (0.5 to 5.0)

1.0

Floating electrodes survey inversion method (0=use fixed water layer, 1=Incorporate water layer into the model)

1

Resistivity variation within water layer (0=allow resistivity to vary freely,1=minimise variation)

1

Use sparse inversion method for very long survey lines (0=No, 1=Yes)

0

Optimize Jacobian matrix calculation (0=No, 1=Yes)

0

Automatically switch electrodes for negative geometric factor (0=No, 1=Yes)

1

Force resistance value to be consistant with the geometric factor (0=No, 1=Yes)

0

Shift the electrodes to round up positions of electrodes (0=No, 1=Yes)

0

Use difference of measurements in time-lapse inversion (0=No,1=Yes)

0

Use active constraint balancing (0=No,1=Yes)

0

D

Type of active constraints (0=Normal,1=Reverse)

0

Lower damping factor limit for active constraints

0.4000

Upper damping factor limit for active constraints

2.5000

Water resistivity variation damping factor

8.0000

Use automatic calculation for change of damping factor with depth (0=No,1=Yes)

0